



M E T O C E A N
S O L U T I O N S

CRUDE SHIPPING PROJECT, WHANGAREI HARBOUR

Establishment of numerical models of wind,
wave, current and sediment dynamics

Report prepared for
Chancery Green for Refining NZ

Specialists in
Oceanography and
Meteorology

MetOcean Solutions Ltd: Report P0297-01

July 2017

Report status

Version	Date	Status	Approved by
RevA	15/06/2016	Draft for internal review	Monetti
RevB	17/06/2016	Draft for internal review	McComb
RevC	22/06/2016	Draft for client review	Gardiner
RevD	02/08/2016	Updated draft for internal review	Monetti
RevE	12/08/2016	Updated draft for client review	Gardiner
RevF	12/10/2016	Updated for client review	Monetti
RevG	19/01/2017	Updated for client review	Monetti
Rev0	07/02/2017	Draft for public consultation	Monetti
Rev1	25/07/2017	Final version	Monetti

It is the responsibility of the reader to verify the currency of the version number of this report.

Acknowledgements

Thanks to Ross Sneddon from the Cawthron Institute for ADCP deployment and data collection.

Thanks to Ricky Eyre from Northland Regional Council for supplying LIDAR and single-beam data for Whangarei Harbour, Stuart Caie from LINZ for supplying offshore multi-beam data and historic survey data of Mair Bank and Jae Staite from Northport Ltd for supplying multi-beam survey data for main channel and multiple historic surveys of Mair Bank.

The information, including the intellectual property, contained in this report is confidential and proprietary to MetOcean Solutions Ltd. It may be used by the persons to whom it is provided for the stated purpose for which it is provided, and must not be imparted to any third person without the prior written approval of MetOcean Solutions Ltd. MetOcean Solutions Ltd reserves all legal rights and remedies in relation to any infringement of its rights in respect of its confidential information.

EXECUTIVE SUMMARY

Refining NZ is investigating options for the deepening and the realignment of the shipping channel leading to the Marsden Point Refinery at the entrance to Whangarei Harbour. MetOcean Solutions Ltd (MSL) participation in the effects assessment for the project has involved an evaluation of the effects of the channel deepening on the wave, current and sediment dynamics of the harbour entrance, the effects of dredging and disposal on water quality, and the effects of sediment disposal on the receiving environment. This has been undertaken through the use of a suite of numerical model investigations supported by empirical data, observations and historical and contemporary oceanographic measurements.

The study investigations are presented in technical reference documents. The present report (MSL Report P0297-01) provides details on the establishment of numerical models for wind, wave, current and sediment dynamics, and the data collection program that was undertaken to support the model establishment and to validate the numerical schemes. The second report MSL Report P0297-02 (MSL, 2016) summarises the existing physical environment and outlining the likely effects of the Crude Shipping Project on the waves, hydrodynamics and short- and long-term sediment dynamics. These reports should be read together.

The dominant physical processes at regional and local scales were replicated through the application of industry-standard numerical models based on published scientific methodologies and the background knowledge acquired from previous numerical modelling studies. Several models were investigated and the most appropriate ones chosen for the domain of application. Wherever possible, models were validated using historical and contemporary oceanographic data sets.

Wave modelling

The open-source SWAN model has been used in numerous studies around the world to simulate the coastal spectral wave transformation processes. Here, the model was used to hindcast the wave climate and further examine the wave transformation across the ebb tide delta and the nearshore environment in the vicinity of the ebb tide delta and the offshore disposal areas. The model was successfully validated with measurements from 5 locations, and was shown to replicate the wave climate at the entrance of Whangarei Harbour and along Ruakaka Beach. Based on the physical processes involved and the good validation of the model, it is considered an appropriate tool to predict the effect of the channel deepening on the wave climate.

Current modelling

Ocean currents were simulated with two different models to investigate regional and local scales. The open-source ROMS model was used to perform 3D hydrodynamic downscaling of the oceanic and tidal flows over the Hauraki Gulf and Bream Bay and to provide information for the site selection and detailed simulations of the proposed offshore disposal grounds. Validation of ROMS with measured current profile data showed that the model adequately represented the non-tidal flow regime while tidal flows were somewhat under-predicted by the model at Disposal 3.2. In the context of sediment transport, it has been concluded that such biases in the current speed were insufficient to result in measurable changes. The impact of such bias on the plume modelling was investigated by forcing the model with the ADCP measured current profiles. Results did not highlight any increase of the predicted plume extension associated to the release of

sediments compared to the scenarios using the ROMS forcing. At local scale, the open-source SELFE model was used to simulate the 2D tidal flows in the vicinity of the ebb tide shoal, entrance and through the entire Whangarei Harbour. SELFE applies a finite-element mesh to allow resolution over complex bathymetries such as Whangarei Harbour. The model was validated against water levels measured at four locations and current profiles measured over regions of the outer channel where dredging is proposed. The validation showed the model to replicate the governing hydrodynamics of the harbour well, including the phase and amplitude of the tidal elevations and the spatially complex flows along the main shipping channel.

Morphodynamic modelling of the harbour entrance

The open-source Delft3D system was used to run high-resolution process-based morphodynamic simulations based on fully-coupled wave, current and seabed interactions. The morphodynamic system at the Whangarei Harbour entrance is influenced by the shellfish biomass on Mair Bank. Dealing with this unique environment within the numerical framework required the application of a range of published methodology approaches.

Climatic conditions were modelled to consider potential sediment transport and morphology evolution under conceptual and realistic scenarios. Morphological Acceleration Factors (MORFACs) for morphodynamic upscaling were applied to represent the likely short-term and long-term evolution of the seabed. For these scenarios, the sediment grain size distributions of the seabed were initialised from a 6-month fair-weather Bed Composition Generator (BCG) run. The resulting sedimentology was then qualitatively validated against contemporary sediment grain size observations.

Sediment plumes created during dredging

A Lagrangian particle model (ERcore) developed by MSL was used to simulate the likely extent and concentration of sediment plumes created during the dredging operation. This was achieved by simulating a plume continuously over a 28-day period at the various locations along the channel, and performing a subsequent statistical analysis of the predicted plume concentrations and extents. The plume dispersion associated with two different trailing suction hopper dredgers (TSHD), one cutter suction dredger (CSD) and one backhoe dredger (BHD) was simulated in the present study. The depth-averaged SELFE tidal currents were used as the environmental driver. A sensitivity analysis of the plume model considering more conservative scenarios was also carried out to assess the impact of several model parameters on the predicted plume extension.

Sediment plumes created during disposal

The same Lagrangian particle model (ERcore) was also used to simulate the likely extent and concentration of sediment plumes created during the disposal operation. The 3D ROMS model and the measured current profile data were used as the environmental drivers to the plume modelling. Using measured data at the disposal site addresses the identified underestimation of tidal current speed in the ROMS model. Plumes were simulated over a 6-month period at 5 sites within the proposed offshore disposal ground 3.2, applying the same probabilistic approach to determine plume extent and concentration as for the dredging process. The modelling included three phases of convective descent, dynamic collapse and

passive plume dispersion, using release depths according to the type of vessel involved.

Morphodynamic modelling of the disposal grounds

The Delft-3D modelling system was used to simulate the evolution of the proposed disposal grounds. A sequence of 16 representative wave and tide scenarios were run combined with weighted morphological acceleration factors to predict the long-term movement of material from the ground.

After an iterative process involving consideration of various alternatives and refinement of the preferred disposal areas, MetOcean modelled two offshore disposal sites. The first of these offshore disposal sites is referenced as Disposal Site 3.2, and is modelled for the placement of up to 97.5% of the capital dredge volume and up to 100% of the maintenance dredge volume. The capital dredge volume for this area is estimated at 3.7 million m³, and the maintenance dredge volumes are estimated as 125,000 m³ per annum (Tonkin and Taylor, 2016a). Therefore, as a conservative estimate that 97.5% of the capital dredge volume, and the full amount of the maintenance dredge volume will be placed in Area 3.2, a 4 m high disposal mound was modelled over a proposed 2 km² area – equivalent to a total volume of 8 million m³. The effect of the disposal mound on the wave climate within Bream Bay was assessed based on the wave modelling of the 16 representative scenarios including both the pre-disposal and the post-disposal bathymetries in the model.

Additionally, the Disposal Site 1.2 was designed for the disposal of 2.5 – 5% of the capital dredge and up to 100% of the maintenance dredge volume. The assessment of the disposal dynamics for the maintenance volumes was undertaken based on the numerical modelling of a representative value for a low mound, which was taken to be a 0.6 m high disposal mound (1.5 million m³) defined on the ebb tide delta and corresponding to 5% of the capital dredge volume and 100% of the maintenance dredge volume over 10 years. Such approach is particularly conservative as the disposal mound will be continuously eroded between each disposal due to the relative low water depth (less than 10 m) characterising the southern flank of the tidal delta.

As for the offshore disposal mound, the long-term evolution of the disposal ground was simulated using a sequence of 16 representative wave and tide scenarios combined with weighted morphological acceleration factors.

TABLE OF CONTENTS

Executive summary	ii
1. Introduction	2
1.1. Report structure	2
1.2. Study area.....	4
1.3. Proposed channel deepening design	5
1.4. Proposed offshore disposal ground designs.....	7
1.5. Additional Northport berth	8
2. Wind modelling.....	9
2.1. Model approach	9
2.2. Model validation	9
3. Wave modelling.....	13
3.1. Model approach	13
3.1.1. Model description.....	13
3.1.2. Pertinence of the model for the present study	13
3.1.3. Model domain and boundary conditions	14
3.1.4. Post-processing	16
3.2. Model validation	17
3.2.1. Frequency range and accuracy measures	18
3.2.2. Validation results.....	18
4. Regional hydrodynamic modelling.....	22
4.1. Model approach	22
4.1.1. Modelling description and pertinence of the model.....	22
4.1.2. Model domains.....	22
4.1.3. Atmospheric forcing	25
4.1.4. Open boundary conditions	25
4.1.5. Tidal forcing	25
4.1.6. Model calibration.....	25
4.2. Model validation	25
4.2.1. Current measurement program	25
4.2.2. Validation	26
5. Harbour tidal hydrodynamic modelling	31
5.1. Model approach	31
5.1.1. Model description.....	31
5.1.2. Pertinence of the model for the present study	31
5.1.3. High-resolution bathymetry and domain	32
5.1.4. Open boundary conditions	32
5.2. Model validation	32
5.2.1. Data collection program	32
5.2.2. Validation results.....	33
6. Sediment transport modelling.....	41
6.1. Modelling system	41
6.1.1. Delft3D-WAVE (SWAN)	41
6.1.2. Delft3D-FLOW	42

6.1.3. Delft3D-MOR	43
6.1.4. Pertinence of the model	44
6.2. Model domains.....	44
6.3. Modelling approach.....	46
6.3.1. Hydrodynamic and wave forcing	46
6.3.2. Initial bed configuration and composition.....	52
6.4. Delft3D – FLOW hydrodynamic validation	53
6.5. Morphodynamic validation.....	57
7. Dredge plume modelling	59
7.1. Trajectory modelling.....	59
7.2. Particle size distribution and settling velocity	61
7.3. Dredging scenarios	62
7.3.1. TSHD.....	62
7.3.2. BHD.....	64
7.3.3. CSD.....	65
7.4. Post-processing	66
7.4.1. Concentration and depositional thickness computation	66
7.4.2. Application to the present study	67
7.5. Sites for dredge plume modelling	67
8. Disposal plume modelling	70
8.1. Trajectory modelling.....	70
8.2. Simulated scenarios.....	70
8.2.1. Sources terms.....	70
8.2.2. Sediment distribution and settling velocity	74
8.2.3. Release sites and events	74
9. Disposal ground modelling	76
9.1. Modelling approach.....	76
9.2. Model domains.....	77
References.....	79
Appendix A – Location of instruments	82
Appendix B – Measured Currents.....	83
Appendix C – Location of release sites.....	89

LIST OF FIGURES

Figure 1.1	Flow chart showing the numerical modelling process for the study. Red lines indicate hydrodynamics; blue indicates waves; green indicate wind and yellow lines indicates bathymetry.....	3
Figure 1.2	Maps of Whangarei Harbour (top) and its entrance (bottom) with the locations used in the present study for the establishment of the numerical models and the description of the effect of the channel deepening on the coastal dynamics.	4
Figure 1.3	Depths (upper plot) and depth differences (lower plot) between the Option 4.2 channel design and the existing channel configuration. Positive amplitudes indicate a deepening of the channel.	6
Figure 1.4	Location of Disposal grounds 1.2 and 3.2 (indicated by coloured diagonal cross-hatch polygons) for the disposal of capital and maintenance volumes. 3 Mile Reef indicated by a green polygon is a sensitive reef for its benthic encrusting communities.	7
Figure 1.5	Satellite image showing the NorthPort Berth4 reclaim area included in the hydrodynamic model bathymetry.	8
Figure 2.1	Location of the wind station (red circle) at Marsden Point. Geographic coordinates are provided in Appendix A.	9
Figure 2.2	Time series plot of the measured and hindcast wind speed and wind direction at Marsden Point (year 1979). Note only a portion of the 12 years of data used for validation is shown here for better visualisation.	11
Figure 2.3	Time series plot of the measured and hindcast wind direction at Marsden Point (year 1979). Note only a portion of the 12 years of data used for validation is shown here for better visualisation.	11
Figure 2.4	Scatter and Quantile-Quantile plots of the measured and hindcast wind speed at Marsden Point (1979-1990). Also shown are the lines of equivalence.	12
Figure 2.5	Modelled (left) and measured (right) annual wind rose at position WS shown on Figure 2.1. Geographic coordinates of this location are provided in Appendix A.	12
Figure 2.6	Histograms of measured and hindcast wind directions at Marsden Point (1979-1990).	12
Figure 3.1	Water depth and model domains used to reproduce the spectral wave transformation from offshore to nearshore. The geographical extent of each domain is shown by the red rectangles.	15
Figure 3.2	Locations of the instruments (red circles) deployed for measuring the wave conditions along Ruakaka Beach and offshore of the entrance.	17
Figure 3.3	Time series of measured (blue) and modelled (red) significant wave height H_s at the WRB site.	19
Figure 3.4	Scatter diagram (left) and quantile-quantile plot (right) of measured and modelled significant wave height H_s at WRB site.	19
Figure 3.5	Time series of measured (blue) and modelled (red) mean absolute period from the second spectral moment T_{m02} at the WRB site.	20
Figure 3.6	Time series of measured (blue) and hindcast (red) significant wave height H_s at site W1.	20
Figure 3.7	Time series of measured (blue) and hindcast (red) significant wave height H_s at site W2.	21
Figure 3.8	Time series of measured (blue) and hindcast (red) significant wave height H_s at site W3.	21

Figure 3.9	Time series of measured (blue) and hindcast (red) significant wave height H_s at site W4.	21
Figure 4.1	Hydrodynamic hindcast modelling approach with ROMS. Upper panel shows the NZ domain, and HRKI domain and lower panel shows the WHANG domain.	24
Figure 4.2	Location of the four ADCP deployments in Bream Bay between January and July 2016. The geographic coordinates of each position is presented in Table 4.2. Also shown are the proposed disposal grounds 3.2 and 1.2.	26
Figure 4.3	Time series of modelled and measured non-tidal depth-averaged current velocity at position ADCP2 from 5 March to 14 April 2016.	27
Figure 4.4	Time series of modelled and measured tidal depth-averaged current velocity at position ADCP2 from 5 March to 14 April 2016.	28
Figure 4.5	Measured depth-averaged current rose at position ADCP2 (5 March – 14 April 2016).	28
Figure 4.6	Modelled depth-averaged current rose at position ADCP2 (5 March – 14 April 2016).	29
Figure 4.7	Quantile-Quantile plots of the measured and modelled non-tidal (top) and tidal (bottom) depth-averaged current speed at position ADCP2 (5 March – 14 April 2016).	30
Figure 5.1	Model depth and mesh of the Whangarei Harbour and surrounds. Depths are given in metres below Mean Sea Level (MSL) The mesh covers the offshore region, including the ebb tidal delta, while salient bathymetric features are represented inside the harbour.	32
Figure 5.2	Locations of current velocity measurements (Zone A in green, B, in red and C in orange) and water level measurements (K17, P10, W2 and Parua) used to calibrate and validate the SELFE (and Delft3D) tidal model within Whangarei Harbour and Bream Bay.	34
Figure 5.3	Measured and modelled water level comparisons at site k17.	34
Figure 5.4	Measured and modelled water level comparisons at site p10.	35
Figure 5.5	Measured and modelled water level comparisons at site Parua.	35
Figure 5.6	Measured and modelled water level comparisons at site W2.	36
Figure 5.7	Modelled (SELFE) and measured velocity comparisons within Zone A (Figure 5.2) for the peak ebb (upper) and flood (lower) tidal stages.	37
Figure 5.8	Modelled (SELFE) and measured velocity comparisons within Zone B (Figure 5.2) for the peak ebb (left) and flood (right) tidal stages.	38
Figure 5.9	Modelled (SELFE) and measured velocity comparisons within Zone C (Figure 5.2) for the peak ebb (left) and flood (right) tidal stages.	39
Figure 5.10	Quantile – Quantile plots of the measured and modelled (SELFE) peak tidal ebb and flood current speed (m/s) along the vessel tracks within zones A and B for both peak ebb and flood stages. The root mean squared errors corresponding to the different distributions are presented in the top-left corner of each plot.	40
Figure 6.1	Delft3D – FLOW model grid (right) and depths (left).	45
Figure 6.2	Delft3D – WAVE model grids for the modelling of the wave spectral transformation from the offshore region to the coast. The BND position indicates the site used to extract the wave climate described in Section 6.3.1.	46
Figure 6.3	Comparison of the best tide, pure M2 tide, 1.1 M2, 1.2 M2 and 1.3 M2 tide curves at the harbour entrance.	47

Figure 6.4	Scatter plot of wave heights as a function of wave directions for the 10-year time series, with delimitation of bins (red boxes). Red dots are the representative conditions of each bin.....	49
Figure 6.5	Reduced average annual wave climate based on the 10-year wave hindcast using four directional bins and four wave height bins (i.e. 16 wave classes). Colours indicate the probability of occurrence of a given class. The white dots are the representative wave condition of each wave class. Wave classes are summarised in Table 6.1.	49
Figure 6.6	Time series of significant wave height and peak direction at location BND (see Figure 6.2) for December 2014 and January 2015. Wave conditions during periods 1) and 2) were used to simulate the sediment transport at Whangarei Harbour during fair-weather and storm conditions.	51
Figure 6.7	Bed stratigraphy approach implemented in Delft3D to initialise the bed composition over the domain.	53
Figure 6.8	Modelled (Delft3D) and measured velocity comparisons within Zone A (Figure 5.2) for the ebb (upper) and flood (lower) tidal stages.....	54
Figure 6.9	Modelled (Delft3D) and measured velocity comparisons within Zone B (Figure 5.2) for the ebb (left) and flood (right) tidal stages.....	55
Figure 6.10	Modelled (Delft3D) and measured velocity comparisons within Zone C (Figure 5.2) for the ebb (left) and flood (right) tidal stages.	56
Figure 6.11	Quantile – Quantile plots of the measured and modelled (Delft3D) peak tidal ebb and flood current speed (m/s) along the vessel tracks within Zones A and B for both peak ebb and flood stages. The root mean squared errors corresponding to the different distributions are presented in the top-left corner of each plot.....	57
Figure 7.1	Sources of a dredge plume for a Trailing Suction Hopper Dredger: 1-Drag Head, 2-Overflow, 3-Propeller wash (after Becker J. et al., 2015).....	63
Figure 7.2	Percentages of sediment transferred from the near-field density driven plume to the far-field plume during overflowing	64
Figure 7.3	Source of a dredge plume for a Backhoe Dredger (after Becker et al., 2015).	65
Figure 7.4	Source of a dredge plume for a Cutter Suction Dredger (after Becker et al., 2015).....	66
Figure 7.5	Simulated release sites along the dredged channel. Existing depth and depth changes are provided in Table 7.2. Geographic coordinates are presented in Appendix B.	69
Figure 8.1	Three main phases occurring during the disposal of dredged material: 1) convective descent, 2) dynamic collapse, and 3) passive plume dispersion.	72
Figure 8.2	Percentages of sediment transferred from the near-field density driven plume to the far-field plume.	73
Figure 8.3	Location of the sites over the disposal ground used for the release of particles as part of the disposal plume modelling. The green polygon indicates the contour of a reef classified as sensitive.	75
Figure 9.1	Bathymetry and Delft3D – FLOW model grid for the proposed disposal ground modelling.	77
Figure 9.2	Delft3D –WAVE model grid for the proposed disposal ground modelling. Location (BND) for representative wave climate is shown at the centre of the eastern boundary.....	78

LIST OF TABLES

Table 2.1	Comparison between measured and hindcast wind data. Accuracy measures for wind speed and direction at Marsden Point (1979-1990).	10
Table 3.1	Boundary, resolution and limits defined for each SWAN nest.	14
Table 3.2	Measured wave data sources used for the hindcast validation.	18
Table 4.1	ROMS model nests configurations.	23
Table 4.2	Details of the current measurement program undertaken in Bream Bay from January to July 2016.	26
Table 6.1	Wave classification based on an average annual wave climate defined from a 10-year hindcast.	50
Table 7.1	Representative median grain sizes, settling velocities, and proportions of total volume released for the 3 discrete sediment classes considered.	62
Table 7.2	Depths and depth changes of release sites along the dredged channel.	68
Table 8.1	Details of the dredging vessels likely to be used for dredging and disposal works.	73
Table 8.2	Source terms and release depths.	73
Table 8.3	Summary of simulation periods.	75

1. INTRODUCTION

Refining NZ (RNZ) is investigating options for the deepening and the realignment of the shipping channel leading to the Marsden Point Refinery at the entrance to Whangarei Harbour. Increasing the navigable depth is necessary to allow vessels with increased draft to safely transit to the refinery. MetOcean Solutions Ltd (MSL) has been contracted to provide coastal oceanographic expertise and investigate the potential effects of channel deepening on the physical environment. The scope of work includes i) an evaluation of the wave, hydrodynamic and sediment dynamic regime throughout the Whangarei Harbour entrance region, ii) consideration of the effects of capital dredging on this environment, iii) potential effects on the coastal sediment budgets, iv) the stability of the adjacent beaches and the sub-tidal delta, and v) the effects of dredging and disposal on water quality in the receiving environment. A flow chart of the study processes is shown on Figure 1.1, and a map of Whangarei Harbour with the different locations referred to in the study is presented in Figure 1.2. Figure 1.3 presents a map showing the location of the proposed deepening. The location of the proposed disposal grounds for the placement of capital and maintenance volumes is shown in Figure 1.4.

The study investigations are presented in two reports:

- The present report is a technical reference document that details the establishment of numerical models for wind, wave, current and sediment dynamics, and the data collection program that was undertaken to support the model establishment and to validate the numerical schemes.
- The second report (MSL Report P0297-02) first characterises the existing environment and then investigates the likely physical effects of the Crude Shipping Project.

We recommend that the two reports be read together, in order to gain a complete understanding of our assessment approach and findings.

1.1. Report structure

The numerical modelling approach applied to characterise the regional wind and wave climate in the study area, is described in Sections 2 and 3 respectively, including validation against contemporary wind and wave data. Sections 4 and 5 explain the regional and nearshore hydrodynamic modelling techniques and present validations of the models used. Section 6 outlines the nearshore and harbour channel sediment transport modelling methods. The plume modelling approach used to consider the effects of dredging and disposal is detailed in Sections 7 and 8, respectively. The methods used to estimate the sediment transport from the preferred offshore disposal ground is provided in Section 9. An executive summary is presented at the beginning of the report.

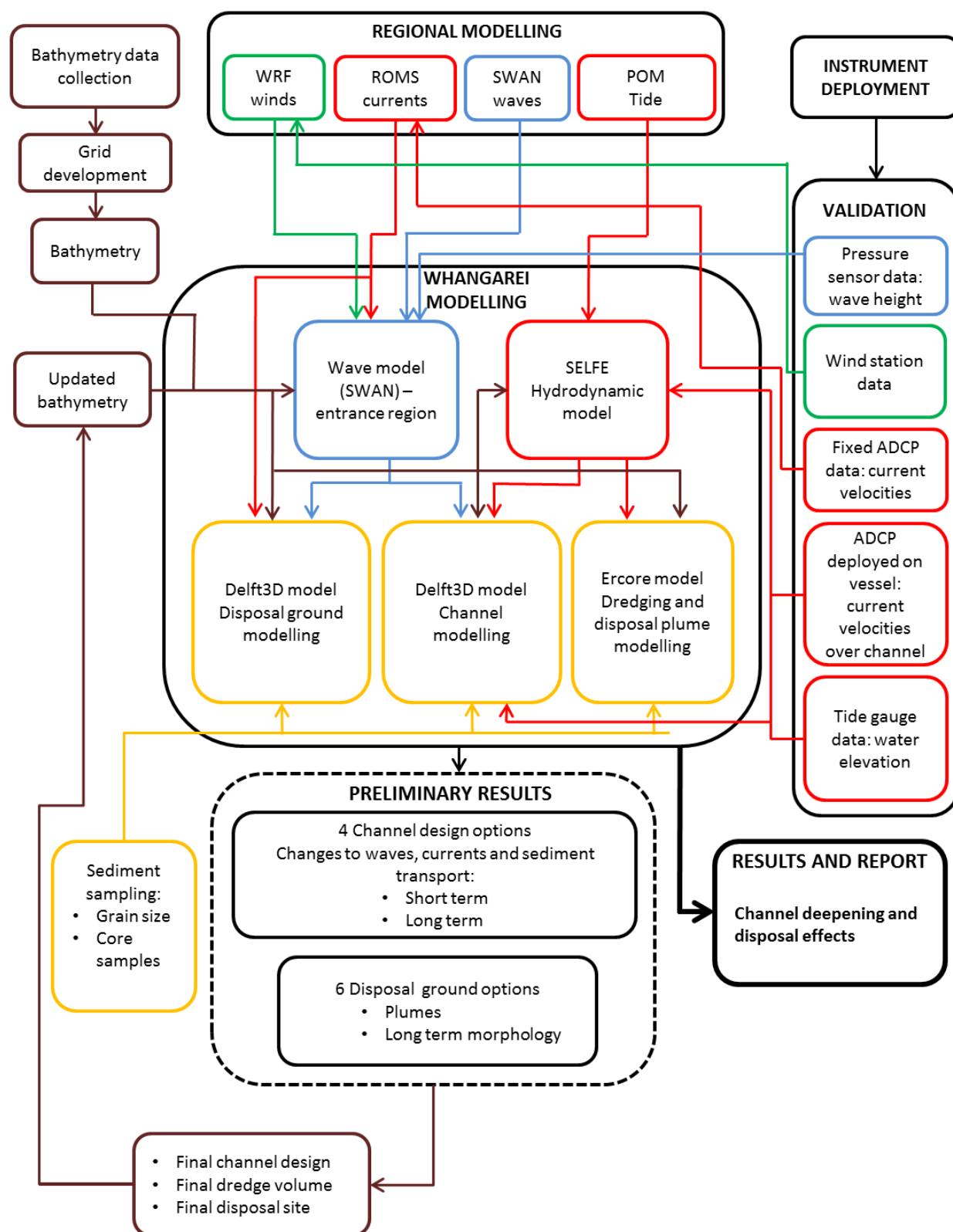


Figure 1.1 Flow chart showing the numerical modelling process for the study. Red lines indicate hydrodynamics; blue indicates waves; green indicate wind and yellow lines indicates bathymetry.

1.2. Study area

The different locations referred in the present report for the validation process and the description of the effect of the deepening channel on the coastal dynamics at Whangarei Harbour (MSL Report P0297-02) have been summarised in Figure 1.2.



Figure 1.2 Maps of Whangarei Harbour (top) and its entrance (bottom) with the locations used in the present study for the establishment of the numerical models and the description of the effect of the channel deepening on the coastal dynamics.

1.3. Proposed channel deepening design

RNZ commissioned Royal Haskoning DHV (RHDHV) to define an optimal navigation channel design, including the associated dredging requirements, in order to provide high water access for vessels with increased draft to safely transit to the RNZ Crude Jetty.

Different options for the channel design (RHDHV Shipping Channel - Concept Design Report, Royal HaskoningDHV, 2016a) were provided and discussed with RNZ. An Under Keel Clearance study was completed by OMC in the OMC International (2016) - Mardsen Point Channel Optimisation report, based on the channel designs provided by RHDHV and the long period wave analysis performed by MSL. Further assessment of the channel was undertaken from a navigation perspective (RHDHV Report - Desktop Simulation Study, Royal HaskoningDHV, 2015). The Option 4.2 was the stated preferred option from a channel design perspective and was confirmed via the alternative assessment work presented in Tonkin and Taylor (2016a).

For the present study, Option 4.2 has been adopted as the design case for the numerical modelling. Details about the characteristics of the proposed channel and corresponding dredging requirements are described in Royal HaskoningDHV, 2016b, as part of the dredging methodology assessment provided by RHDHV to RNZ.

An overview of the proposed channel design (Option 4.2) and the resultant differences between existing and post-dredging bathymetries are shown on Figure 1.3 based on the depth datasets used by MSL to setup the model water depth.

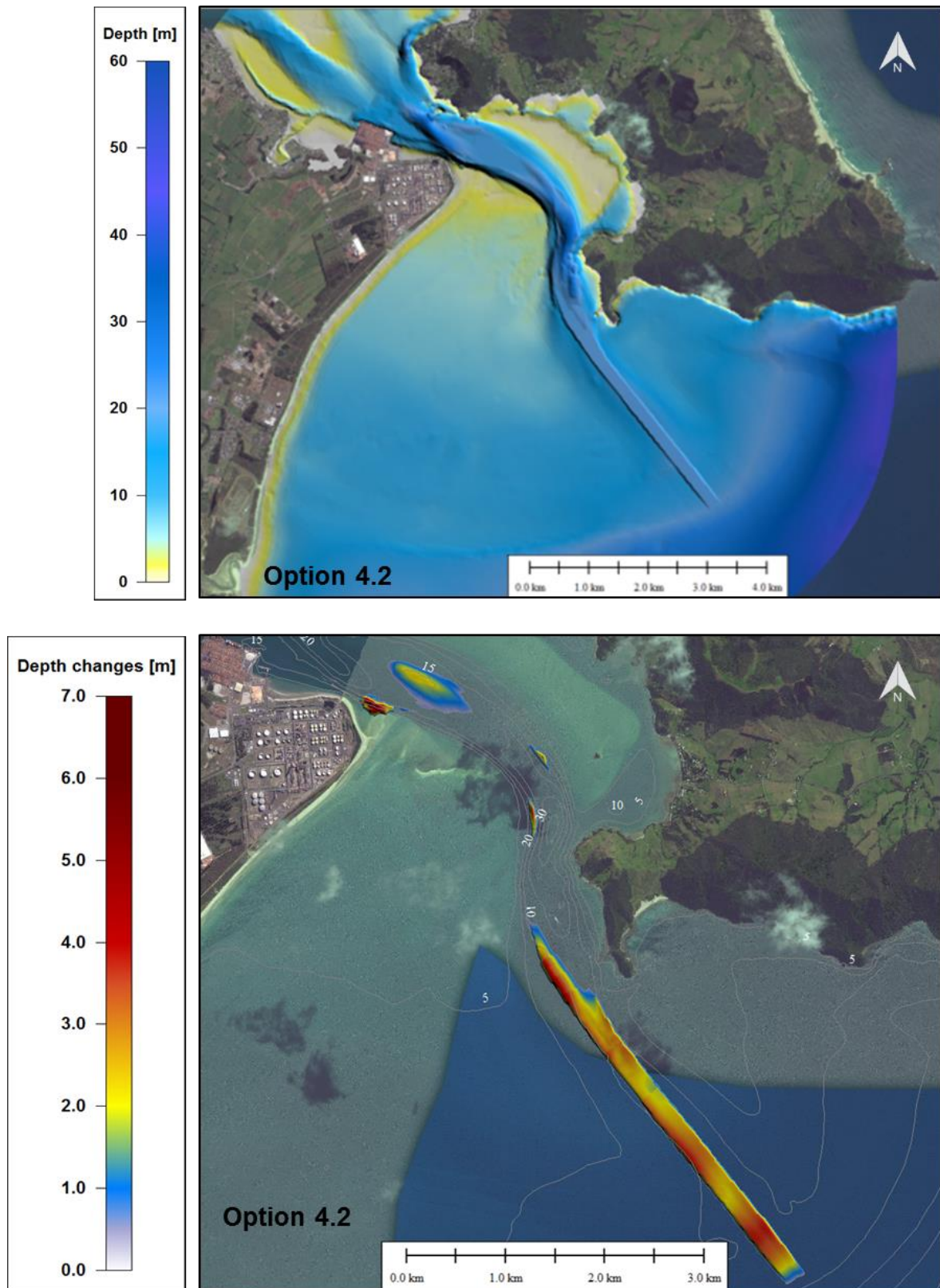


Figure 1.3 Depths (upper plot) and depth differences (lower plot) between the Option 4.2 channel design and the existing channel configuration. Positive amplitudes indicate a deepening of the channel.

1.4. Proposed offshore disposal ground designs

In consultation with Royal HaskoningDHV, Tonkin + Taylor, and MetOcean Solutions, as well as expert consultants from a range of other disciplines, the client went through a selection process which led to the identification of the preferred locations to dispose the capital and maintenance dredge volumes from the Crude Shipping Project. That process is described in the Tonkin and Taylor report (2016). In this context, two offshore disposal sites have been identified by RNZ as potential options for the disposal of capital and maintenance volumes (see Figure 1.4):

- Disposal Site 1.2 (yellow polygon) is located over the south-western flank of the tidal delta where depths range between 2 and 10 m. Its distance from Ruakaka Beach and Busby Head is approximately 2 km and 1.6 km, respectively. This disposal site is considered by RNZ as the preferred option for the placement of maintenance volume and up to 5% of the capital dredging volume, and the site has therefore been investigated in the present study.
- Disposal Site 3.2 (red polygon) is an area measuring approximately 2 km², which ranges in depth from 41 to 48 m. This option for the disposal of capital and maintenance volumes is located approximately 3.5 km to the South of Bream Head and 700 m to the east of 3 Mile Reef. Its distance from Busby Head and the inlet entrance is approximately 7 km. This disposal site is considered the preferred option for the placement of up to 95% of the capital volume and up to 100% of the maintenance volume by RNZ and the area was therefore investigated in the present study

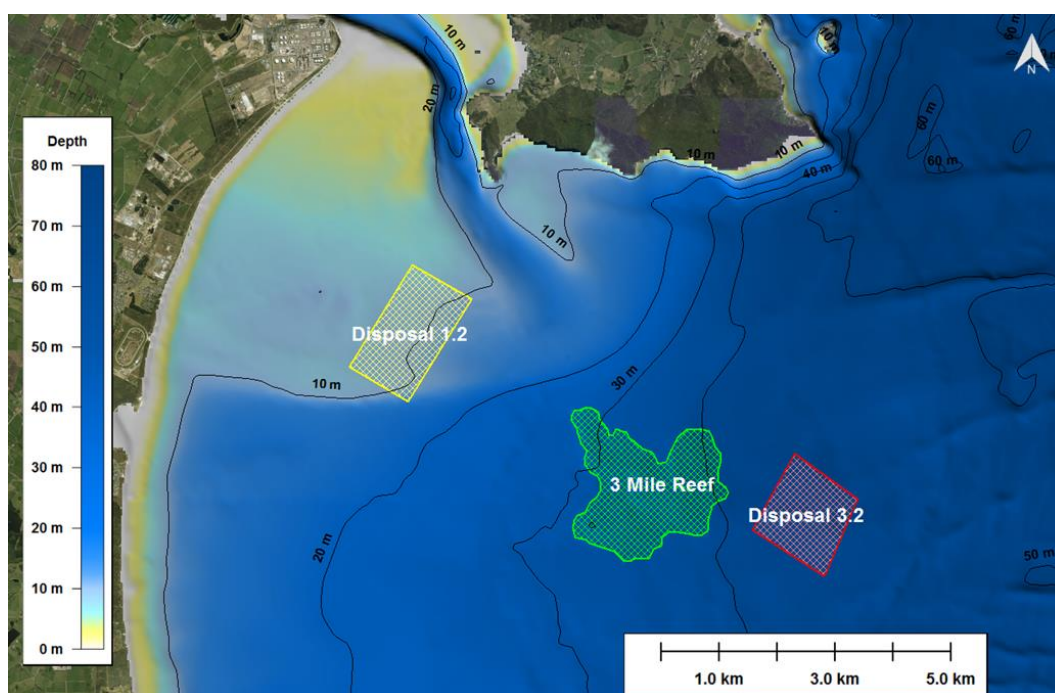


Figure 1.4 Location of Disposal grounds 1.2 and 3.2 (indicated by coloured diagonal cross-hatch polygons) for the disposal of capital and maintenance volumes. 3 Mile Reef indicated by a green polygon is a sensitive reef for its benthic encrusting communities.

1.5. Additional Northport berth

Additionally, the numerical modelling considered the existing Northport facilities, including Berths 1-3. It has also taken into account unimplemented resource consents held by NorthPort in respect of an additional proposed berth, known as Berth 4 (there are a series of consents issues by Northland Regional Council relating to the reclamation, construction, and use of Berth 4, primarily those consents numbered CON20030505523). As required pursuant to the RMA, the modelling included Berth 4 (see reclaim area in Figure 1.5) as if those resource consents had been given effect to as part of the “existing environment”.



Figure 1.5 Satellite image showing the NorthPort Berth4 reclaim area included in the hydrodynamic model bathymetry.

2. WIND MODELLING

The numerical modelling of the atmospheric dynamics at Whangarei was undertaken by MSL to provide the wind conditions required to force the regional hydrodynamic and wave models presented in Sections 3 and 4.

2.1. Model approach

The near-surface wind field was prescribed by a 36-year (1979-2014) regional atmospheric hindcast carried out by MSL. The WRF (Weather Research and Forecasting) model was established over all of New Zealand at hourly intervals and at approximately 12 km resolution. The hindcast was specifically tuned to provide appropriate marine wind fields for metocean studies around the country. The WRF model boundaries were sourced from the CFSR (Climate Forecast System Reanalysis) dataset distributed by NOAA, which was available at hourly intervals and 0.31° spatial resolution. While the WRF hindcast produced atmospheric parameters at hourly intervals over the 36 years, only the near surface wind field (i.e. 10 minute mean at 10 m elevation) is used here.

2.2. Model validation

Validation of the WRF hindcast was undertaken at the Marsden Point wind station situated at 35.840 S, 174.487 E (WGS84) as shown in Figure 2.1. Wind data were recorded at approximately 10 m elevation above mean sea level between 1979 and 1990.

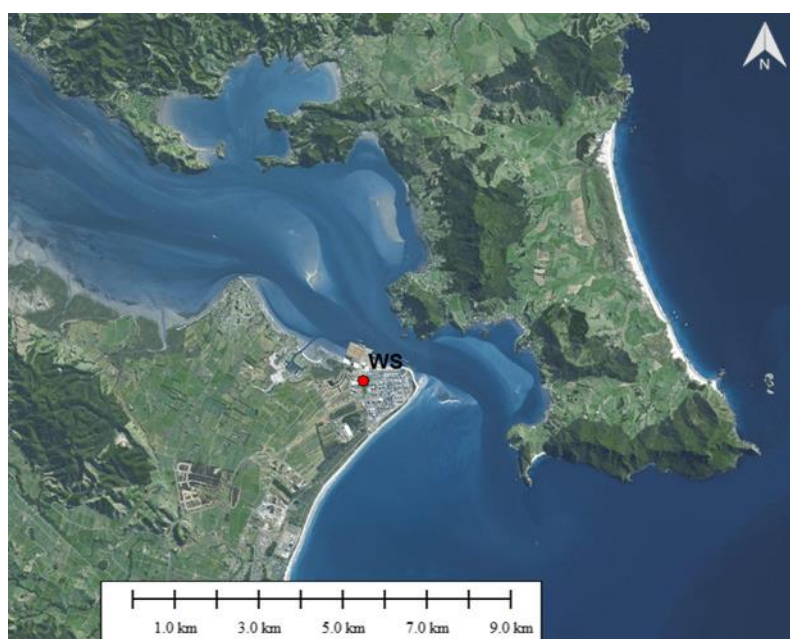


Figure 2.1 Location of the wind station (red circle) at Marsden Point. Geographic coordinates are provided in Appendix A.

The quantitative validation shows the model to exhibit a reasonable correspondence with the measured data (

Table 2.1). The hindcast wind speed was biased slightly high (0.59 ms^{-1}). The time series of measured and hindcast wind speed and direction are provided in Figure 2.2 and Figure 2.3 respectively, while the scatter and quantile-quantile (Q-Q) plots

for the wind speed validation are presented in Figure 2.4. These figures illustrate the good consistency between the measured and hindcast wind speed data.

The comparison between modelled and measured annual wind roses at Marsden Point shown on Figure 2.5 indicates that the model realistically replicates the regional coastal wind climate, albeit with a relative low bias of approximately 0.7 m.s⁻¹ in speed and 11 degrees in direction, and illustrates that it does not include the influence of the local topography on the micro-scale wind regime. The topography of Mount Mania, Whangarei Heads, Bream Head and Ruakaka Forest creates wind corridors over some areas and provides sheltering for others; these are not fully replicated in the model given the resolution of the model grid is only 12 km. This spatial variability of the wind fields onshore is not expected to significantly affect the wave and current generation over the study area. On Figure 2.6, the distribution of wind directions are shown as histograms instead of Q-Q plots, which is more suitable for directional comparisons. The predominance of winds incoming from the SW sector is consistent between the measured and hindcast data, and the northeast and east sector winds are also relatively well replicated by the hindcast.

In summary, the model adequately replicates the regional wind dynamics, and it was therefore assessed that it is suitable for the forcing of the hydrodynamic and wave models.

Table 2.1 Comparison between measured and hindcast wind data. Accuracy measures for wind speed and direction at Marsden Point (1979-1990).

Parameter	Wind speed	Wind direction
MAE	1.92 ms ⁻¹	31 deg.
RMSE	2.44 ms ⁻¹	44 deg.
MRAE	0.59	0.31
BIAS	0.67 ms ⁻¹	-11 deg.
Scatter Index	0.47	0.22

$$\text{Mean absolute error (MAE):} \quad \overline{|x_h - x_m|} \quad (2.1)$$

$$\text{Root Mean Square Error (RMSE):} \quad \sqrt{\overline{(x_h - x_m)^2}} \quad (2.2)$$

$$\text{Mean absolute relative error (MRAE):} \quad \overline{\left| \frac{x_h - x_m}{x_m} \right|} \quad (2.3)$$

$$\text{Bias:} \quad \overline{x_h - x_m} \quad (2.4)$$

Scatter Index (SI):
$$\frac{\sqrt{(x_h - x_m)^2}}{x_h} \quad (2.5)$$

Where h and m indicate hindcast and measured data, respectively.

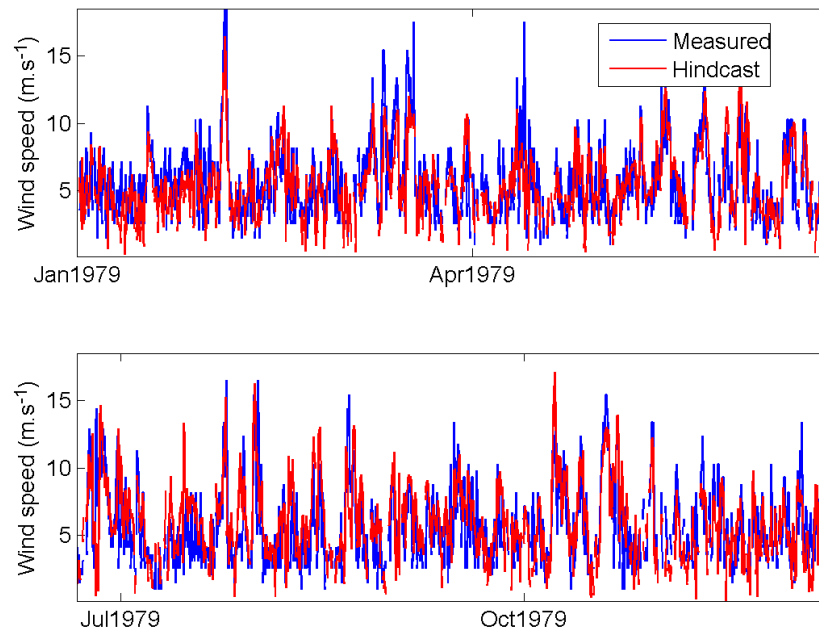


Figure 2.2 Time series plot of the measured and hindcast wind speed and wind direction at Marsden Point (year 1979). Note only a portion of the 12 years of data used for validation is shown here for better visualisation.

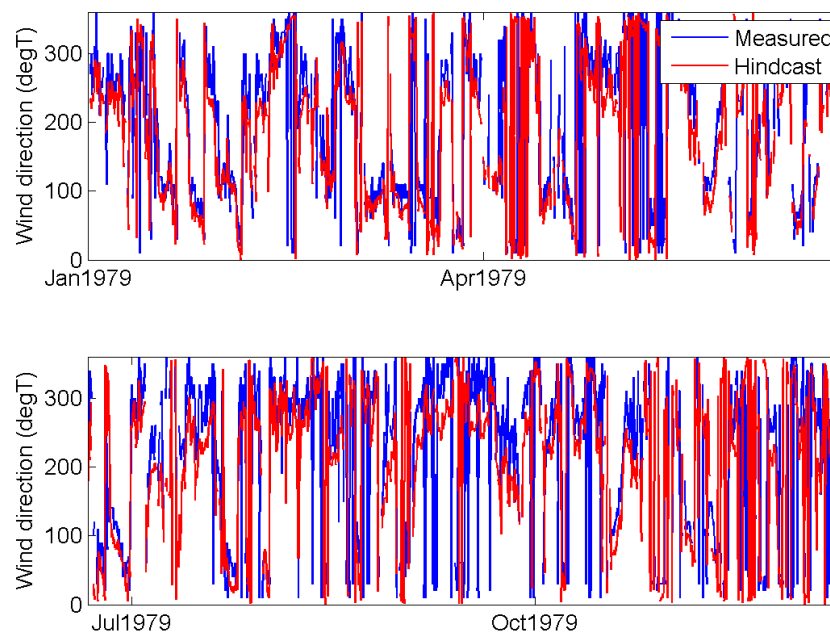


Figure 2.3 Time series plot of the measured and hindcast wind direction at Marsden Point (year 1979). Note only a portion of the 12 years of data used for validation is shown here for better visualisation.

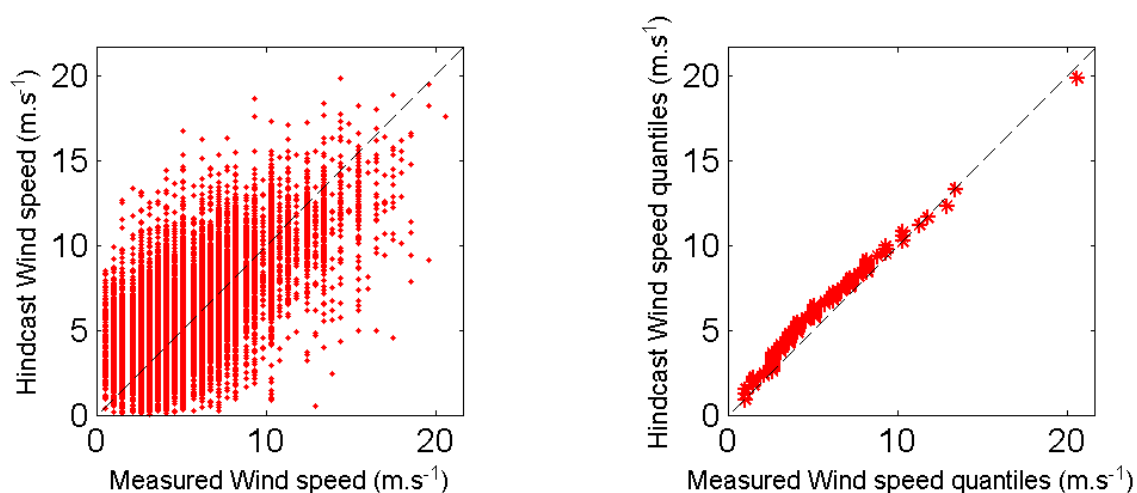


Figure 2.4 Scatter and Quantile-Quantile plots of the measured and hindcast wind speed at Marsden Point (1979-1990). Also shown are the lines of equivalence.

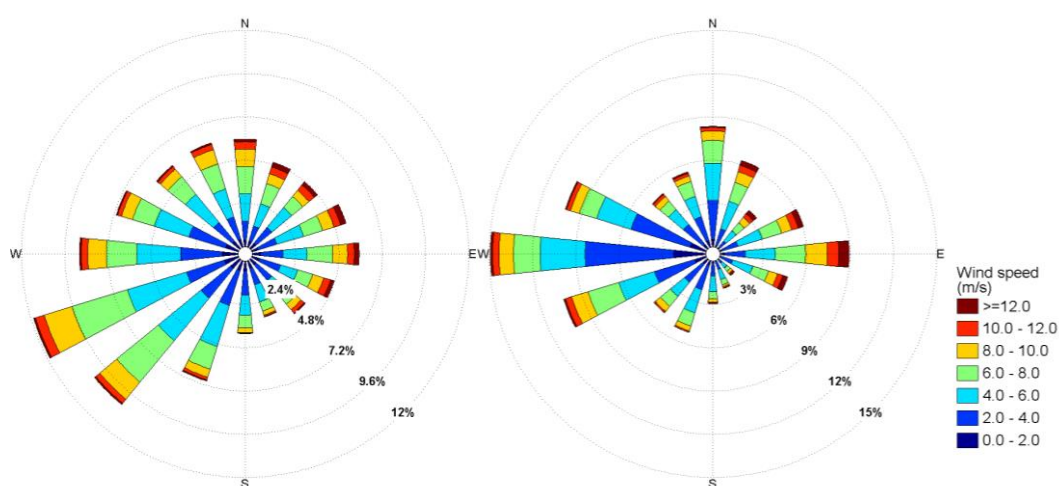


Figure 2.5 Modelled (left) and measured (right) annual wind rose at position WS shown on Figure 2.1. Geographic coordinates of this location are provided in Appendix A.

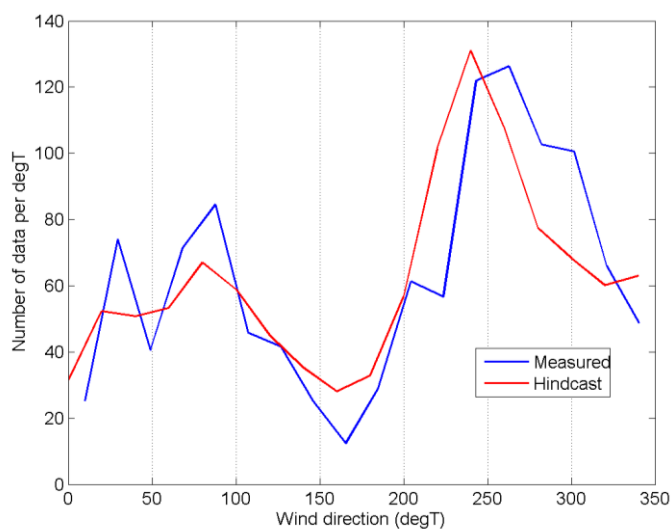


Figure 2.6 Histograms of measured and hindcast wind directions at Marsden Point (1979-1990).

3. WAVE MODELLING

This section details the numerical wave hindcast modelling used to characterise the regional wave climate as well as the nearshore wave transformations from offshore and into the harbour entrance.

3.1. Model approach

3.1.1. Model description

A modified version of SWAN¹ (Simulating Waves Nearshore) was used for the hindcast wave modelling for the project. The wave hindcast extended over a 36-year period between 1979 and 2015.

SWAN is a third generation ocean wave propagation model which solves the spectral action density balance equation for wavenumber-direction spectra. This means that the growth, refraction, and decay of each component of the complete sea state, each with a specific frequency and direction, is solved, giving a complete and realistic description of the wave field as it changes in time and space. A detailed description of the model equations, parameterisations and numerical schemes can be found in Holthuijsen (2007) or the SWAN documentation². Physical processes that are simulated include the generation of waves by surface wind, dissipation by white-capping, resonant nonlinear interaction between the wave components, bottom friction and depth limited breaking. All 3rd generation physics are included. The BYDRZ physics package developed for WW3 model, which accounts for the effects of full air flow separation and therefore relative reduction of the input at strong wind forcing, was implemented in SWAN and used for the hindcast. The Collins (1972) friction scheme was used for wave dissipation by bottom friction.

The solution of the wave field is found for the non-stationary (time-stepping) mode. Boundary conditions, wind forcing and resulting solutions are all time dependent, allowing the model to capture the growth, development and decay of the wave field.

3.1.2. Pertinence of the model for the present study

The SWAN model was selected in the present study for its unconditionally stable numerical scheme and its ability to accurately reproduce the wave spectral transformations from deep to shallow water regions over complicated nearshore bathymetry. SWAN is considered the most suitable tool to compute the offshore-to-nearshore transformation of wave fields. Other types of models, notably non-hydrostatic or Boussinesq-type phase resolving time-domain models have a more complete description of the (nonlinear) wave transformation and resolve the wave shape, but are impractical to apply over large domains and/or over long-term periods.

SWAN has widely been applied all over the world in many coastal wave studies and successfully validated against measured data. Dodet (2013) investigated the wave-current interactions in a wave-dominated tidal inlet (Albufeira Lagoon) and showed that SWAN was able to faithfully represent the wave dynamics at the seaward entrance of the delta and within the inlet. The authors of that study used a three-level nested design structure within SWAN forced by WW3 spectra outputs

¹ Modified from SWAN version of the 40.91 release (publicly available code)

² http://swanmodel.sourceforge.net/online_doc/online_doc.htm

and coupled with a high-resolution hydrodynamic model. This corresponds to the same approach applied in the present study of the entrance to Whangarei Harbour.

3.1.3. Model domain and boundary conditions

The wave hindcast involved three-level SWAN downscaling to model the nearshore region at approximately 50 m resolution. Full spectral boundaries for the parent domain were prescribed from MSL implementation of WW3 global wave model (Tolman, 1991) with the Tolman and Chalikov (1996) physics.

The limits and resolutions for each SWAN nest are shown in Table 3.1 and Figure 3.1. The parent domain was forced with full spectral boundaries from WW3 and provided boundaries to run a first SWAN child at 0.0015 degree. A second child nest with about 50 m resolution was defined to resolve the complex bathymetric features near the shore. All nests were configured with 24 frequency bins (logarithmic scale from 0.04 to 0.66 Hz) and 36 directional bins. SWAN was run with wind fields specified from the MSL WRF New Zealand reanalysis.

Table 3.1 Boundary, resolution and limits defined for each SWAN nest.

Domain	Boundary	Longitude (degree)			Latitude (degree)		
		x1	x2	dx	y1	y2	Dy
Parent	WW3	174.45	176.15	0.009	-37.23	-35.23	0.009
Child 1	Parent	174.451	174.8	0.0015	-36.04	-35.8	0.0015
Child 2	Child 1	174.458	174.558	0.0005	-35.925	-35.825	0.0005

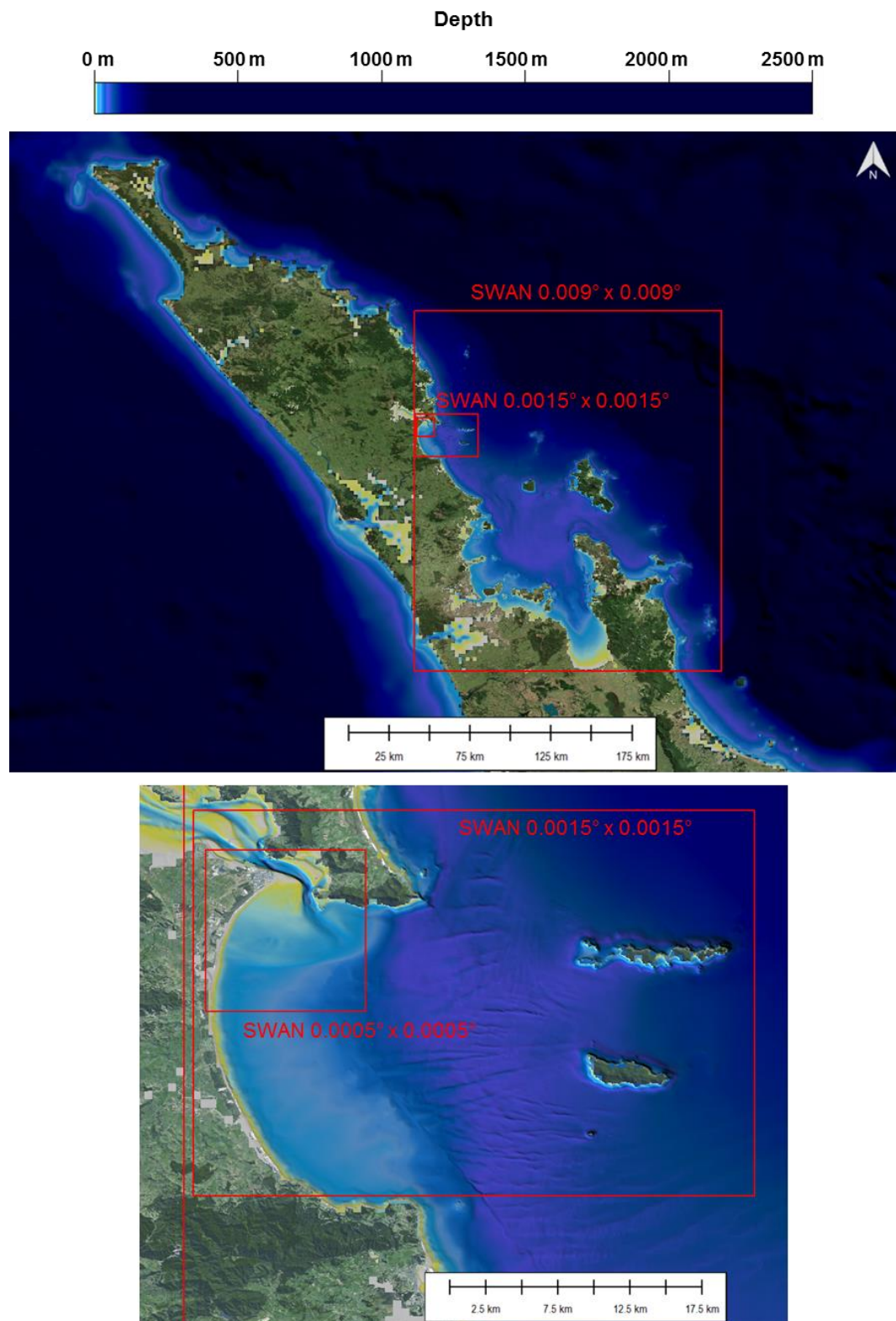


Figure 3.1 Water depth and model domains used to reproduce the spectral wave transformation from offshore to nearshore. The geographical extent of each domain is shown by the red rectangles.

3.1.4. Post-processing

Two-dimensional frequency-direction wave spectra were output at hourly intervals from the highest resolution SWAN domain at four nearshore. The spectra were post-processed to calculate wave statistics for the total wave field, as well as for sea and swell components. One – dimensional frequency spectra, spectral moments, significant wave height, mean direction at peak frequency and peak wave period were calculated based on the equations provided below:

- One-dimensional frequency spectra:

$$S_n(f) = \int_{-\pi}^{\pi} E_n(f, \theta) d\theta \quad (3.1)$$

- Spectral moments were calculated as:

$$m_x = \int \int f^x E(f, \theta) df d\theta \quad (3.2)$$

- Significant wave height , mean direction at peak frequency and peak wave period defined as:

$$H_s = 4\sqrt{m_0} \quad (3.3)$$

$$Dpm = \tan^{-1} \frac{\int_{-\pi}^{\pi} E(f_p, \theta) \sin\theta d\theta}{\int_{-\pi}^{\pi} E(f_p, \theta) \cos\theta d\theta} \quad (3.4)$$

$$T_p = \frac{1}{f_p} \quad (3.5)$$

where f_p is the peak wave frequency of the one-dimensional spectra and $E(f_p, \theta)$ is the energy contained in the peak wave frequency band.

- Mean wave periods were defined from the first and second spectral moments as:

$$T_{m01} = \frac{m_1}{m_0}, \quad T_{m02} = \frac{m_2}{m_0} \quad (3.6)$$

- Spectral width parameter was calculated as:

$$S_{we} = \sqrt{\frac{1 - m_2^2}{m_0 m_4}} \quad (3.7)$$

3.2. Model validation

A program of wave measurements was undertaken to validate the nearshore wave transformation model. This involved the deployments of a waverider buoy and pressure sensors. The validation data locations are shown on Figure 3.2 and the observational durations are specified in Table 3.2.

The model wave hindcast was first validated against the offshore waverider buoy (WRB) data to ensure the sequence of hindcast model domains could reproduce the wave boundary conditions to the study area. The second step was to demonstrate the ability of the nearshore model to capture the governing wave dynamics across the ebb tide delta from the nearshore wave data sites (W1 – W4) along Ruakaka Beach (Figure 3.2). Note that the water depth at these nearshore sites ranged from 2.8 to 7 m (see Table 3.2).

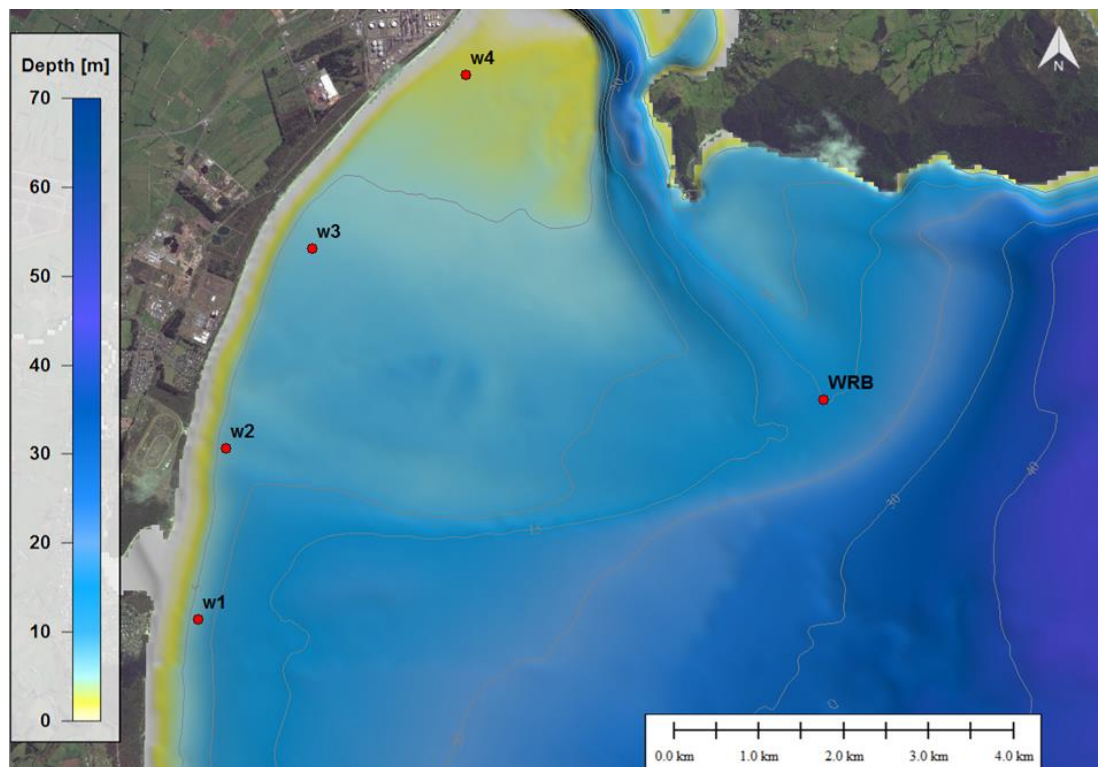


Figure 3.2 Locations of the instruments (red circles) deployed for measuring the wave conditions along Ruakaka Beach and offshore of the entrance.

Table 3.2 Measured wave data sources used for the hindcast validation.

Site name	Water depth (m)	Data coverage
WRB	15.0	continuous
W1	6.9	10/07 to 08/08 2015
W2	7.0	10/07 to 08/08 2015
W3	6.9	10/07 to 08/08 2015
W4	2.8	10/07 to 08/08 2015

3.2.1. Frequency range and accuracy measures

The wave spectra (measured and modelled) at the nearshore sites W1 – W4 were integrated over the 0.04 – 0.25 Hz range, while the entire frequency range was used at site WRB. Co-temporal, co-located wave parameters calculated from the hindcast model and from the measurements were compared directly.

3.2.2. Validation results

Comparisons between measured and modelled significant wave heights (Figure 3.3 and Figure 3.4) at location WRB outside the ebb-tidal delta indicate that the model adequately predicts the time-varying wave conditions. On average the hindcast wave heights were biased slightly high (0.07 m in absolute value) while the hindcast peak wave period was biased slightly low, by about 0.7 s (see Figure 3.5). The model tends to slightly under-predict the wave heights in the range low energy range (Figure 3.4) which could be due to a slight underestimation of the local wind wave growth. Moderate energy swell events (1-2 m in height) are slightly overestimated, which is due to the incident directional spectra from WW3 having a slightly high bias along the east coast of New Zealand.

The hindcast results for the nested inner wave domain, which includes the ebb tide delta and the harbour entrance region, are provided in Figure 3.5 to Figure 3.9. Here the time series of measured and predicted wave heights are co-plotted, showing a general agreement with the time varying conditions and also the gradient in wave energy that decreases with distance to the north along Ruakaka Beach. Site W1 exhibits some anomalous behaviour however, with the model over-predicting the wave height for one event, which is being well replicated at the other sites. Close examination of the model results indicates that strong wave refraction over the ebb tide delta causes zones of high and low wave energy to be distributed along the beach. The location of these zones depends on the incident wave period and wave direction. So, while the hindcast boundary spectra to the inner nest are a very good estimate, it is not a perfect replication of the 2D wave spectra and subtle differences in the incoming wave directionality will be readily expressed in the nearshore results. This is made particularly evident on the ebb tide delta because the waves travel for several km slightly oblique to the bathymetric contours, and therefore refraction effects on the nearshore wave conditions becomes highly evident. The measured and modelled data clearly shows that the shape of the ebb tide delta causes distinct redistribution of the wave energy along the shore, an important finding highlighting the influence of the offshore bathymetry on the nearshore wave conditions.

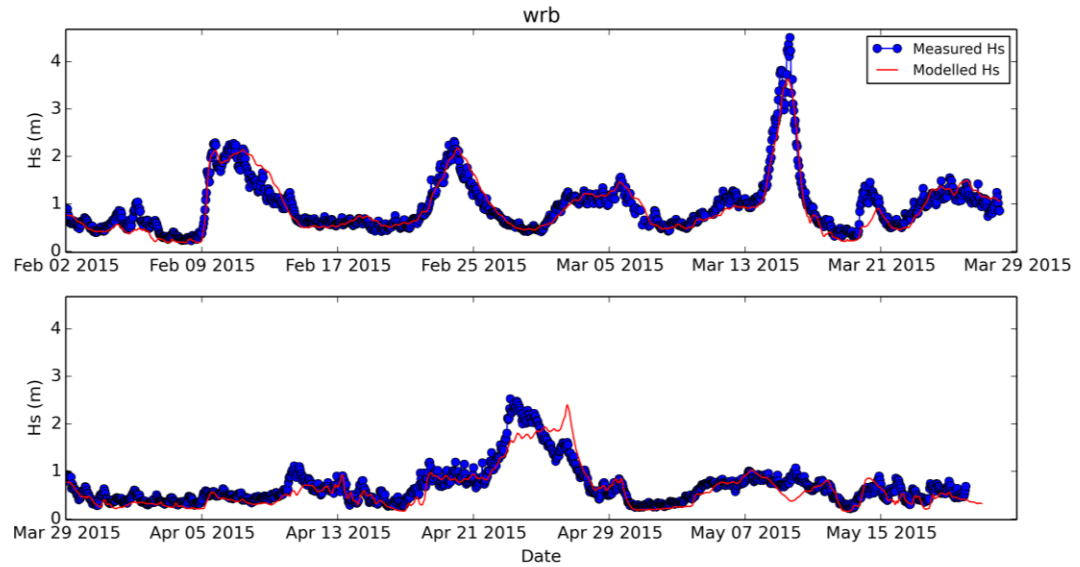


Figure 3.3 Time series of measured (blue) and modelled (red) significant wave height H_s at the WRB site.

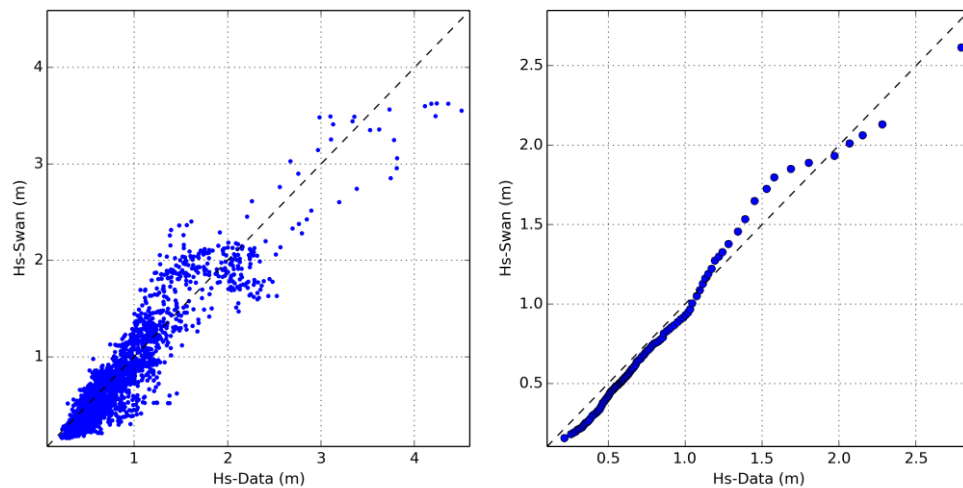


Figure 3.4 Scatter diagram (left) and quantile-quantile plot (right) of measured and modelled significant wave height H_s at WRB site.

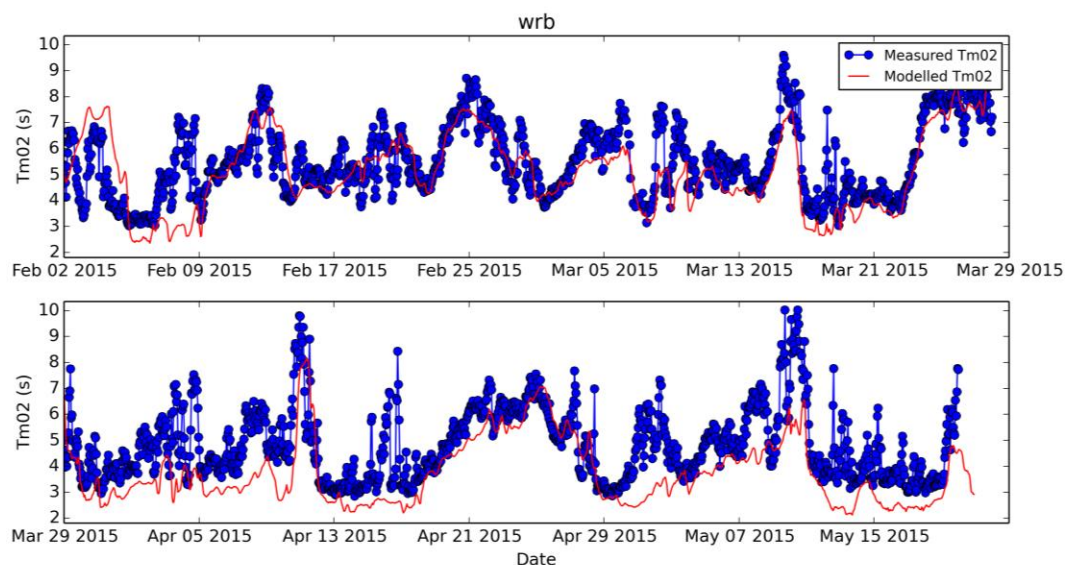


Figure 3.5 Time series of measured (blue) and modelled (red) mean absolute period from the second spectral moment T_{m02} at the WRB site.

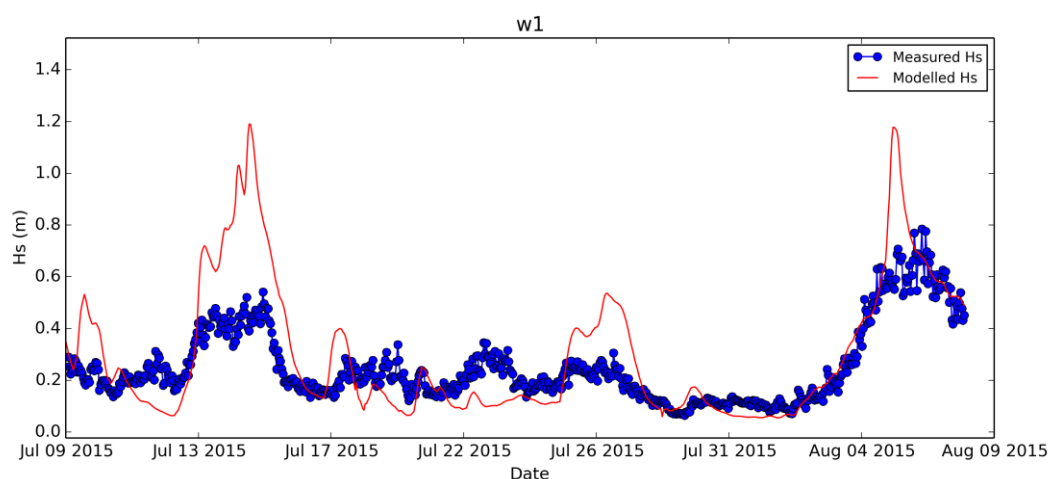


Figure 3.6 Time series of measured (blue) and hindcast (red) significant wave height H_s at site W1.

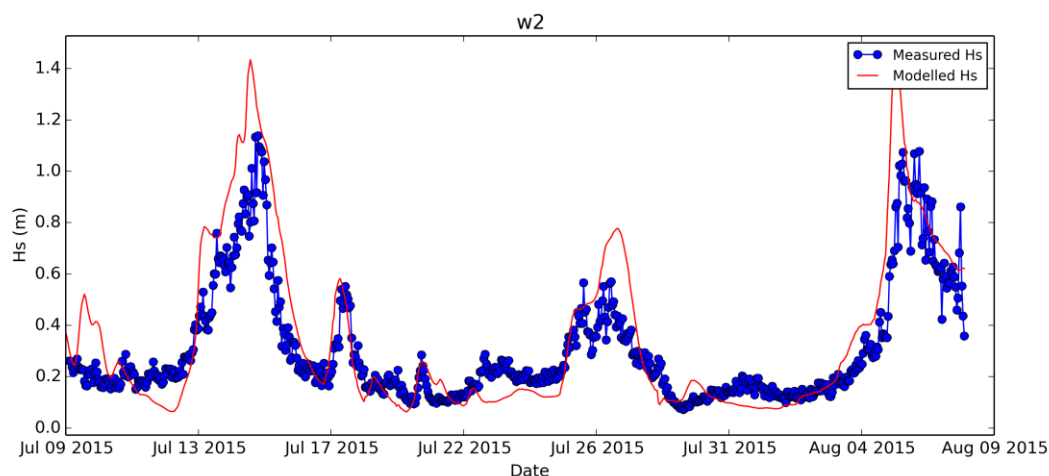


Figure 3.7 Time series of measured (blue) and hindcast (red) significant wave height H_s at site W2.

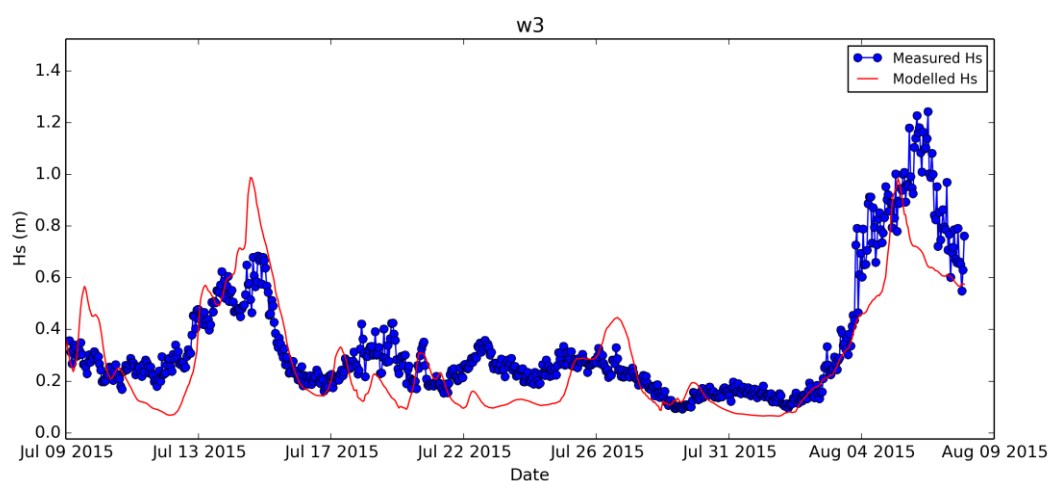


Figure 3.8 Time series of measured (blue) and hindcast (red) significant wave height H_s at site W3.

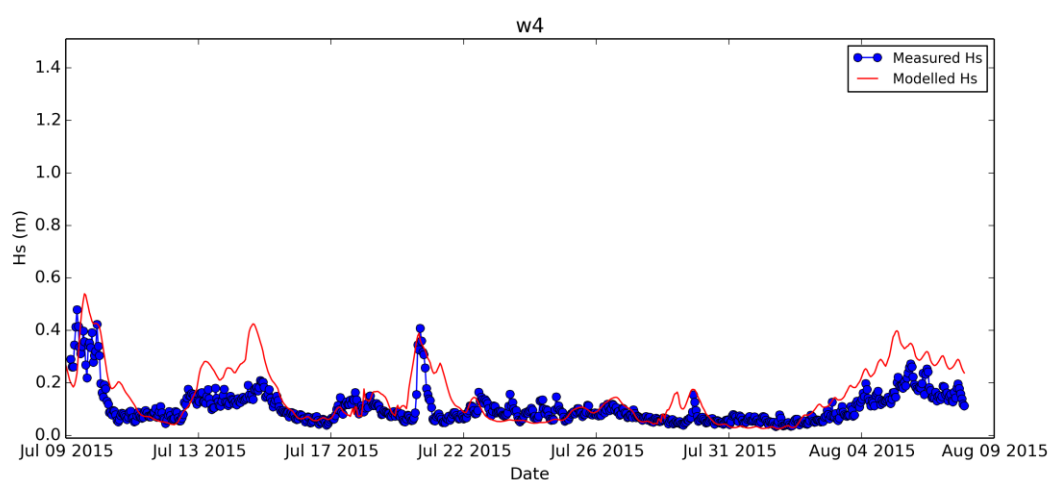


Figure 3.9 Time series of measured (blue) and hindcast (red) significant wave height H_s at site W4.

4. REGIONAL HYDRODYNAMIC MODELLING

Characterising the circulation in the continental shelf waters adjacent to Whangarei Harbour is important when considering the local scale hydrodynamic and sediment transport processes, as it prescribes the boundary conditions for the nearshore and harbour entrance numerical modelling. The presence of strong, along-shelf winds and offshore oceanic boundary currents year round can all play a role in forcing the circulation near the coast. A careful modelling strategy is required to reproduce the different spatial and temporal scales and circulation phenomena at the shelf and deep ocean environments and adequately feed the local scale models. This section describes the modelling studies that were undertaken to characterise regional hydrodynamics.

4.1. Model approach

4.1.1. Modelling description and pertinence of the model

A 10-year hindcast was performed using the ROMS hydrodynamic model version 3.7 (Regional Ocean Modelling System, described in Haidvogel (2008) to characterise the tidal and residual shelf scale circulation regime. The application of the ROMS model at regional scale fully captures the interaction of the wind and tidal circulation with the morphology of the Hauraki Gulf. This modelling tool has been used widely in the scientific and commercial consultancy communities for a wide range of ocean basin at regional and coastal scales.

ROMS has a curvilinear horizontal coordinate system and solves the hydrostatic, primitive equations subject to a free-surface condition. It is a state-of-the-art model widely used for regional and coastal dynamics assessment. Its terrain-following vertical coordinate system results in accurate modelling of shelf seas with variable bathymetry, allowing the vertical resolution to be inversely proportional to the local depth. Besides tidal and wind-driven currents, ROMS resolves frontal structures and baroclinic pressure gradients quite well. Vertical mixing may be resolved by different separate turbulent closure schemes, that are flexible to shallow and deep water dynamics. These features make ROMS particularly well-adapted for the modelling of regional hydrodynamic systems and ROMS is one of the hydrodynamic models most used for regional study applications. It is a modern code which captures sub-, meso- and macro-scale hydrodynamic mechanisms while maintaining robustness, accuracy and numerical stability.

4.1.2. Model domains

The hindcast setup was configured with a three-level nesting (Figure 4.1, top) approach to best transfer the energy gradually from larger to smaller coastal scales, and to properly resolve the flow associated with local and remote forcing, both essential for the resultant currents in the area of interest. The open boundary conditions that were imposed to the highest level nest (NZ) consisted of tri-dimensional velocity, temperature, salinity and sea surface height fields derived from the 6-hourly Climate Forecast System Reanalysis (CFSR) product (Saha et al., 2010) from the National Centers for Environmental Prediction (NCEP), which consisted of a 0.5 degree global reanalysis with comprehensive data assimilation.

The larger scale ROMS nest encompassed the area shown in the lower panel of Figure 4.1 with 7 km horizontal resolution, the goal of which was to absorb the basin scale circulation estimated by the CFSR global reanalysis, thus avoiding a large parent-to-child resolution step. This domain, called NZ hereinafter, was able

to more adequately capture the oceanic circulation and its variability. The second domain (HRKI) covered the entire Hauraki Gulf and continental shelf surrounding the area of interest with a horizontal resolution of 1.7 km. With this grid spacing, the local bathymetry was more accurately captured resulting in fine scale representation of the local coastal currents. The third domain (WHANG) covers the continental shelf near the area of interest with a much higher resolution (350 m), and resolved the detailed, local wind-driven and tidal circulation, producing accurate currents and thermohaline fields to support the subsequent local scale hydrodynamic and sediment models.

The 3D flow and thermohaline fields were transferred from the top level domains to the refined ones by the offline one-way nesting technique commonly used with ROMS.CFSR 3D fields were fed to NZ at 6-hourly intervals and NZ-HRKI and HRKI-WHANG ROMS at 3-hourly intervals.

All ROMS domains were submitted to spin-up phases prior to the 10-year hindcast period to allow the adjustment of the coarser initial conditions to higher resolution and its better represented bathymetry. The spin-up times were hierarchically established according to the main scales that each one was required to resolve. This information, along with all other relevant information for each of the hydrodynamic model domains considered for this study, is summarised in Table 4.1. The bathymetry for the ROMS grids was derived from electronic navigation charts and field data whenever available.

Table 4.1 ROMS model nests configurations.

Model Settings	NZ	HRKI	WHANG
Horiz Resolution	8 km (0.08° x 0.06°)	1.7 km (0.02° x 0.02°)	350 m (0.004° x 0.004°)
Vertical layers	30	19	15
Tidal forcing	No	No	Yes
Meteo forcing	MSL WRF NZRA	MSL WRF NZRA	MSL WRF NZRA

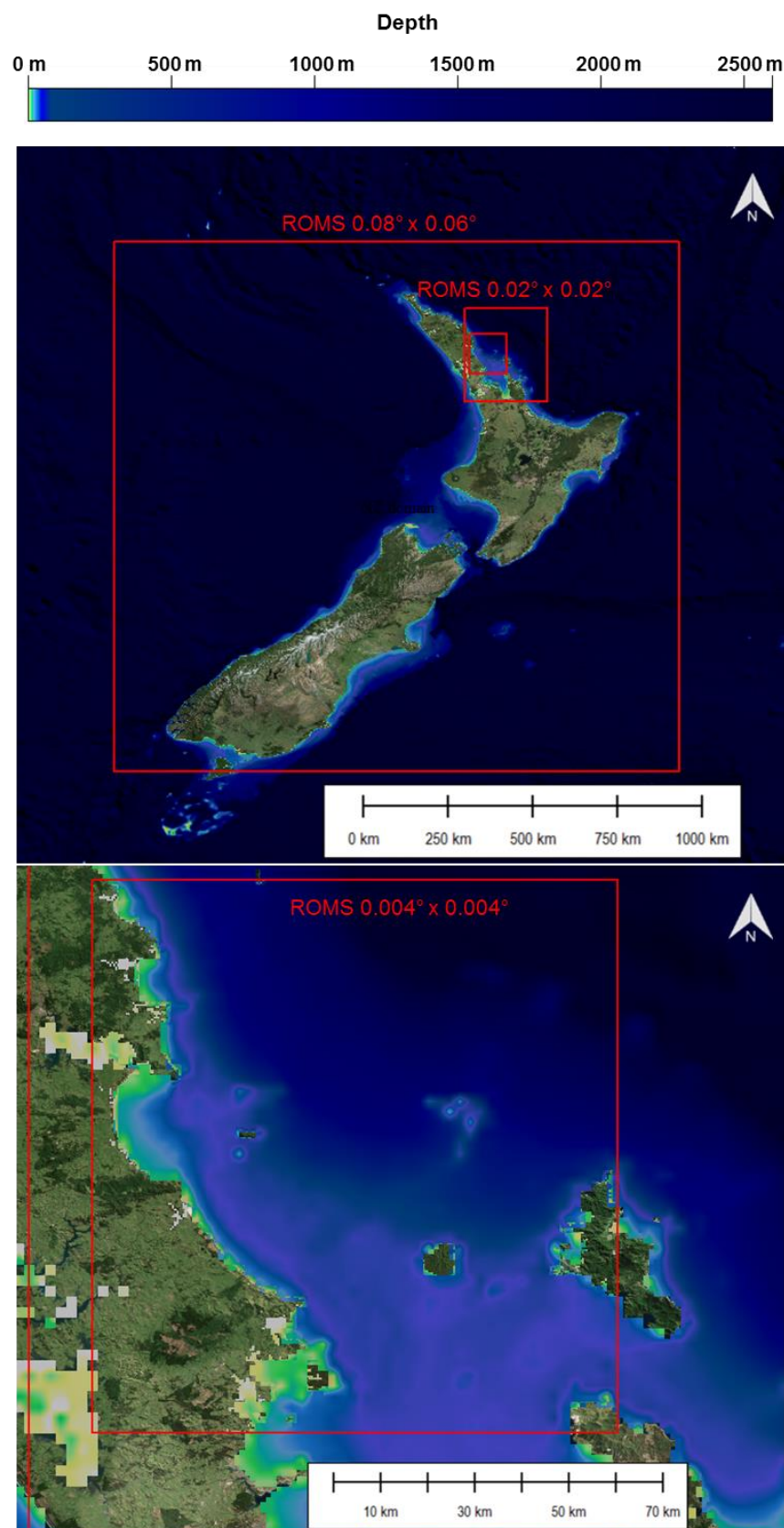


Figure 4.1 Hydrodynamic hindcast modelling approach with ROMS. Upper panel shows the NZ domain, and HRKI domain and lower panel shows the WHANG domain.

4.1.3. Atmospheric forcing

Atmospheric forcing for ROMS was derived from the WRF model outputs described in Section 2. Horizontal resolution varied from 16 to 4 km in the ROMS modelling area. Atmospheric fields consisted of winds, atmospheric pressure, relative humidity, surface temperature, long and short wave radiation and precipitation rate, imposed at hourly intervals to provide air-sea fluxes to drive ROMS in all domains, using a *bulk flux* parameterisation (Fairall et al., 2003).

4.1.4. Open boundary conditions

High frequency (6-hourly for CFSR-NZ and 3-hourly for NZ-HRKI and HRKI-WHANG) open boundary 3D thermohaline, velocity and sea surface height fields were included for all domains. Passive/active prescriptions were applied for all 3D variables at the open boundaries, where a radiation scheme was applied when outflows were estimated by ROMS algorithms. Where inflow was detected, a nudging condition was applied, allowing the penetration of 3D transports and T-S from the external sources, a key setting to guarantee the deep ocean circulation contributions to the smaller scales. To account for the fast propagating tidal oscillations, 2D velocities and surface elevations were treated with *Flather* and *Chapman* schemes, respectively.

4.1.5. Tidal forcing

ROMS WHANG was forced at the open boundaries by tidal elevations and currents, harmonic constituents derived from a MetOcean Solutions' New Zealand 2D hydrodynamic model consisting of a 5 km resolution grid, which was in turn forced at its open boundaries by the renowned OTIS Atlantic Ocean solution (Oregon State University Tidal Inverse Solution (Egbert and Erofeeva, 2002)).

4.1.6. Model calibration

Through comprehensive testing of model parameters such as sub-grid scale parameterisations, forcing sources and grid settings including open boundary locations, spatial resolution and downscaling rate between parent and child grids, the model was calibrated with respect to available published literature and representation of the main identified forcing mechanisms. Numerical diagnosis such as checking kinetic energy equilibrium and trends in the 3D fields were successfully conducted.

4.2. Model validation

4.2.1. Current measurement program

Four ADCP measurement campaigns were undertaken between January and July 2016 at four different locations (see Figure 4.2). For each deployment, the ADCP was installed on the seabed facing upwards and recording data in 5-minute bursts every 30 minutes. The vertical bins ranged between 0.5 and 5 m depending on the water depth at the deployment location. The water depth and period of each deployment are summarised in Table 4.2 while the geographic coordinates of each deployment are provided in Appendix A and time series plots of the depth-average data in Appendix B.

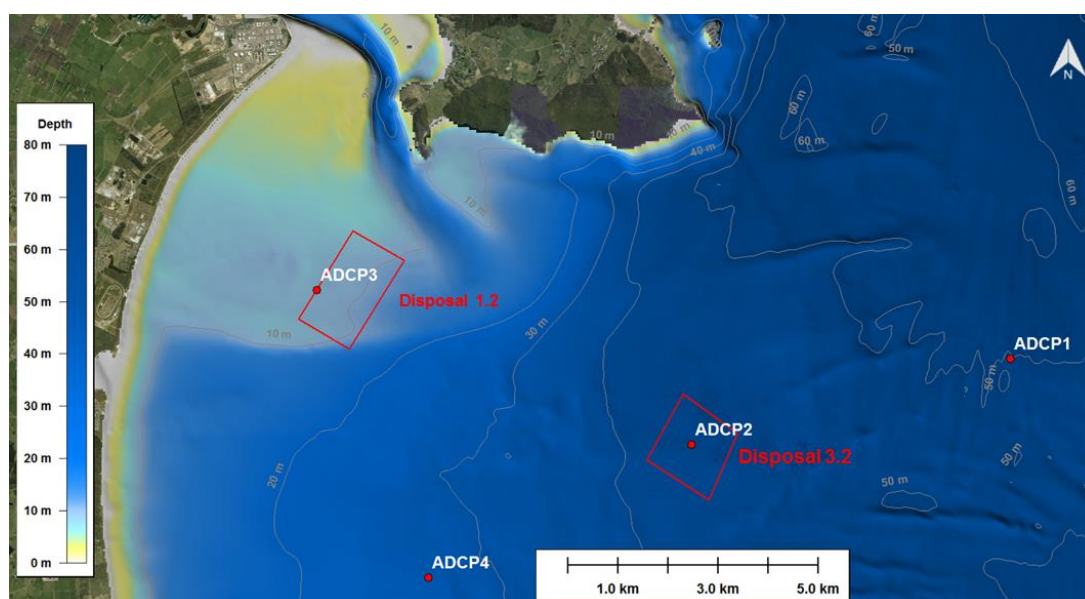


Figure 4.2 Location of the four ADCP deployments in Bream Bay between January and July 2016. The geographic coordinates of each position is presented in Table 4.2. Also shown are the proposed disposal grounds 3.2 and 1.2.

Table 4.2 Details of the current measurement program undertaken in Bream Bay from January to July 2016.

Position	Depth (m)	Measurement period (2016)
ADCP1	50	15 Jan - 5 Mar
ADCP2	44	5 Mar - 14 Apr
ADCP3	9	17 Apr - 3 Jun
ADCP4	25	12 Jun – 14 Jul

4.2.2. Validation

In addition to the 10-year ROMS hindcast used in the study, the ROMS model was run over a two-month period between March and May 2016 to allow the co-temporal validation of the model with measured data at position ADCP2, located at the centre of the proposed disposal ground 3.2 illustrated in Figure 4.2. The validation of the model at position ADCP2 allows a good assessment of the performance of the regional model, which was used to force both the disposal plume and the disposal ground models.

The model outputs were archived at 5-minute intervals to be consistent with the ADCP data, and the modelled and measured current speeds were vertically-averaged from 10 to 30 m depth for the time-domain comparison. Because the measured data duration was not long enough to resolve all tidal components by harmonic decomposition, a 25-hour filter was applied to separate the tidal and non-tidal flows for the validation.

The measured and modelled depth-averaged current velocities (Figure 4.3 - Figure 4.7) indicate that the model faithfully predicts the northeast-southwest bi-modal circulation at position ADCP2. The residual (non-tidal) component of the current is reasonably well replicated by the model, as shown on the Q-Q plot (Figure 4.7, top

plot). The correlation between the model and measured dominant V-component of the non-tidal velocity provides a good level of confidence in the model. Given that the U-component of the velocity is very low (rarely exceeding 0.05 m.s^{-1}), the relative low correlation between the measured and the modelled data for this component is assumed to have minor importance on the model performance assessment.

On the other hand, the tidal component is under-predicted by around 20%. This results in a total bias (tidal and non-tidal components) ranging between 5 – 20% of the existing current speed (i.e. between $0.005 - 0.03 \text{ m/s}$). The impact of such bias on the prediction of sediment transport has to be considered based on the local sedimentology, the ratio between currents and waves and the water depth. In this regard, it seemed preferable to discuss the consequences of such bias in the context of short-term and long-term sediment transports caused by the placement of material over the offshore disposal area. This bias in modelled data is therefore considered in the interpretation of the disposal plume and ground modelling results in MSL Report P0297-02 (MSL, 2016). Note that a scenario including the use of measured current profiles as forcing within the sediment transport model was performed to assess the impact of such bias on the model results. Conclusions are also presented in MSL Report P0297-02.

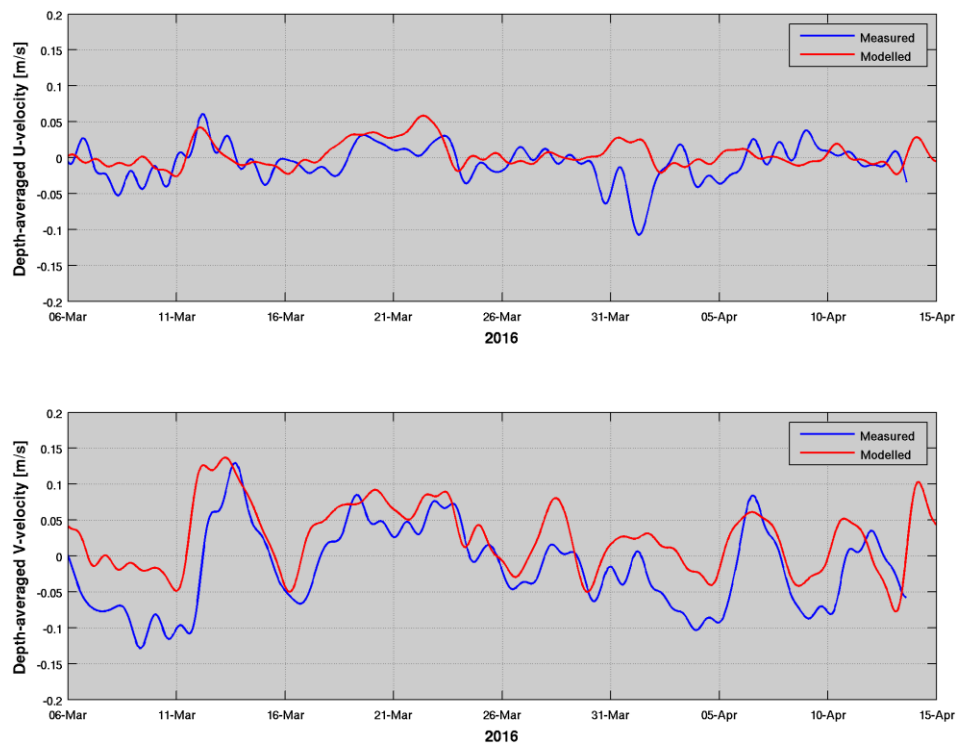


Figure 4.3 Time series of modelled and measured non-tidal depth-averaged current velocity at position ADCP2 from 5 March to 14 April 2016.

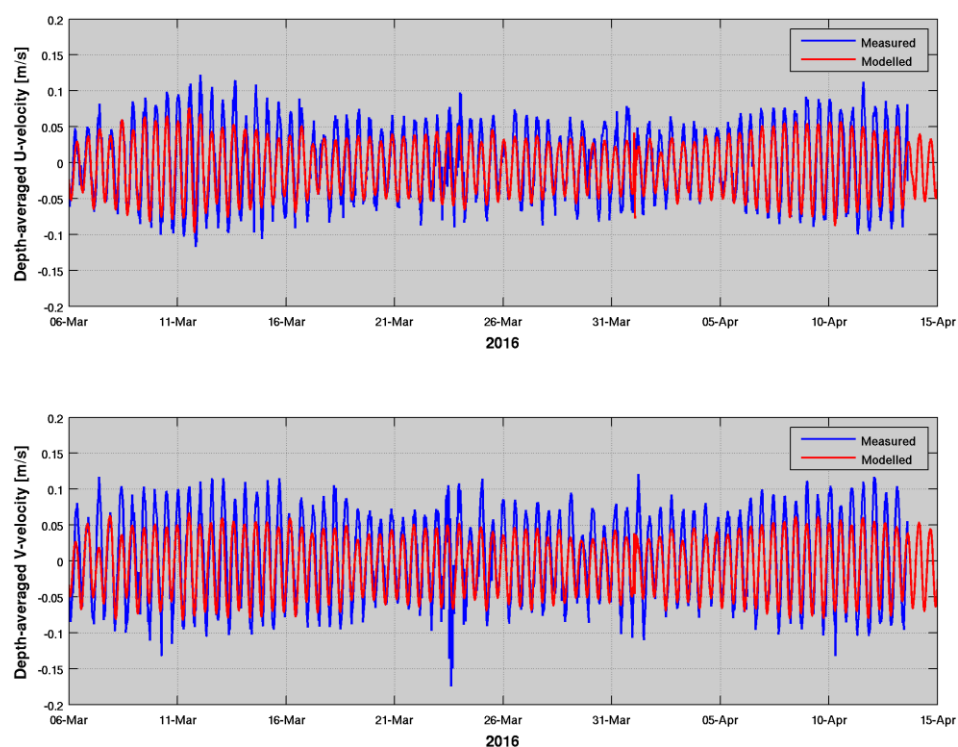


Figure 4.4 Time series of modelled and measured tidal depth-averaged current velocity at position ADCP2 from 5 March to 14 April 2016.

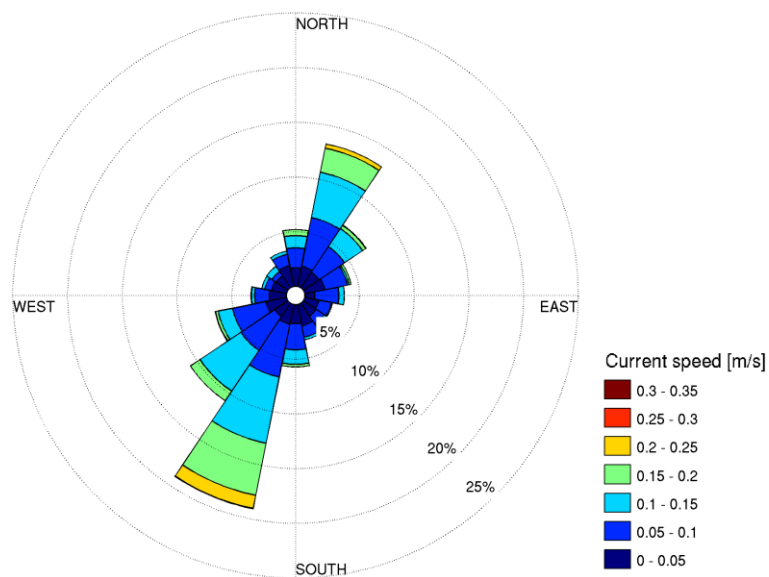


Figure 4.5 Measured depth-averaged current rose at position ADCP2 (5 March – 14 April 2016).

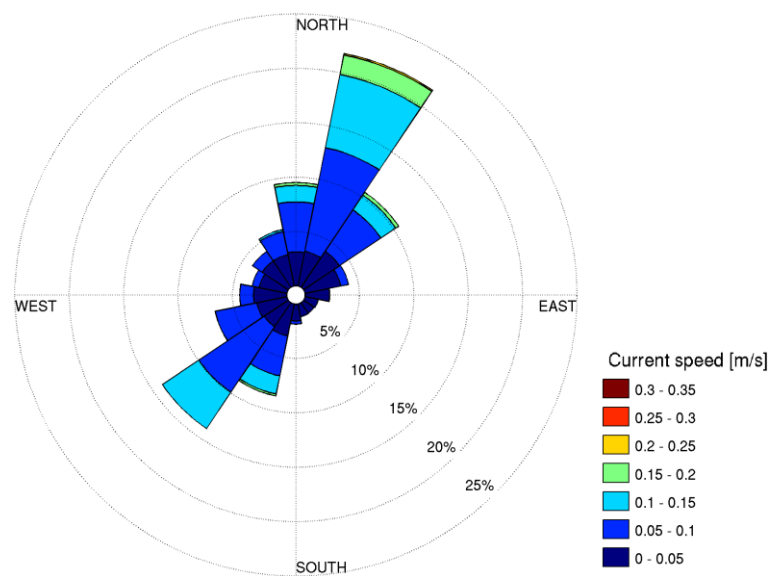


Figure 4.6 Modelled depth-averaged current rose at position ADCP2 (5 March – 14 April 2016).

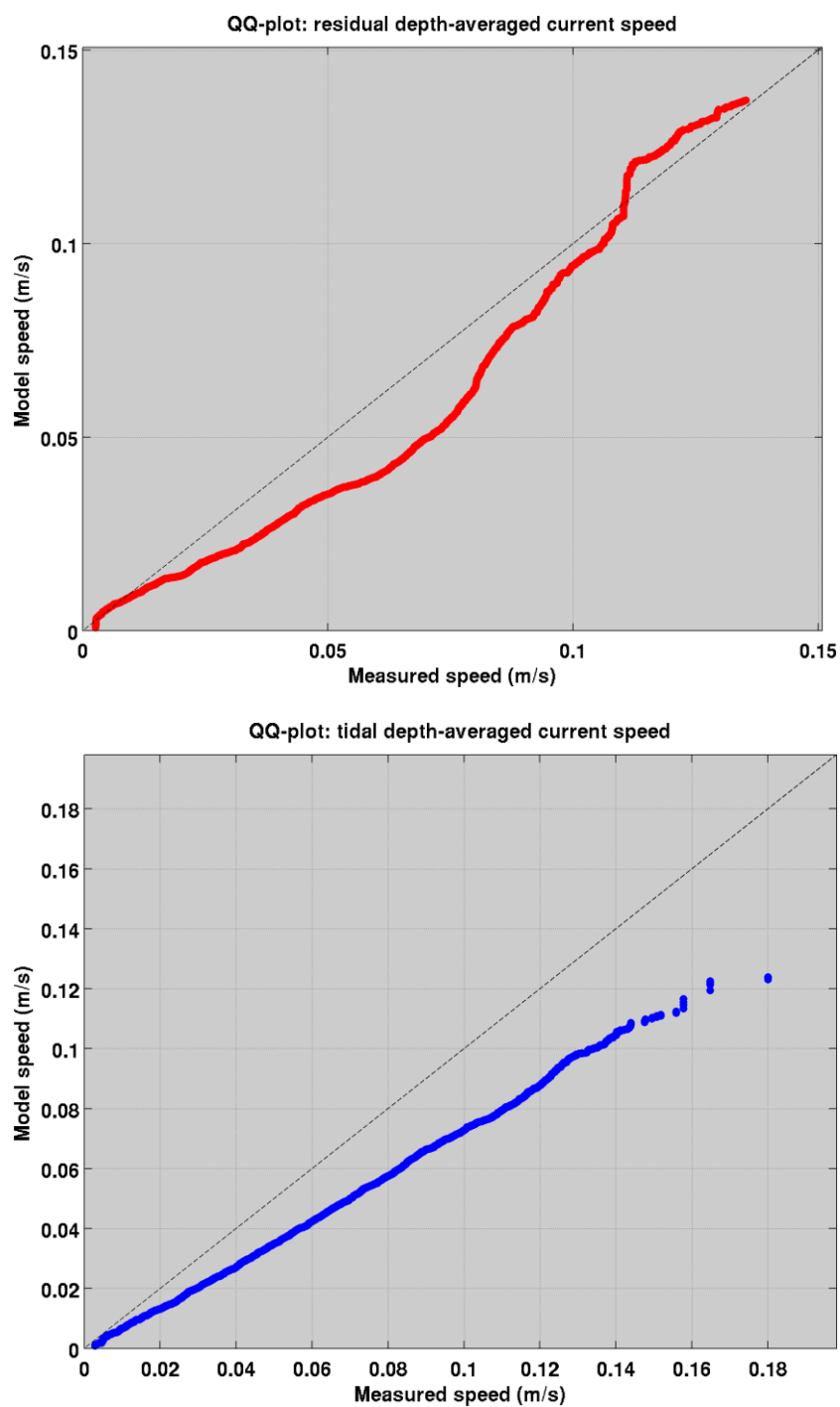


Figure 4.7 Quantile-Quantile plots of the measured and modelled non-tidal (top) and tidal (bottom) depth-averaged current speed at position ADCP2 (5 March – 14 April 2016).

5. HARBOUR TIDAL HYDRODYNAMIC MODELLING

Whangarei Harbour is characterised by a relative complex morphology with numerous channels, sand banks and small islands. In this context, a regional model such as ROMS is not the best option to accurately replicate the tidal flows over the study area and an alternate model, SELFE, was used that was better suited.

This section details the set-up of the high-resolution hydrodynamic modelling that was undertaken to simulate the tidal dynamics over Whangarei Harbour, given that the non-tidal component was of low importance. This nearshore hydrodynamic modelling stage aimed to provide the boundary conditions to the morphological model and assess the effect of the channel deepening on the local tidal dynamics.

The model water elevation and current velocities were validated at several positions within Whangarei Harbour and over the navigation channel using contemporary measured data. The key aim of the present numerical modelling was to capture both the temporal and spatial variability of the tidal dynamics to anticipate the changes in amplitude and phase caused by a different channel configuration.

5.1. Model approach

5.1.1. Model description

SELFE is a prognostic finite-element unstructured-grid model designed to simulate 3D baroclinic, 3D barotropic or 2D barotropic circulation. The barotropic mode equations employ a semi-implicit finite-element Eulerian-Lagrangian algorithm to solve the shallow-water equations, forced by relevant physical processes (atmospheric, oceanic and fluvial forcing). SELFE uses either pure terrain-following sigma, or S-layer coordinates in the vertical, or a hybrid system using both S and Z-layers as required and uses sophisticated vertical turbulent closure models. A detailed description of the SELFE model formulation, governing equations and numerics can be found in Zhang and Baptista (2008).

The SELFE model is physically realistic, in that well understood laws of motion and mass conservation are implemented. Therefore water mass is generally conserved within the model although it can be added or removed at open boundaries (e.g. through tidal motion at the ocean boundaries, or river discharges) and water is redistributed by incorporating aspects of the real-world systems (e.g. bathymetric information, forcing by tides and wind). The model transports water and other constituents (e.g. salt, temperature, turbulence) through the use of triangular volumes (connected 3-D polyhedrons) of varying size and is described as an unstructured finite element model.

5.1.2. Pertinence of the model for the present study

SELFE has been used for the present study as it provides robust capability to replicate the key hydrodynamic processes in shallow and intertidal environments. An important feature is its capability to simulate wetting and drying in shallow areas. The model sensitivity to bottom friction considered as a determinant mechanism in shallow waters has been demonstrated in the past. Moreover, the unstructured triangular grid approach implemented in SELFE allows for increase in model in the channel, along adjacent beaches and over sand banks without increasing dramatically the total computational runtime.

The SELFE model has been extensively applied to study circulation in coastal margins (bays, estuaries, tidal inlets and rivers) around the world (www.strccmop.org), including reported excellent representation of the hydrodynamic in a wave-dominated tidal inlet (Dodet, 2013).

5.1.3. High-resolution bathymetry and domain

Model bathymetries were derived from a combination of relevant ENC (Electronic Navigation Charts), LIDAR, and survey data (single-beam and multi-beam surveys). All data were converted to a common horizontal projection (NZTM), and reduced to a common vertical datum.

The model domain extents and bathymetry are shown in Figure 5.1. The domain was chosen to be sufficiently large to ensure the appropriate tidal boundaries (elevations and velocities) could be applied. The mesh resolution varies from approximately 300 m in the offshore, to ~5 m nearshore and around salient features.

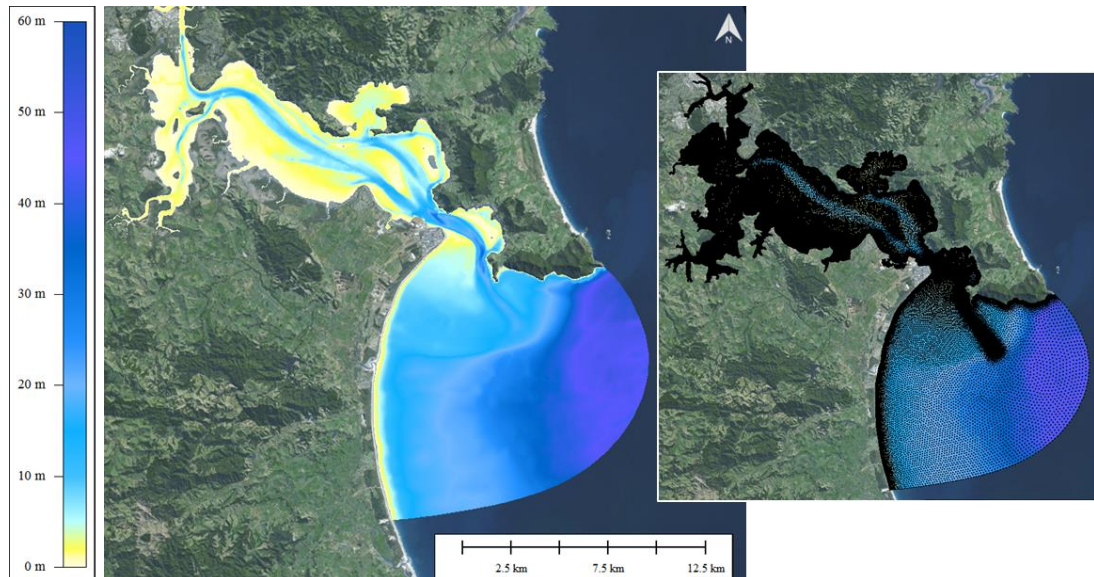


Figure 5.1 Model depth and mesh of the Whangarei Harbour and surrounds. Depths are given in metres below Mean Sea Level (MSL) The mesh covers the offshore region, including the ebb tidal delta, while salient bathymetric features are represented inside the harbour.

5.1.4. Open boundary conditions

A national New Zealand tidal solution derived from an implementation of the Princeton Ocean Model (POM) nested within the TPXO7.2 Pacific inverse tidal dataset (Egbert and Erofeeva, 2002) was used to prescribe the tidal elevation and current velocity at the boundaries of the grid. Depth dependent velocities along the offshore boundaries were defined using a standard logarithmic velocity profile (Van Rijn, 1993).

5.2. Model validation

5.2.1. Data collection program

A targeted measurement campaign was undertaken to provide data specifically for model validation. There were two components; water level measurements at four

locations in the harbour over one month and a moving vessel ADCP survey in the entrance region. ADCP moving vessel deployments have the benefit of providing 3-dimensional velocity data over different sections of the navigation channel thereby allowing a spatial time-dependent validation of the tidal models. Note however that velocity data provided by ADCP moving vessel deployments are slightly degraded by various factors such as Doppler noise, large sampling volume and beam divergence over rapidly changing bathymetry. Nonetheless, it was the preferred method to provide a spatial validation source in the complex tidal flows of the entrance.

In the present study, the ADCP moving vessel deployment was undertaken over three different zones A, B, C illustrated on Figure 5.2 from 19 May to 21 May 2015. Current velocities were measured during 13 hours through each area to capture the peak ebb and flood tidal stages.

5.2.2. Validation results

Comparisons between the measured and predicted water levels (Figure 5.3 to Figure 5.6) indicate that the model reproduces the tidal water elevation variability within Whangarei Harbour well. The magnitude and timing of the tidal propagation throughout the harbour confirms both the suitability of the tidal boundary conditions as well as the ability of the model to replicate the hydrodynamics, which include the prescription of the bathymetry and the frictional parameterisation.

The validation of the depth-averaged flows in the channel indicates an acceptable capability to replicate the complex tidal hydrodynamics at the Whangarei Harbour entrance. Snapshots of the measured and modelled flows are presented in Figure 5.7 to Figure 5.9 for the peak tidal ebb and flood situation. Here, the modelled depth-averaged currents are plotted with co-located measured values. The modelled speeds and directions show good correspondence with the measurements in most of the areas, including the zones of high flow and the recirculating eddy features on the channel margins. This relative good agreement between modelled and measured data is also outlined by the Q-Q plots calculated from the peak ebb and flood tidal velocities for all the measured locations. Note that no statistics are provided for Zone C due to insufficient measured data for a meaningful analysis.

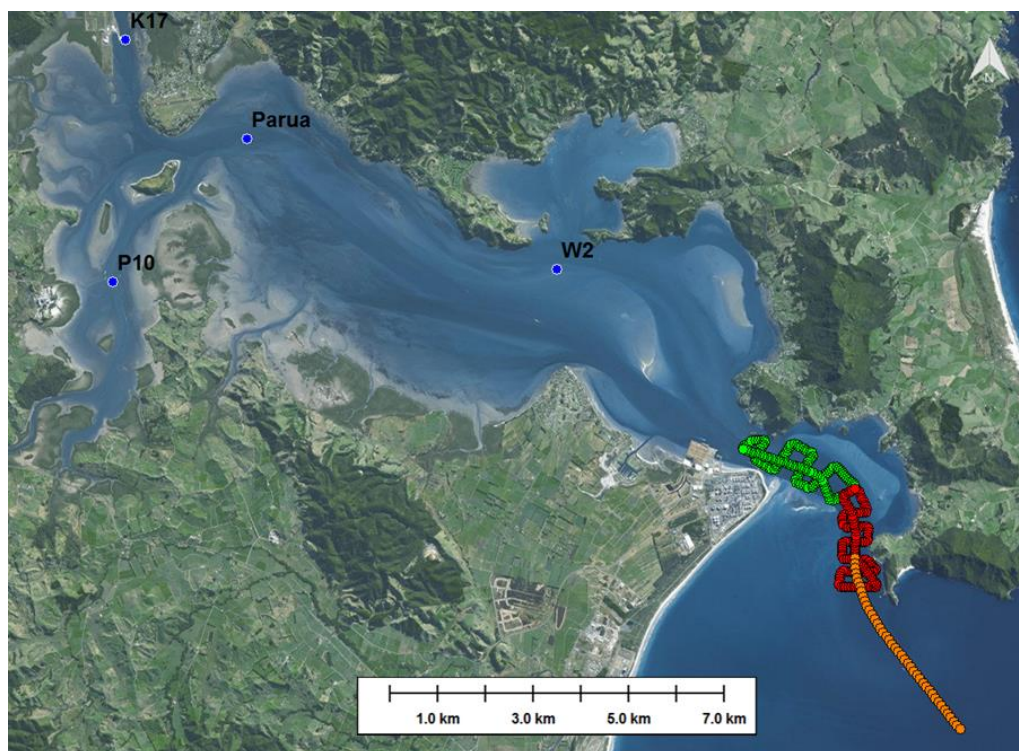


Figure 5.2 Locations of current velocity measurements (Zone A in green, B, in red and C in orange) and water level measurements (K17, P10, W2 and Parua) used to calibrate and validate the SELFE (and Delft3D) tidal model within Whangarei Harbour and Bream Bay.

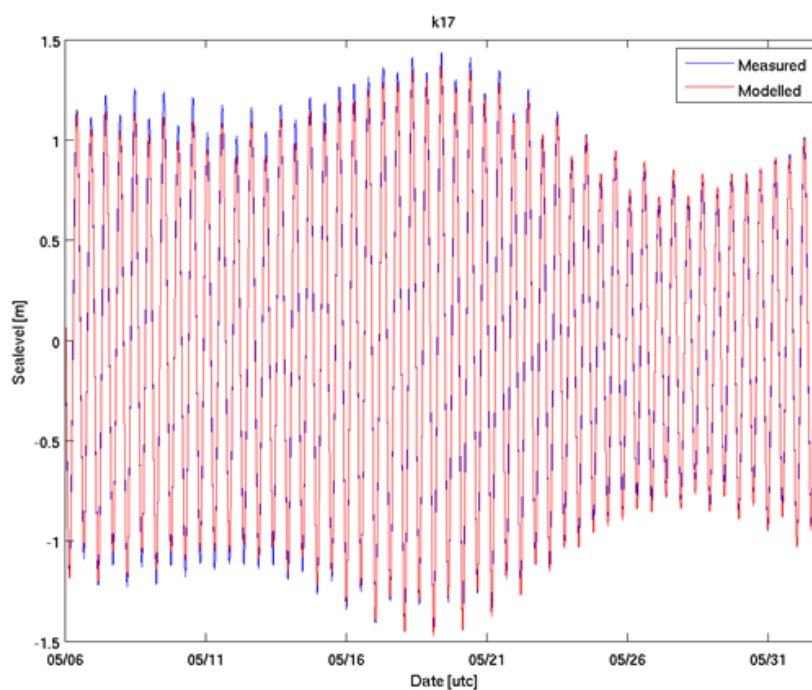


Figure 5.3 Measured and modelled water level comparisons at site k17.

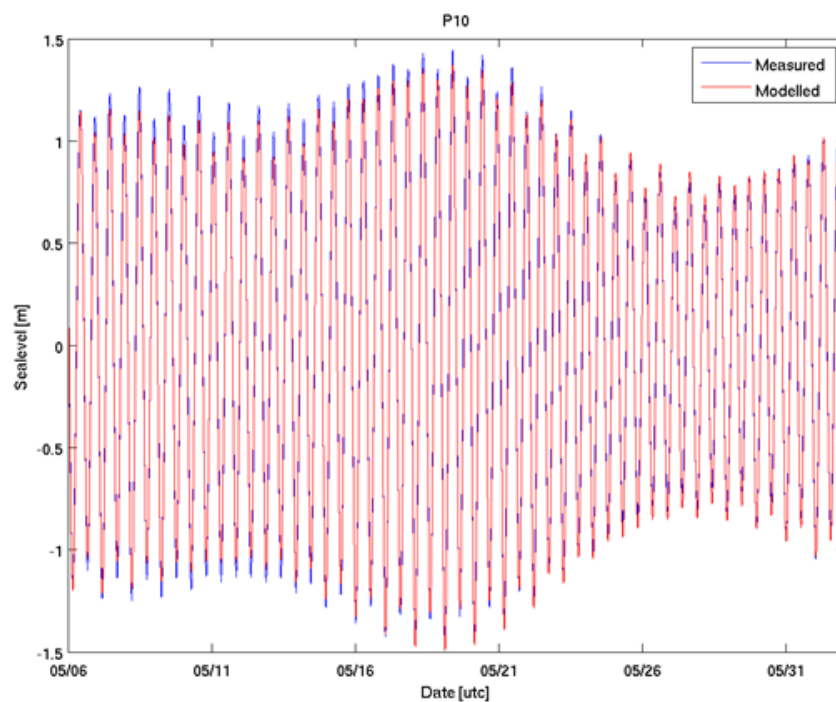


Figure 5.4 Measured and modelled water level comparisons at site p10.

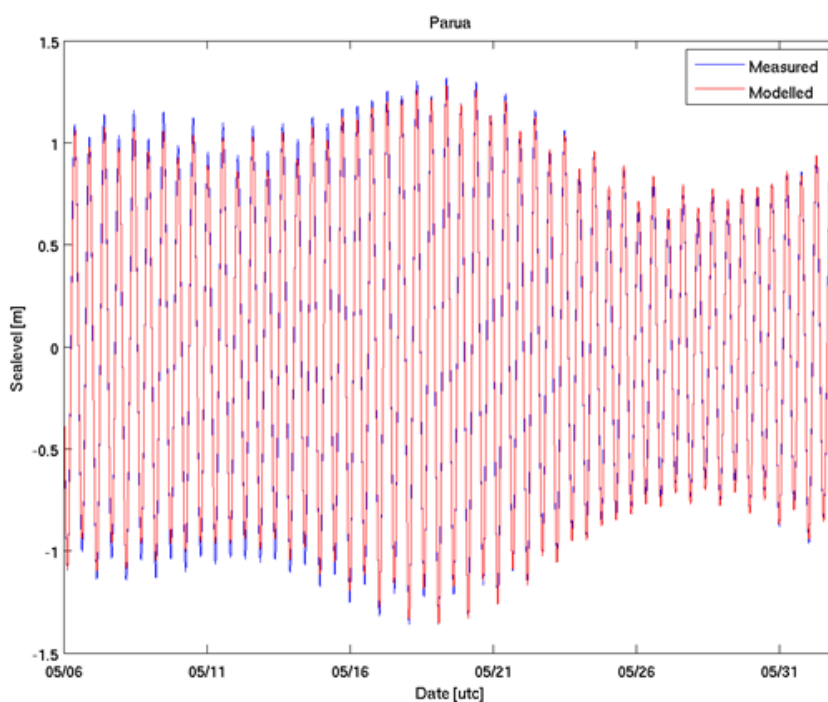


Figure 5.5 Measured and modelled water level comparisons at site Parua.

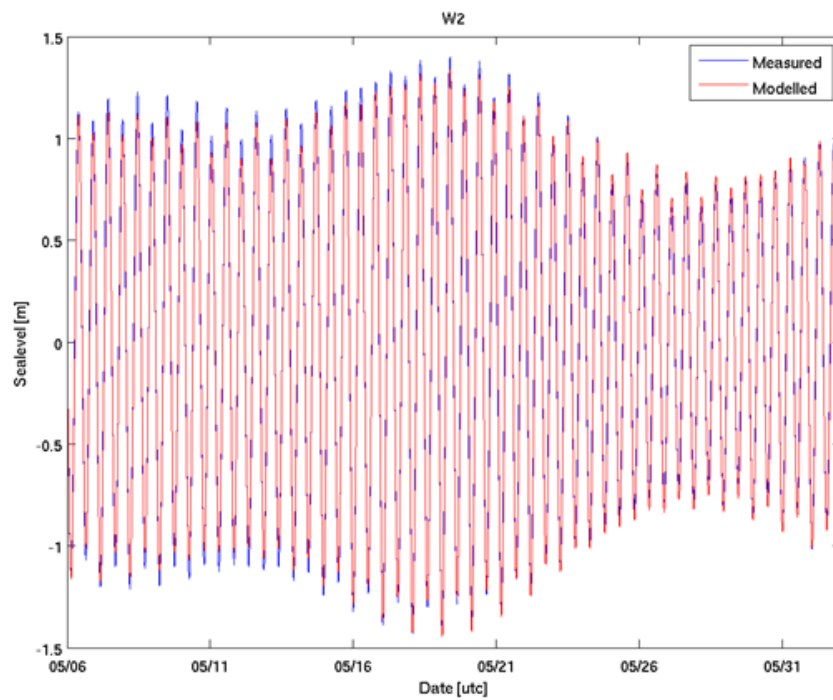


Figure 5.6 Measured and modelled water level comparisons at site W2.

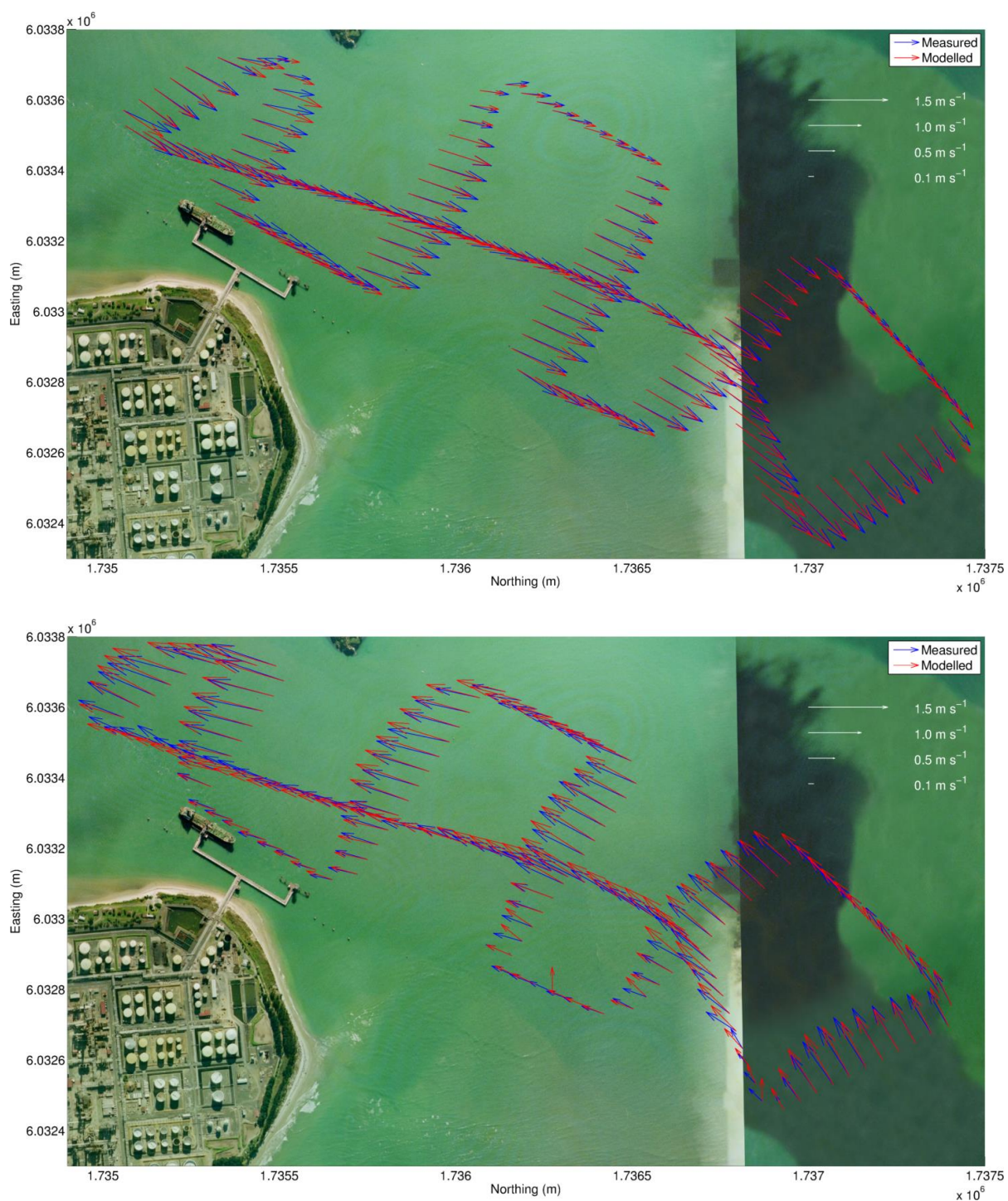


Figure 5.7 Modelled (SELFE) and measured velocity comparisons within Zone A (Figure 5.2) for the peak ebb (upper) and flood (lower) tidal stages.

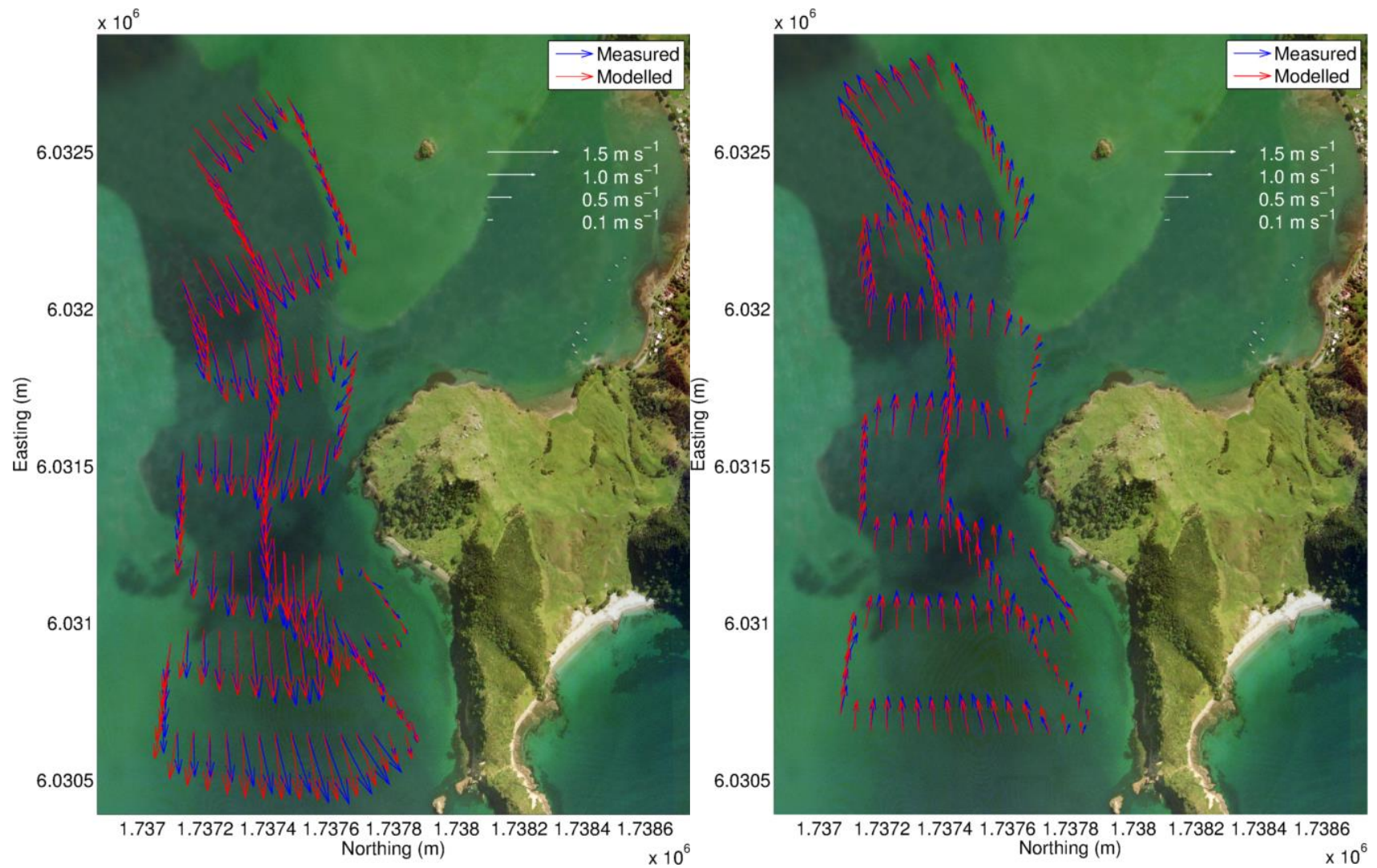


Figure 5.8 Modelled (SELFE) and measured velocity comparisons within Zone B (Figure 5.2) for the peak ebb (left) and flood (right) tidal stages.

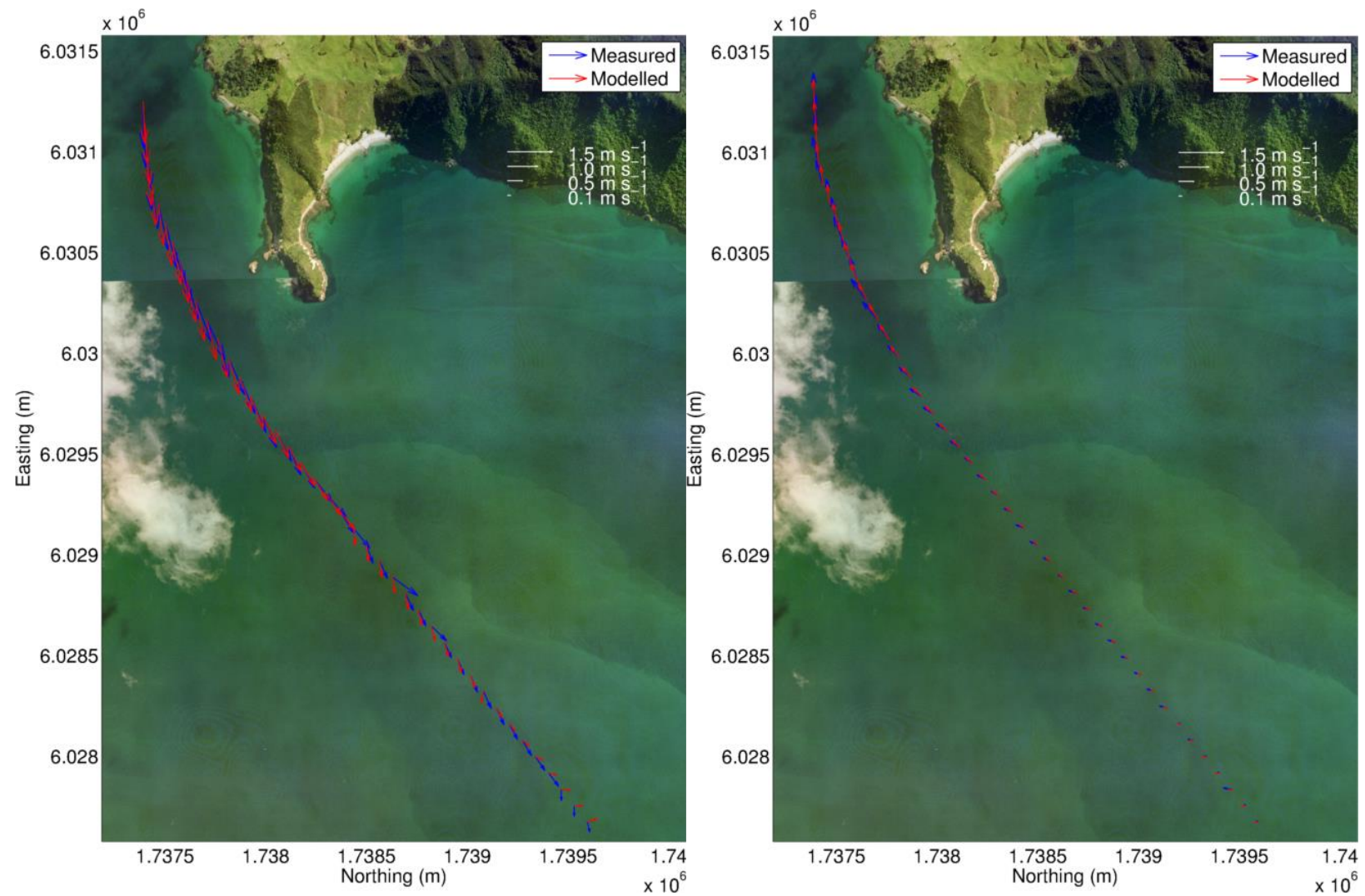


Figure 5.9 Modelled (SELFE) and measured velocity comparisons within Zone C (Figure 5.2) for the peak ebb (left) and flood (right) tidal stages.

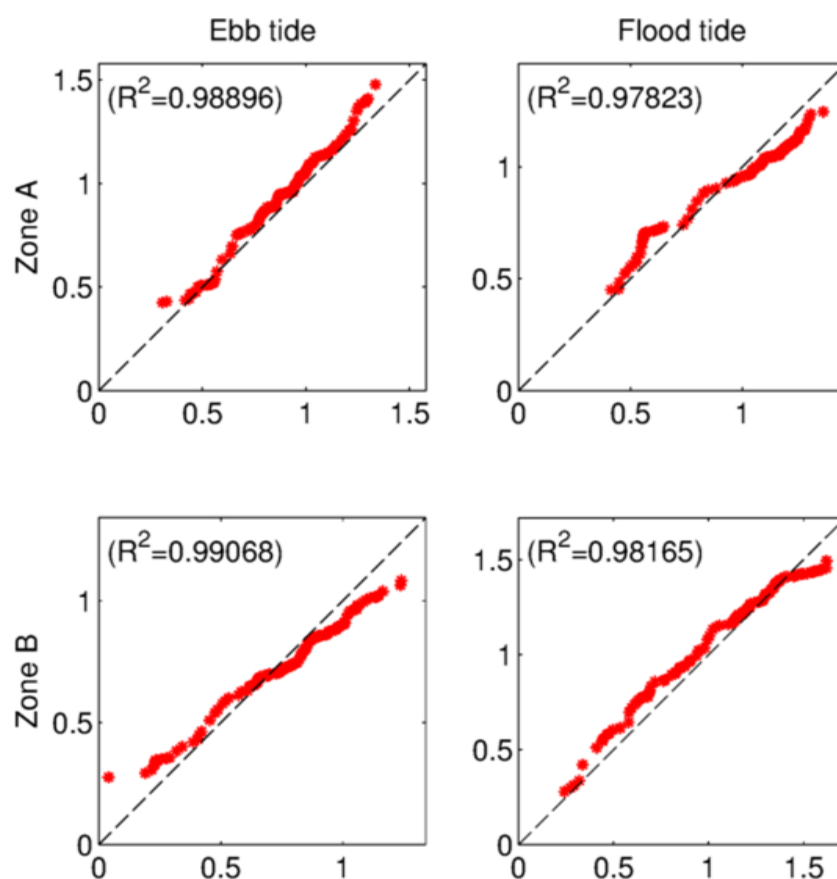


Figure 5.10 Quantile – Quantile plots of the measured and modelled (SELF) peak tidal ebb and flood current speed (m/s) along the vessel tracks within zones A and B for both peak ebb and flood stages. The root mean squared errors corresponding to the different distributions are presented in the top-left corner of each plot.

6. SEDIMENT TRANSPORT MODELLING

Nearshore wave and tidal models were previously established at the entrance to Whangarei Harbour and the surroundings. One of the purposes of these models was to provide high-resolution data to force the morphological model. Indeed, the overall response of the coastal morphodynamic is largely controlled by the interactions between currents, waves and sediments. In this context, a fully coupled numerical model is required to capture the short-, medium- and long-term morphological processes that affect the study area in order that the effect of the channel deepening on the existing coastal dynamics can be anticipated. The fully coupled process-based numerical model, Delft3D, was thus implemented based on the wave and tidal conditions provided by SWAN and SELFE, respectively.

This section provides an overview of the model as well as the different approaches and settings used to undertake the sediment transport modelling in this highly complex region. The validation of the hydrodynamic component of the model applied to assess the model performance is also presented using the same methodology as previously applied for the SELFE model validation.

6.1. Modelling system

The modelling system Delft3D (Lesser et al., 2004) was used to set up and run high-resolution process-based morphodynamic models. The software is based on interlinking three separate components that together simulate flow, waves and sediment transport. The three components are fully coupled to simulate morphodynamic feedbacks. An overview of the main parameters and components is given in this section.

6.1.1. Delft3D-WAVE (SWAN)

The third-generation SWAN model (Simulating WAVes Nearshore) was used as the wave module (Booij et al., 1999; Ris et al., 1999). SWAN computes the evolution of random, short-crested waves in coastal regions with deep, intermediate and shallow water depths. The SWAN model accounts for (refractive) propagation due to depth and current and can represent the processes of wave generation by wind, dissipation due to white-capping, bottom friction and depth-induced wave breaking, and non-linear wave-wave interactions explicitly with state-of-the-art formulations (Deltares, 2013a)).

For the present work, the local wave model boundary conditions were nested with 2D spectral boundaries obtained from a regional scale grid forced either by representative wave events (i.e. accelerated morphological simulations) or real hindcast conditions (i.e. real-time simulations). The nesting allows the retention of spatial variability in the incident wave field due to large scale regional refraction and sheltering effects. Bottom friction was modelled using the formulation of Collins (1972) and the default coefficient value was 0.016. Dissipation by friction and wave breaking was applied in the model. The formulation of Van der Westhuysen et al. (2007) was used to reproduce the wave dissipation due to whitecapping.

Hindcast conditions available at hourly intervals were applied as offshore boundary conditions. This coincides with the interval of the sequential two-way coupling between SWAN and the hydrodynamic module (Delft3D – FLOW) that allows the exchange of relevant parameters on curvilinear model grids via a communication file. Wave parameters and the forcing terms associated with the wave radiation stresses computed by SWAN were read by the FLOW module to model the

hydrodynamic conditions. At the end of each assigned 60 minute runtime, bottom elevation, water level and current fields were used as input to the computation in SWAN. The model loops through these sequential module applications until the end of the complete simulation. Morphodynamic modelling is thus performed through the implementation of a fully coupled wave – hydrodynamic system based on wave and current interactions.

In the scientific community, there is an on-going debate about the vertical distribution of wave-induced radiation stresses that generally split up into a surface component, a bottom component and a body force and their implementation within 3D momentum equations (Ardhuin and Roland, 2013; Ardhuin et al., 2008; Bennis et al., 2011). The debate indicates that important wave-induced processes interacting with the flow circulation may still be inadequately implemented in Delft3D. These limitations are accepted in the present study considering that they do not fundamentally impact the sedimentology and morphology in the area of interest.

6.1.2. Delft3D-FLOW

The base hydrodynamics were computed in the Delft3D – FLOW module, which can be used in a full 3D or 2DH (depth averaged) mode. The hydrodynamic module Delft3D-FLOW solves the Navier-Stokes equations for an incompressible fluid under the shallow water and Boussinesq assumptions. The system solves the horizontal equations of motion, the continuity equation, the transport equations for conservative constituents, and a turbulence closure scheme. The details of equations and associated sub-models are fully described in Lesser et al. (2004) and in (Deltares, 2013b).

In a tidal inlet environment, the 3D mode is more appropriate than 2D as the cross-shore velocity profile in nearshore areas where breaking waves cause return flow and exhibit a strong vertical shear (Ranasinghe et al., 1999), which can significantly affect bed dynamics of deltas. A calibration process based on a comparison between 2D and 3D modes of Delft3D highlighted important wave effects in the 3D simulation, as wave-induced mass flux adjusted for the vertical non-uniform Stokes drift, additional turbulence and vertical mixing processes and streaming as an additional wave-induced shear stress in the wave boundary layer (Walstra et al., 2001). The model consisted of 10 *sigma* layers in the vertical direction focused on the surface and on the bottom levels of the water column to better reproduce wave – current interactions and sediment transport processes. Model domains implemented in the present study are presented in Section 6.2.

Bed shear stresses were computed using a quadratic friction law. The non-linear enhancement of the bed shear stress in the presence of waves was taken into account by means of the wave-current interaction model of Fredsøe (1984). Turbulence effects were modelled using constant background horizontal and vertical eddy viscosity and eddy diffusivity coefficients. Horizontal background eddy viscosity was set $1 \text{ m}^2 \text{ s}^{-1}$ while diffusivity was equal to $1 \text{ m}^2 \text{ s}^{-1}$. A value of $10\text{e-}6$ was used for the vertical background viscosity and diffusivity. The bottom roughness distribution used in this study was based on Manning formulation (depth dependency) with a coefficient of 0.02, which is commonly used in Delft3D (Deltares, 2013b).

Current and water elevation conditions at open boundaries were prescribed based on tidal constituents generated from the high resolution SELFE tidal model (see Section 5). Hydrodynamic conditions were provided at intervals of 15 min to the Delft3D – FLOW module. The set value for the numerical time step was 3 s based

on a stability criterion defined for a Courant Number lower than 10 in Delft3D-FLOW (Deltares, 2013b).

6.1.3. Delft3D-MOR

The module Delft3D-MOR combines the information provided by the flow and wave modules to compute the sediment transport fluxes at each computational time step. The seabed level can then be updated as a result of the sediment sink and sources terms and computed transport gradients.

Data on bed composition and sediment properties are essential to adequately predict morphodynamics in nearshore regions, particularly in tidal inlet environments where the seabed composition is usually divided into several fractions of sediments from silty cohesive material to non-cohesive fine gravel.

In the present study, based on vibrocore results (Tonkin and Taylor, 2016c), model simulations were restricted to non-cohesive sand fractions with a grain size of 200 μm for the potential sediment fluxes approach, and from 100 to 10000 μm for the sediment transport pathways approach. For such an approach, a set of four layers was implemented, including the active layer and the base well mixed layer. Details on the methodology used to generate the bed composition with a multi-layer seabed scheme are discussed in Section 6.3.2.

The biomass of pipi over Mair Bank was mimicked by adding a fraction (80%) of coarse gravel in the uppermost layer of the bed layer model, the so-called active layer. This approach aims to decrease the sediment transport and thus reproduce the overall stability of Mair Bank as observed in Morgan et al. (2011). The potential erodibility of Mair Bank suggested by the shear stress values decreases because the Pipi population causes an increase in the shear stress resistance, as first described in (Black, 1983) and repeated in other studies completed since then.

For non-cohesive sediments, the total sediment transport is defined as the sum of the suspended load and bedload transport. The sediment transport predictor TRANSPOR 2004 of Van Rijn et al. (2004) was used in the present study rather than the default (Van Rijn, 1993) due to the recalibration against new data and the extension of the model to incorporate the wave zone. The approach first computed the magnitude and direction of the bed-load sand transport used by Van Rijn. The computed sediment transport vectors were then relocated from water level points to velocity points using an upwind computational scheme to ensure numerical stability.

The slope of the banks and of the channel is an important factor to consider in a tidal inlet environment. In tidal inlet environments, the non-cohesive bedload transport definitions in the model have a bed slope effect, which represents a gradient in the initial direction of sediment transport. The Bagnold (1966) equations were used for longitudinal transport (*AlfaBs*) and Van Rijn (1993) for the transverse direction (*AlfaBn*). It is reported that *AlfaBs* was of lesser importance in model calibration compared with *AlfaBn* which can cause 'unrealistic incision of the main tidal channel' (Van der Wegen and Roelvink, 2008; Dastgheib, 2012; Dissanayake et al., 2012). The default value (*AlfaBn* 1.5) commonly leads to unrealistic channel slope with gradients larger than the angle of repose. However, calibration processes have shown that decreasing the default values (as suggested in Dissanayake et al. (2012)) leads to significant erosion of the edges of the channel, as a result infilling the channel, particularly to the east and northeast of Mair Bank. In reality, long-term bathymetry surveys between 2000 and 2015 have demonstrated that the channel is morphologically stable (MSL Report P0297-02).

The steep channel slope suggests some degree of cohesiveness and armouring induced by many decades of morphodynamics which cannot be fully reproduced by the model. Consequently, the channel stability was modelled within Delft3D - MOR using the non-restrictive upper range of values for the longitudinal and transverse bed slope factors (1.0 *AlfaBs* and 1.5 *AlfaBn*).

The erosion of dry cells in Delft3D was controlled by the drycell erosion factor (DCE, *thetSd* keyword in Delft3D) to simulate bank erosion. The DCE default value was originally set to zero in Delft3D. However, calibration processes showed that as suggested in Dissanayake et al (2012) large cell erosion factors produced better representations of the ebb-delta than did low values. Unrealistic seaward extensions of the delta in long term simulations were observed, which is contrary to the evolution of Mair Bank described in Morgan et al. (2011) and Williams and Hume (2014). The use of larger values, 0.5 (50% of erosion in neighbouring dry cell) as defined in the present study, is predicted to improve the model's capability to reproduce the channel morphological variability.

In Delft3D, a commonly used approach for the bed composition modelling is based on 2DH computations as a well-mixed single layer including one or several grain sizes of sediments. However, another approach described in Dastgheib (2012) incorporates the concept of layered bed stratigraphy. The bathymetry is subdivided into cells with a specific thickness and a specific fraction of different sediment grain size. The uppermost sediment layer corresponding to the transport layer (or active layer) imports sediments when sedimentation happens and export sediments when erosion happens. In case of deposition, sediment is imported to the transport layer by settling from the water column where it is mixed and redistributed to the underlayer, thereby maintaining its defined constant thickness. In case of erosion, the transport layer imports sediment from the underlayer directly beneath it to replenish and thereby retains its defined constant thickness. The underlayer is indirectly eroded. Conceptually, a layered bed stratigraphy permits specifications of bed composition and sediment characteristics corresponding to the hydrodynamic conditions and the bathymetry.

Both approaches described above have been used in the present study to simulate the potential sediment fluxes and the evolution of the sea bed. Configurations of the underlayers and sediment grain size distribution are described in Section 6.1.2. More information on numerical aspects can be found in the Deltares (2013b).

6.1.4. Pertinence of the model

Interactions between morphological, tidal and wave components play a major role in the dynamics of coastal areas such as bays, estuaries and inlets. In this context, using a process-based model as Delft3D, which integrates a fully 2-way coupled system between these components, is particularly pertinent. Delft3D has been specifically developed to simulate the physics of such complex regions and it provides the necessary multi-disciplinary approach and numerical modelling. Moreover, the Delft3D model has been successfully applied worldwide for a large range of coastal studies over both short – term and long – term periods. In New Zealand, the model has been successfully used at Port Otago (Weppe et al., 2015) and Tauranga Harbour (Ramli et al., 2015).

6.2. Model domains

The Delft3D - FLOW model grid covers the northern region of Bream Bay from the Ruakaka river mouth to Bream Head, and Whangarei Harbour entrance from Mair

Bank to One Tree Point, with grid resolutions of approximately 12 m over Mair Bank and within the inlet channel, and 150 m close to Ruakaka and Bream Head (Figure 6.1).

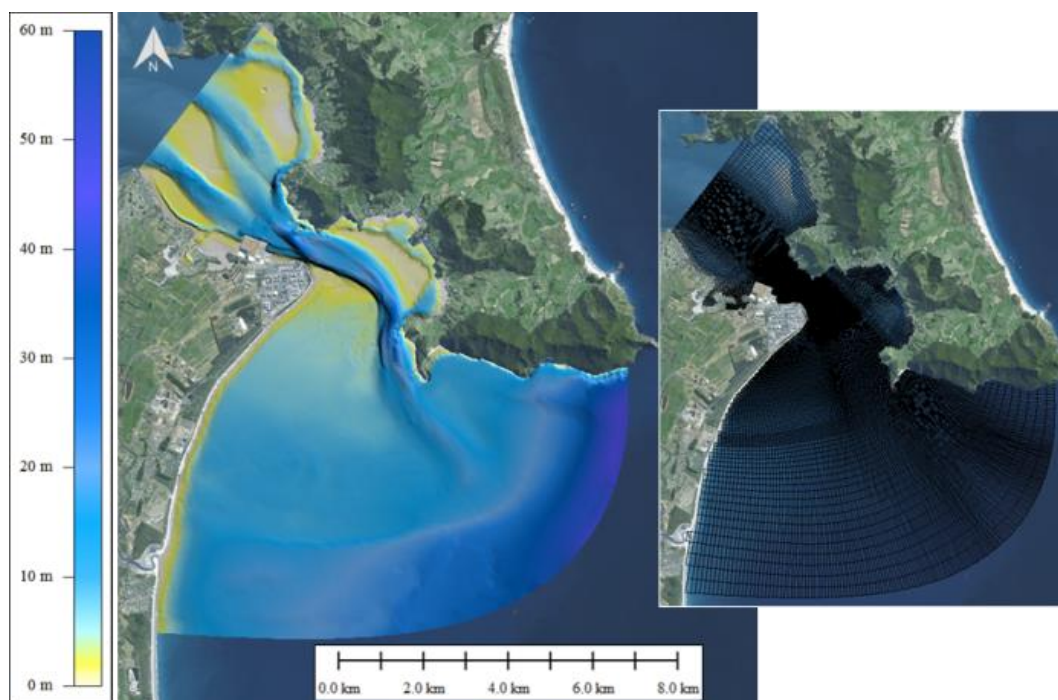


Figure 6.1 Delft3D – FLOW model grid (right) and depths (left).

A one-way online nesting technique was used for the wave modelling based on the implementation of multiple model grids with different grid resolutions. The coarse grid defined within Delft3D – WAVE covers the northern region of Hauraki Gulf, including Mokohinau Islands and Great Barrier Island, with resolutions ranging from 500 m to 3 km (see Figure 6.2). Boundary conditions were nested offline within a coarser regional SWAN domain described in Section 5. The fine grid used in the wave model is slightly more extended along the seaward boundary than the Delft3D – FLOW grid to more accurately force the hydrodynamic model.

The configuration of the model domains has been set-up to fully replicate important physical features in the study area such as:

- The retention of spatial variability in the incident wave field due to both large and high resolution scale regional refraction and sheltering effects.
- The inclusion of the ebb-jet flow extension at the delta entrance.
- The local hydrodynamic current patterns due to the presence of marginal channels sand banks within the harbour.
- The 3-dimensional wave – current interactions over Mair Bank and within the main channel.

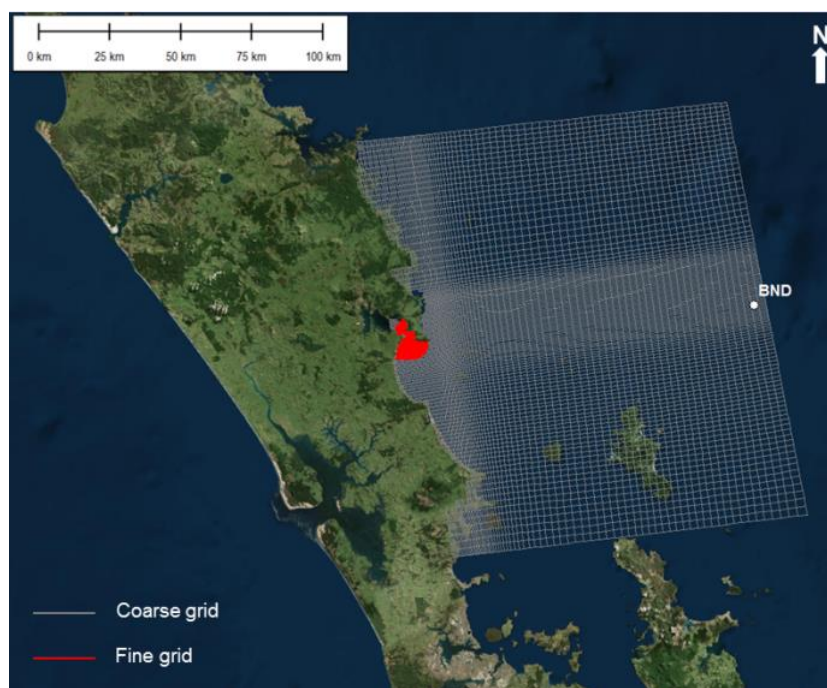


Figure 6.2 Delft3D – WAVE model grids for the modelling of the wave spectral transformation from the offshore region to the coast. The BND position indicates the site used to extract the wave climate described in Section 6.3.1.

6.3. Modelling approach

The main challenge with applying process-based models to predict morphological evolution is that the morphological behaviour of coastal systems generally develops over time scales several orders of magnitude larger than the time scale of the hydrodynamic fluctuations driving the sediment transport (i.e. hours to days versus years to decades and more). This means that while a model system is able to predict the time series of instantaneous hydrodynamics and sediment transport, it will require an unfeasibly long period of time to compute a multi-year real time simulation. Instead, several strategies are commonly used to understand and reproduce morphological dynamics.

The approach employed here combines the reduction of the input forcing (waves and tides) with the use of realistic simulations for both fair-weather and storm conditions. Input reduction essentially means selecting a limited number of representative forcing conditions (i.e. waves and tides) that will reproduce the medium-term residual sediment transport patterns and associated morphological evolution (De Vriend et al., 1993). The application of these techniques to the present study is explained in the following sections.

6.3.1. Hydrodynamic and wave forcing

a) Discrete wave scenarios

- Tidal input reduction

Astronomical tides are deterministic and can therefore be accurately predicted for any period of time. However, tidal oscillations exhibit significant long-term modulations (e.g. spring/neap, yearly and nodal cycles), which make chronological simulations of such cycles computationally demanding. The basis for tidal input

reduction is to find a representative tide that most closely reproduce the net and gross sediment transport as the naturally varying tides over the region of interest and for the time period considered, here one year. In the present study, the representative tide was determined following the approach of Latteux (1995), which is commonly applied (e.g. Brown and Davies, 2009; Dastgheib, 2012; Grunnet et al., 2004).

Tidal signals at a reference point located at the harbour entrance were generated from a high resolution tidal constituents grid, and time series of sediment transport were estimated using a simple power law $Q=A.u^b$ (Q is the transport flux, A is a constant factor, u is current velocity, $b=5$ following Engelund and Hansen (1967)). The single tide best reproducing the net and gross transport magnitude of a given cycle relative to the long term mean transport values was identified and used in the representative scenarios (Figure 6.3).

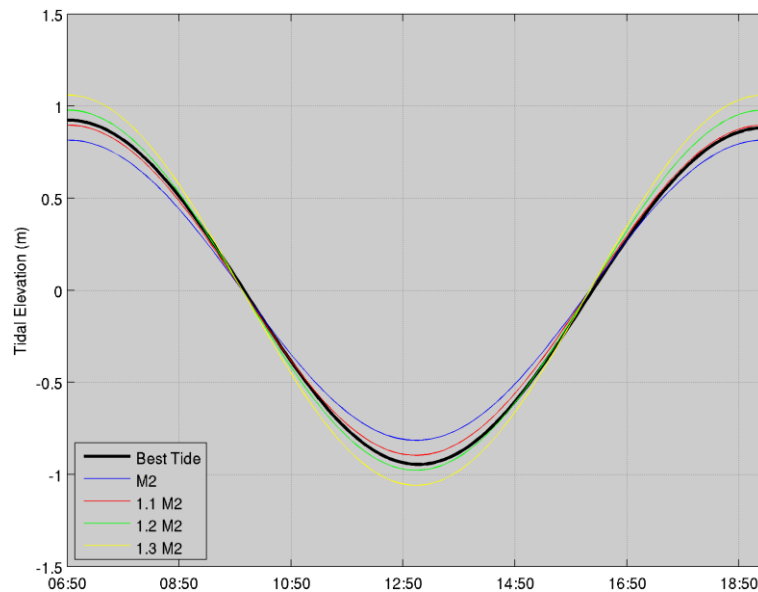


Figure 6.3 Comparison of the best tide, pure M2 tide, 1.1 M2, 1.2 M2 and 1.3 M2 tide curves at the harbour entrance.

- Wave climate reduction

The objective of wave input reduction is to define a set of offshore wave boundary conditions which reproduce the same residual sediment transport patterns and morphological evolution as the real time forcing over a given time period. The approach employed here follows the input reduction framework provided in Lesser (2009) and Walstra et al. (2013).

The first step is the selection of a reduction period, which is the length of the real time wave time series that is used to define the representative conditions. This is typically governed by the time scale of the morphological evolution of interest (e.g. monthly, seasonal or annual behaviour). In the present study, the reduction was undertaken based on a 10 year hindcast wave climate obtained from SWAN simulations to define an average annual wave climate (Section 3). The wave condition timeseries was extracted at the middle of the southern boundary of the wave model domain. In a second step, a set of representative wave classes was defined by distributing the discrete wave data points into a finite number of height and direction bins, and computing a representative value for each bin.

The basic method to determine a representative value within a bin is to use a weighted average of the data points by their frequency of occurrence. To account for the non-linear dependence of sediment transport on wave height, an additional weighting was applied for the computation of the representative height. The initial wave data binning is relatively arbitrary and can be equidistant or non-equidistant (i.e. exhibiting varying bin size). In the non-equidistant case, bins can be defined following either (subjective) scientific judgment or more objective approaches. In the current study, the height and direction bins were defined so that the relative “morphological impact of waves” was similar in each bin (Dastgheib, 2012; Lesser, 2009). The morphological impact of waves of a given wave class was estimated according to the “potential sediment transport” indicator used in Dastgheib (2012).

To automate the determination of bin limits, this indicator was initially computed for a joint probability of wave height and direction with very fine equidistant bins ($\Delta H=0.1$ m, $\Delta \text{Dir}=2$ deg.). Based on the number of directional and wave height bins to be used for the classification, the directional bin limits were determined first, such that the sum of the morphological impact of waves, M_j , within each bin was (approximately) equal. The same principle was then used within each of these directional bins to define the wave height bin limits. This way, the “morphological impact of waves” was similar in each bin.

The wave climate classification (Figure 6.4 and Figure 6.5) used in the following morphological simulations was defined using four directional bins and four wave height bins. The general classification obtained for the wave climate at the reference site reproduced the different levels of wave energy coming in the northeast and southeast directions.

The wave height delimitations were relatively homogeneous regarding the directionality of the wave propagation:

- 1st class with wave heights of 1 – 2 m.
- 2nd class with wave heights of 2 – 2.8 m.
- 3rd class with wave heights of 2.8 – 3.5 m.
- 4th class with wave heights of 3.5 – 5.4 m.

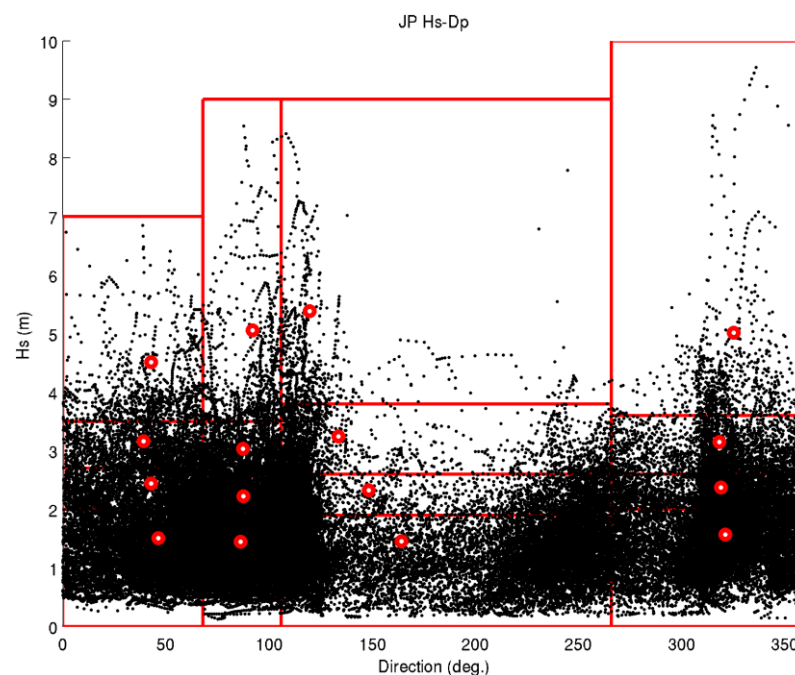


Figure 6.4 Scatter plot of wave heights as a function of wave directions for the 10-year time series, with delimitation of bins (red boxes). Red dots are the representative conditions of each bin.

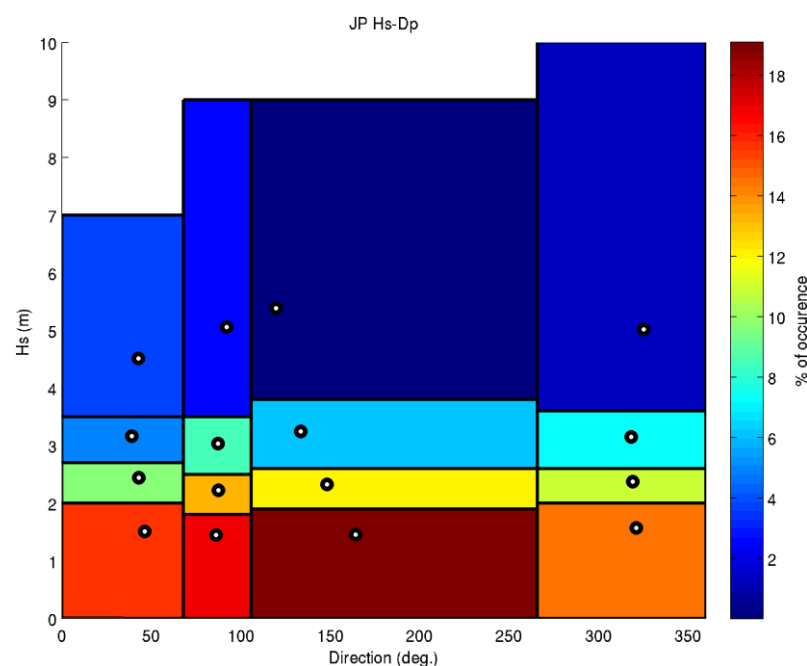


Figure 6.5 Reduced average annual wave climate based on the 10-year wave hindcast using four directional bins and four wave height bins (i.e. 16 wave classes). Colours indicate the probability of occurrence of a given class. The white dots are the representative wave condition of each wave class. Wave classes are summarised in Table 6.1.

Table 6.1 Wave classification based on an average annual wave climate defined from a 10-year hindcast.

Wave class	Representative Hs (m)	Representative Tp (sec)	Representative Dp (deg.)	Probability of occurrence
1	1.5	8.6	46.4	17%
2	2.4	9.0	43.0	4%
3	3.2	9.7	39.1	2%
4	4.5	10.4	42.9	1%
5	1.5	9.1	86.2	18%
6	2.2	10.1	87.6	6%
7	3.0	10.2	87.3	3%
8	5.1	11.0	92.1	1%
9	1.5	7.5	164.3	19%
10	2.3	8.8	148.3	5%
11	3.2	9.2	133.6	2%
12	5.4	10.6	119.7	1%
13	1.6	7.2	321.1	15%
14	2.4	7.4	319.1	4%
15	3.2	8.3	318.3	3%
16	5.0	10.7	325.3	1%

b) Tide-only scenario

A tide-only scenario was run with the best representative tide described in Section 6.3.1 to assess the impact of the tidal flows on the sediment transport dynamics. No wave forcing was considered for this simulation.

c) Historical simulations

The tide-only and discrete wave scenarios were supplemented by historical simulations for both fair-weather and storm conditions (Figure 6.6) based on time series of significant wave height H_s , peak period T_p and peak direction D_p provided by SWAN hindcast (see Section 3).

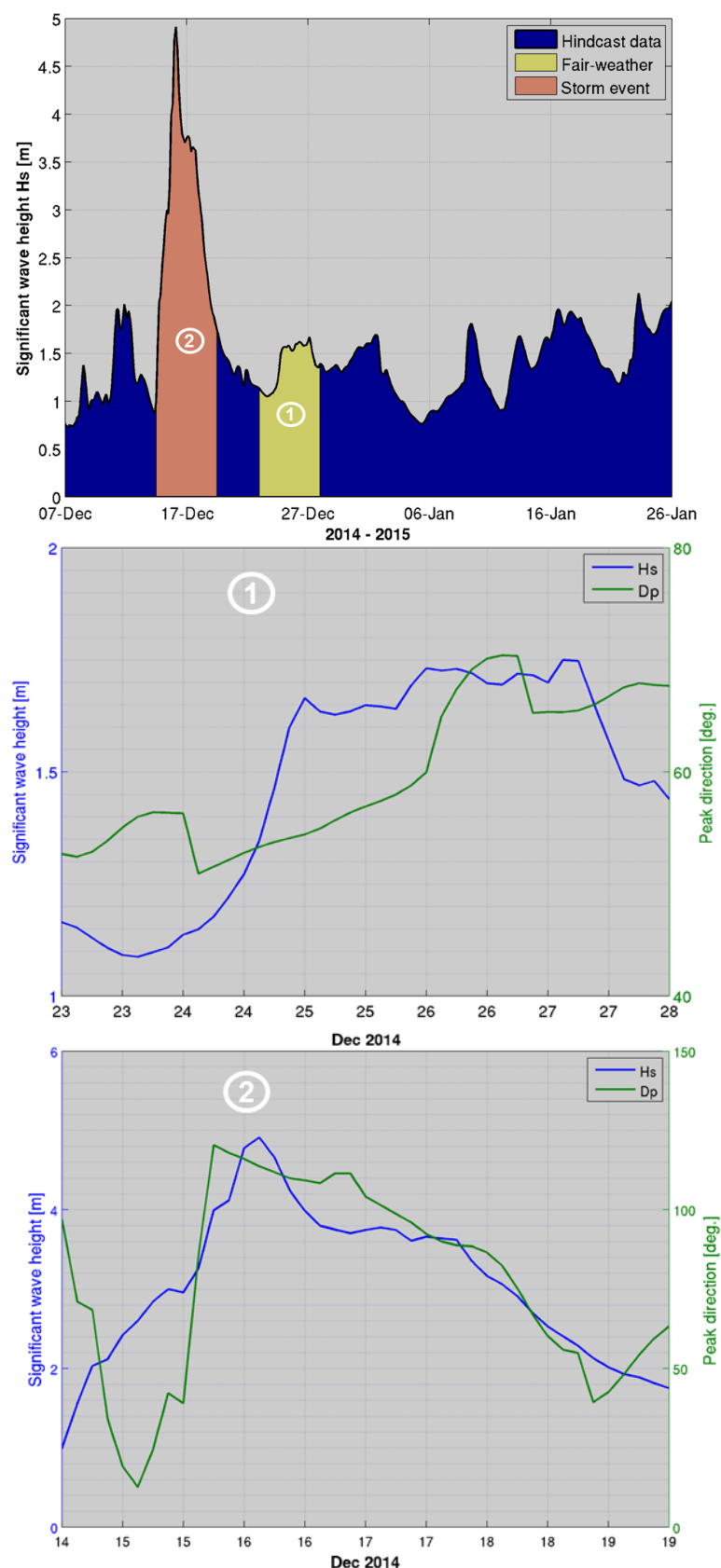


Figure 6.6 Time series of significant wave height and peak direction at location BND (see Figure 6.2) for December 2014 and January 2015. Wave conditions during periods 1) and 2) were used to simulate the sediment transport at Whangarei Harbour during fair-weather and storm conditions.

Firstly, a morphological acceleration factor (Section 6.1.3) of 45 was applied during a simulation of four days to predict the bed evolution that occurred during approximately six months of fair-weather conditions, keeping reasonably fast computations. The aim of this first run was to initialise the sediment grain size distribution over the domain. No bed level update was allowed. More details of the methodology are provided in Section 6.3.2.

In the second phase, the morphodynamic simulation during fair-weather conditions was followed by a 5-day storm simulation without any morphological acceleration ($Morfac = 1$) to avoid unrealistic changes in the bed evolution over a very short period of time due to high energy wave conditions. The distribution of sediment mass fractions characterised by a 6-month tidally dominated environment was directly fed into the subsequent storm event simulation. Note that the bed level update was turned on to reproduce the residual sediment transport, particularly around Mair Bank.

Finally, the 4-day fair weather simulation was rerun with a MORFAC 4 from the 5-day storm simulation outputs to assess the overall morphological response to a sequence of high/low wave energy events. This corresponds to the morphological evolution of 16 days.

6.3.2. Initial bed configuration and composition

The adequate initialisation of spatially varying grain size distribution of bottom sediment in a process-based model is often constrained by a lack of appropriate field data for the entire model domain. As the sea bed composition is partially dependent on the bed shear stress imposed by the local flow and wave environments, using grain-size observations as initial conditions of simulations based on the author's judgement from the limited data available generally led to unrealistic erosion or accretion patterns. Indeed, Camenen and Larroudé (2003) and Pinto et al. (2006) have shown that the physical parameter responsible for the greatest errors in the sediment characteristics is the spatial heterogeneity of grain size distributions of the surface sediment in the area of interest. In accordance, two complementary approaches were implemented to avoid this problem.

First, the conceptual models, including both the “tide-only” and the discrete wave scenarios, were set-up with a homogenous 200 μm grain size sediment layer and a fixed bathymetry to determine the sediment transport fluxes in the system. No modification of the sea bed during the simulation was allowed. Such a method is particularly helpful for giving an overview of the combined effect of the tidal and wave forcing on the seabed. It was assumed that the critical bed shear stress variability determined by the distribution of the sediment grain sizes would make a difference in the results.

The second method applied in the present study is described in Van der Wegen et al. (2011) and based on a bed composition generation (BCG) run or “morphodynamic spin-up”. A synthetic simulation was initiated with a uniform sediment type distribution over two bed layers (the active layer and the underlayer) as described in 0. This is depicted in Figure 6.7. Six sediment fractions (100, 150, 200, 300, 500 and 1000 μm) were available at 16.7% mass each according to the general distribution obtained through the sediment sampling study (Tonkin and Taylor, 2016c). The active layer had a thickness of 0.40 m and the underlayer thickness was 10 m. Note that small active layers result in a rapid coarsening of the system which tend to reduce the spin-up for a gain of computational time. Both layers were set-up with the same fractions of sediment grain size. A spatially

limited active layer including 80% of coarse gravel (>10000 μm grain size) and 20% of medium sand was defined to mimic the biomass of pipi over Mair Bank.

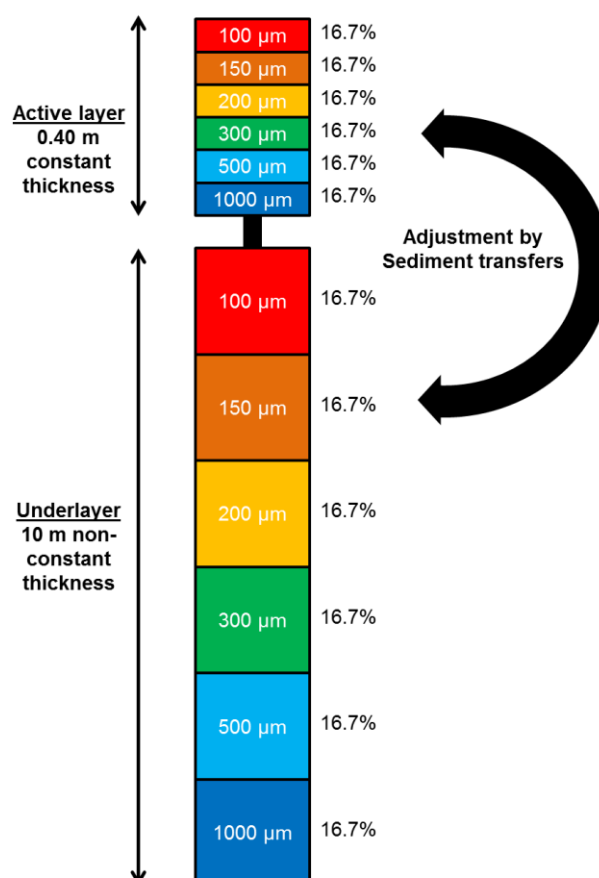


Figure 6.7 Bed stratigraphy approach implemented in Delft3D to initialise the bed composition over the domain.

During the simulation, sediment grain size fractions were redistributed vertically between layers and spatially over the domain in response to the combination of tide-induced currents and low energy wave conditions. At the end of the simulation, the bed composition converged to a more realistic sedimentological setting corresponding to the initial bathymetry, removing errors due to the initial model set-up. The BCG process rendered the model ready to investigate further morphodynamic developments.

6.4. Delft3D – FLOW hydrodynamic validation

The Delft3D – FLOW model was validated based on the measured data provided by the ADCP moving vessel deployment described in Section 5.2.1. Snapshots of measured and modelled peak ebb and flood tidal flows within zones A, B and C over the channel are provided on Figure 6.8, Figure 6.9 and Figure 6.10. Q-Q plots calculated from the measured and modelled peak ebb and flood tidal flows over these areas are presented on Figure 6.11. Note that these values are not co-temporal; the maximums were extracted from the measured and modelled period from that tidal cycle.

The validation of the depth-averaged flows indicates the model adequately replicates the complex tidal hydrodynamics at the Whangarei Harbour entrance. In

Zone A, the model represents the strong tidal flows in the channel between Marsden Point and Mair Bank. Within Zone B, the modelled current fields exhibit good overall agreement with the measured current fields between Mair Bank and the southern margin of Calliope Bank. Both peak tidal ebb and flood current speeds and directions are reasonably well replicated by the model. At Zone C, the peak ebb flows were slightly overestimated.

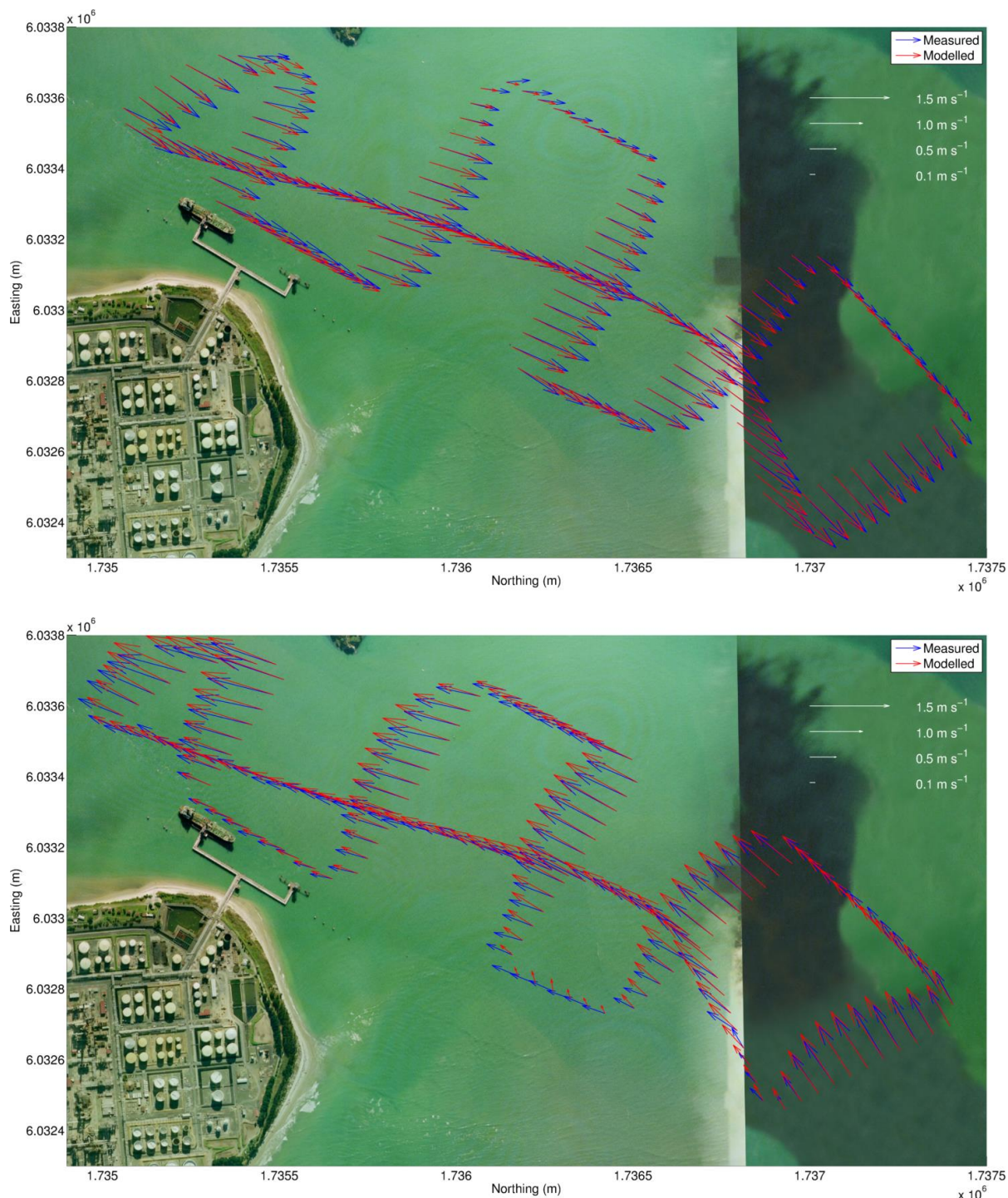


Figure 6.8 Modelled (Delft3D) and measured velocity comparisons within Zone A (Figure 5.2) for the ebb (upper) and flood (lower) tidal stages.

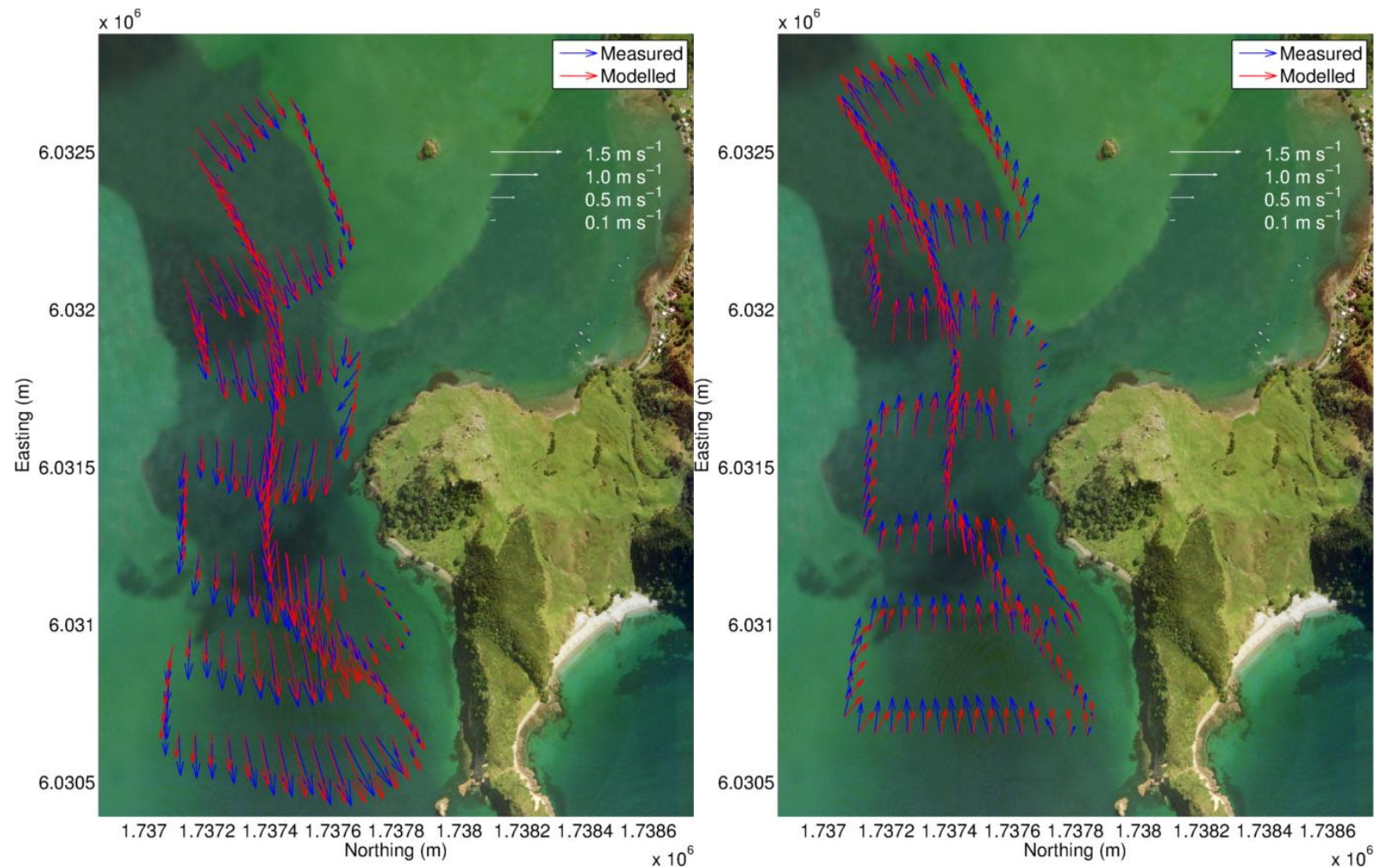


Figure 6.9 Modelled (Delft3D) and measured velocity comparisons within Zone B (Figure 5.2) for the ebb (left) and flood (right) tidal stages.

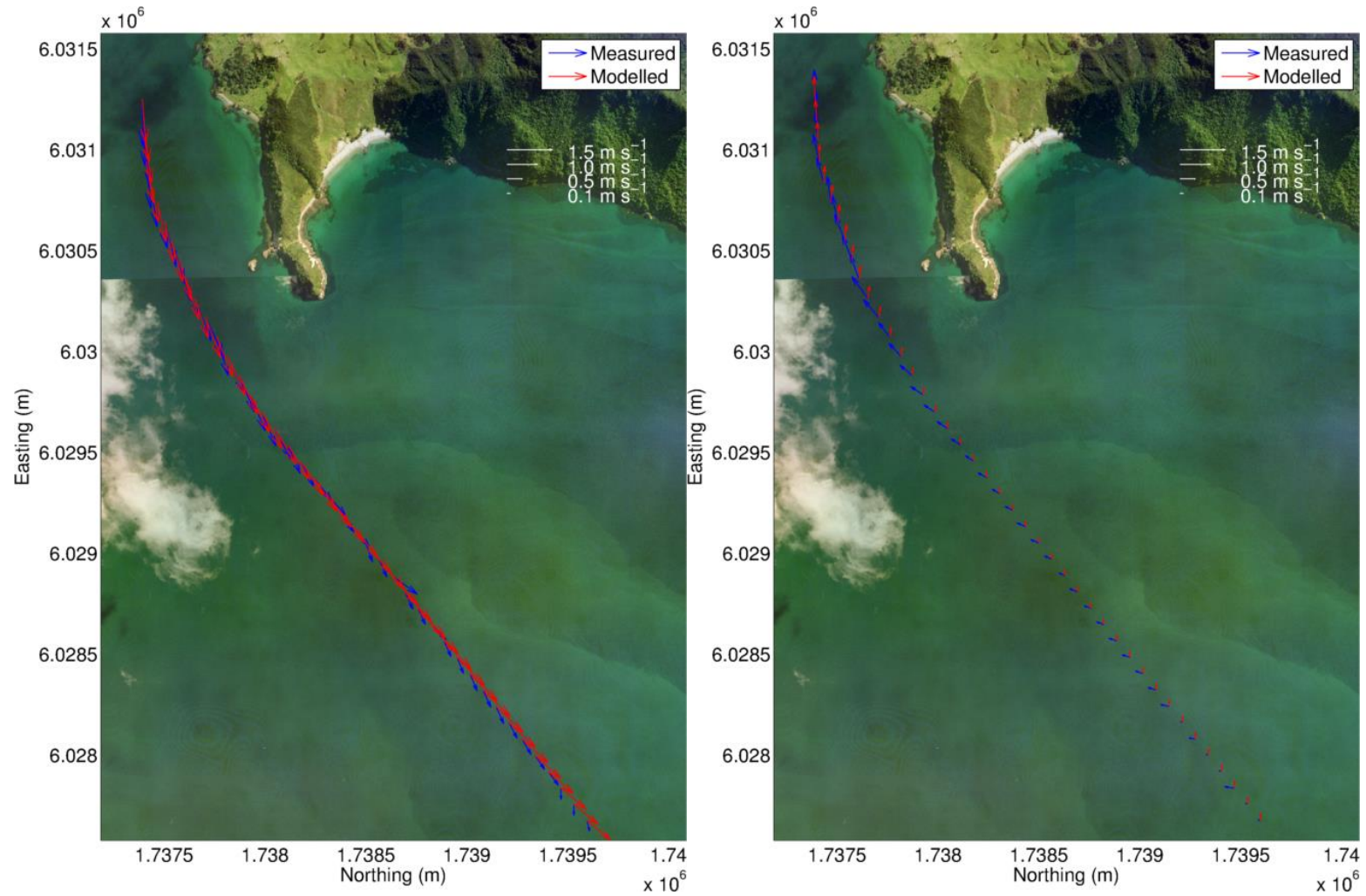


Figure 6.10 Modelled (Delft3D) and measured velocity comparisons within Zone C (Figure 5.2) for the ebb (left) and flood (right) tidal stages.

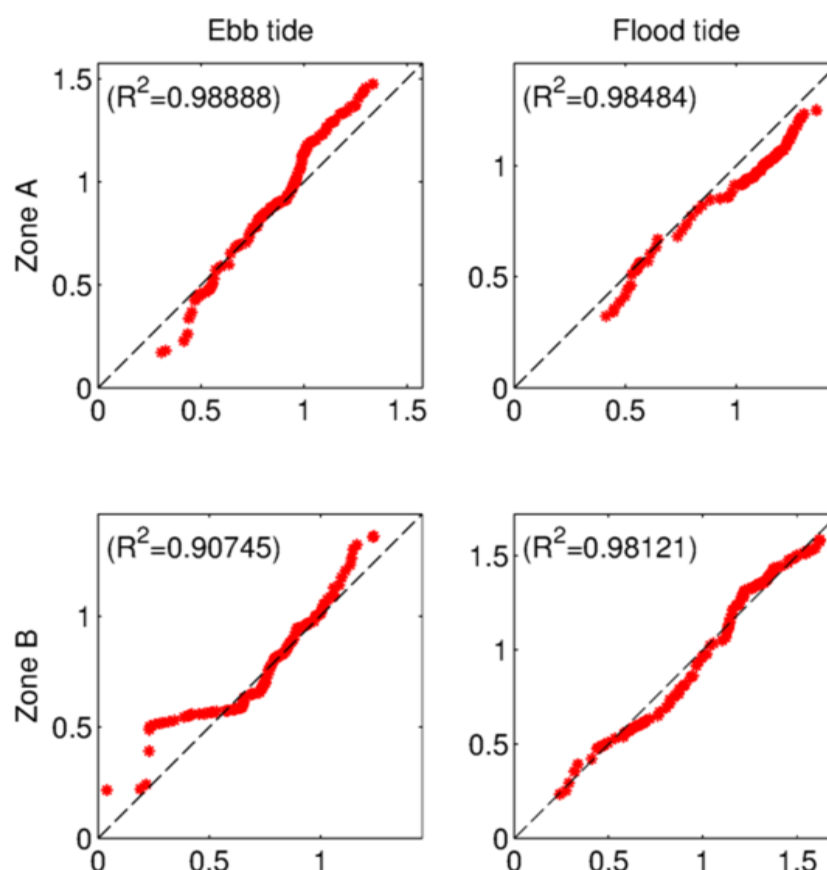


Figure 6.11 Quantile – Quantile plots of the measured and modelled (Delft3D) peak tidal ebb and flood current speed (m/s) along the vessel tracks within Zones A and B for both peak ebb and flood stages. The root mean squared errors corresponding to the different distributions are presented in the top-left corner of each plot.

6.5. Morphodynamic validation

The validation of a morphodynamic model by field observations is generally very difficult to achieve. The complexity of the morphodynamic evolution in a tidal inlet environment driven by both short-term and long-term processes requires appropriate measured data of bathymetry and sediment distribution, which should ideally be available at different time scales and for relatively large areas. Thus, the validation stage can be undertaken on a storm-induced bed evolution or on a long-term bed evolution to verify the level of agreement between the model and the measured data. Both methods provide useful information regarding the capability of the model to predict a range of morphodynamic mechanisms which control the overall tidal inlet dynamics. Analysing storm-induced bed evolution provides both calibration and a quantitative validation of the model configuration, while a long-term bed evolution study is useful in that it qualitatively characterises the overall relevance of the model.

In the present work, more than 15 years of annual bathymetric surveys over Mair Bank and within the tidal inlet channel were available. Such data is particularly valuable for the validation of the model as it describes the relative stability of the system very well. Note however that no validation of a short-term high energy event was possible as detailed pre- and post-storm data are not available. Moreover, the complex interactions between the shell fragment layers, the biomass of *Pipi* and the existing environment (both hydrodynamic and morphodynamic) made a strictly

quantitative validation of the model difficult. Therefore, the sandbar migrations and the sediment grain size distribution obtained from the BCG run were compared qualitatively to the sediment sampling (MSL Report P0297-02). Available historical bed level data and recent sediment sampling inside the tidal inlet channel (Tonkin and Taylor, 2016c; Williams and Hume, 2014) were used for this purpose.

7. DREDGE PLUME MODELLING

The action of dredging the shipping channel will produce a plume of suspended sediments while the dredger is in operation. This section describes the modelling that was undertaken to simulate the extent and duration of such a plume.

An actual release of sediment in the oceanic environment is a process that is finite in time (i.e. occurring at a specific time, over a finite period) and inherently non-deterministic (i.e. controlled by a range of random and unpredictable variables such as currents and turbulences). However, unlike the offshore sediment disposal for which a range of forcing may be significant (i.e. wind, wave, residual currents), tidal forcing dominates the navigation channel from the delta entrance to Mardsen Point, the dredging activities within which are the focus of the present section.

The cyclic nature of tides, as well as the ability to confidently predict tidal hydrodynamics with numerical modelling, simplifies the approach to obtain robust estimations of the sediment dispersion patterns. To ensure the expected variability in plume dispersions is captured; simulations are usually undertaken over two complete spring-neap tidal cycles (~ 28 days).

Patterns of the dredging plume dispersion are initially investigated at key tidal stages including peak flows during ebb and flood phases of neap and spring tides. The full spring-neap tidal cycle simulations capture the entire range of hydrodynamic forcing encountered during a cycle; model outputs were combined and further post-processed into probabilistic suspended sediment concentration (SSC) fields which provide valuable guidance on the extents and magnitudes of dredging-related plumes.

7.1. Trajectory modelling

ERcore, a Lagrangian model, developed by MSL, was used to simulate the trajectories of particles released at the various dredging sites within the channel and turning basin. The model consists of trajectory scheme applied to the existing 2D Eulerian current field (\tilde{u}, \tilde{v}) (Section 0), solving for the motion of discrete particles.

$$\begin{aligned}\frac{dx_p}{dt} &= \tilde{u}(x, y, z, t) + u_t \\ \frac{dy_p}{dt} &= \tilde{v}(x, y, z, t) + v_t \\ \frac{dz_p}{dt} &= -w_s + w_g + w_t\end{aligned}\tag{7.1 a,b,c}$$

where (x_p, y_p, z_p) are the particle coordinates, (u_t, v_t, w_t) are the diffusion components representing turbulent motions, w_s is the particle settling velocity and w_g is a vertical velocity component accounting for bathymetric gradients.

In the horizontal plane, the model uses an Ordinary Differential Equations (ODE) solver, including a 4th order Runge-Kutta method, to calculate the trajectory of a given particle (x_p, y_p) in the time-varying derivative field.

$$\int_t^{t+\Delta t} u_t \cdot dt = \sqrt{6 \cdot k_{u,v} \cdot \Delta t} \cdot \theta(-1,1)\tag{7.2}$$

where $\theta(-1,1)$ is a random number from a uniform distribution between -1 and 1, Δt is the time-step of the model in seconds and $k_{u,v}$ is the horizontal eddy diffusivity coefficient in $\text{m}^2.\text{s}^{-1}$.

In absence of specific field data on diffusive processes, the determination of the diffusion coefficient $k_{u,v}$ is generally based on guidance from empirical relationships. Several relationships are summarized in Fischer et al., 1979 including that of Elder, J.W., 1956 for simple unidirectional shear flows that estimates the longitudinal diffusion coefficient as a function of the water depth and current velocity of the form,

$$k_{u,v} = 5.93 .H .u^* \quad (7.3)$$

where H and u^* are the water depth and friction velocity respectively.

Transverse mixing can be estimated using a relationship of the same form but with reduced proportionality factor (with 50 % error bound).

$$k_{\text{transverse}} \sim 0.6 .H .u^* \quad (7.4)$$

The vertical diffusion is generally expected to be at least one order or magnitude smaller. Elder's formula suggests a vertically averaged value of :

$$k_{\text{vertical}} \sim 0.067 .H .u^* \quad (7.5)$$

Here, both depth and mean current velocities vary along the channel but these equations can still be used to provide a bracketing of reasonable diffusion coefficient values for the present application.

Assuming a generic water depth of 16 metres in the channel and a mean current velocity of 0.8 m.s^{-1} , the above equations yields coefficient of $\sim[3-5] \text{ m}^2.\text{s}^{-1}$, $[0.3-0.5] \text{ m}^2.\text{s}^{-1}$, and $\sim[0.03-0.05] \text{ m}^2.\text{s}^{-1}$ for the longitudinal, transverse and vertical diffusivities respectively.

Furthermore, in numerical models, the role of the horizontal diffusion coefficient is also to implicitly account for sub-grid scale turbulent processes such as eddies that are not explicitly resolved in the model due to the limited resolution. This means that horizontal diffusion must generally increase as grid size increases since eddies of increasing scale are unrepresented. Conversely, the reduction of grid size allows explicit resolution of flow patterns and eddies at finer scales which thereby reduce the required amount of added diffusion.

For dispersion at oceanic scales, (Okubo, A., 1971) notably showed that $k_{u,v}$ varies approximately (with wide scatter) as :

$$k_{u,v} = \alpha .L^{4/3} \quad (7.6)$$

where L is the horizontal scale of the mixing phenomena and α is an empirical proportionality factor. The hydrodynamic model resolution in Whangarei Harbour is generally less than 100 m which yields diffusion coefficient of order $0.1 \text{ m}^2.\text{s}^{-1}$. Here, the average of the longitudinal and lateral diffusivities obtained with the Elder formula yields coefficients of order $\sim 0.1-0.2 \text{ m}^2.\text{s}^{-1}$. Given results provided by the Okubo Equations, a generic diffusion coefficient of $0.1 \text{ m}^2.\text{s}^{-1}$ was eventually selected. Vertical diffusion is not expected to be the dominant process during the

descent of the disposed sediment and a small generic value of $0.0005 \text{ m}^2.\text{s}^{-1}$ was used.

The trajectory of particles in the vertical plane is controlled by the particle's settling velocity w_s , the vertical diffusion component w_t as defined in equation 7.1c, and a component w_g related to the bathymetric gradients to ensure that the trajectory of a particle close to the sea-floor is parallel to it (before settling and diffusion components are applied):

$$w_g = \frac{(h - z)}{h} \left(\tilde{u}(x, y, z, t) \times \frac{dh}{dx} + \tilde{v}(x, y, z, t) \times \frac{dh}{dy} \right) \quad (7.7)$$

where z is the particle elevation above the seabed, h is the water-column height at the particles' horizontal location (x, y) , (\tilde{u}, \tilde{v}) is the current field from equation 7.1

and $\left(\frac{dh}{dx}, \frac{dh}{dy} \right)$ are the bathymetry gradients in the x and y directions, respectively.

Note a logarithmic profile was used to extrapolate the 2D depth-averaged current magnitudes to any water column level (Smart et al., 2002).

In the present model implementation, any particle reaching the shoreline, the seabed or the outside domain boundaries remained at the position of intersection (*i.e.* 'sticky' boundaries), thus allowing no sediment re-suspension.

7.2. Particle size distribution and settling velocity

Representative particle sizes were determined from the observed sediment distribution (Tonkin and Taylor, 2016c). The particle size distribution used for the dredging and disposal plume modelling includes:

- 5% of silt (D50 = 60 μm)
- 26% of fine sand (D50 = 130 μm)
- 59% of medium sand (D50 = 400 μm)

Note that the coarse sand and gravel sediment fractions identified in sampling program were not included in the plume modelling analysis as they settle directly to the bottom and therefore do not contribute to a plume. The very low fraction of clays detected in the sampling results (approx. 0.3%) was considered below the tolerance threshold and was thus not included in the numerical modelling.

A more conservative scenario including 10% silt was tested as part of a sensitivity analysis of the plume model as well as changes to the fall velocity. Assuming 10% silt aims to simulate the case that the dredger encounters silt lenses in the substrate that have not been picked up by the vibro-core programme. Such scenario corresponds to the "worst-case scenario" in terms of plume dispersion as fine silt particles are characterised by low settling velocities making them more mobile than coarse sand particles.

Although general equations are available to compute the settling velocity of individual particles of given sizes (*e.g.* Stokes Law), it is unrealistic to assume that the sediment consists of single particles in the fine silt range ($\sim 60 \mu\text{m}$ or smaller) because of the cohesive nature of material and associated flocculation effects (*e.g.*

Van Rijn, 2007). A representative settling rate of 1 mm.s^{-1} for the flocculated sediment is applied, consistent with the findings of Whitehouse et al (2000) and Smith and Friedrichs (2011). Particle settling velocities were determined using the standard equation of Van Rijn, (1984) for non-cohesive sediment. Dry densities for the silt and sand material were set to 500 kg.m^{-3} and 1650 kg.m^{-3} , respectively. The characteristics of the 3 representative classes and relative proportion of the total volumes are summarized in Table 7.1

Note that simulations considering a settling velocity of 0.4 mm/s associated with finer silt particles were also undertaken to examine the effect of lighter particle dispersion on the plume extension.

Table 7.1 Representative median grain sizes, settling velocities, and proportions of total volume released for the 3 discrete sediment classes considered.

	Representative D50 [microns]	Settling velocity [m/s]	Percentage of total volume [%]
Class 1	60	0.0010	5
Class 2	130	0.0080	26
Class 3	400	0.0365	59

Appropriate simulation time steps were chosen to correctly capture the horizontal trajectories due to the ambient tidal and residual flows. A time step of 60 seconds was applied to ensure sufficient resolution of the vertical settling. The total number of particles released per time-step varied for each of the different size classes according to the different settling rates. This ensured a sufficient number of particles remained in suspension, taking into account the diffusion processes and allowing statistically representative concentrations to be derived. For example, a larger number of medium sand particles were released per discharge event compared to the fine sand since a greater proportion of the medium sand would settle over a given time period due to the higher settling velocities. Each sediment fraction is simulated separately and all results are combined afterwards to produce total suspended sediment concentration (SSC) fields.

7.3. Dredging scenarios

The processes by which sediment is released and suspended in the water column during dredging operations are briefly outlined in the context of the choice of the source term magnitudes and release depths for the particle tracking simulations undertaken in this study.

The dredging method likely to be used in the present case involves the use of two different types of trailing suction hopper dredgers (TSHD) (one large and one smaller), a cutter suction dredger (CSD) and a backhoe dredger (BHD).

7.3.1. TSHD

TSHD are vessel classes operating in two modes: dredging and overflow modes.

During the dredging phase, sediment is sucked into the hopper using a drag head; a fraction of the sediment disturbed by the drag head is not pumped into the hopper and remains suspended in the water column. Sediment suspension is also expected due to the action of propeller wash (Source 1 and 3 respectively in Figure 7.1). These two sources of sediment suspension form a passive plume that is expected to be contained in the bottom part of the water column. In the present

study, the drag head source was defined over the water column at 2 m above seabed, while the propeller source was set to 4 m from the seabed.

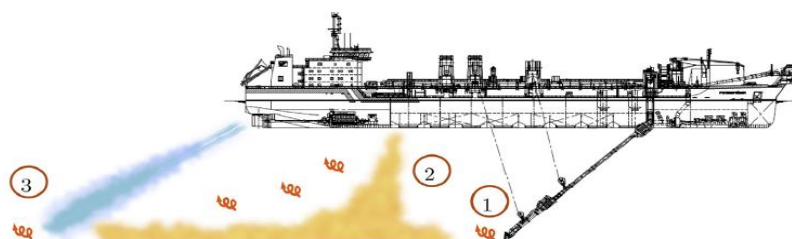


Figure 7.1 Sources of a dredge plume for a Trailing Suction Hopper Dredger: 1-Drag Head, 2-Overflow, 3-Propeller wash (after Becker J. et al., 2015).

The large and small TSHD considered for the present project are characterized by an average dredge work rate of 5400 m³/hour and 1050 m³/hour, respectively. Release rates of 6.15 kg.s⁻¹ (1.5% production rate) and 12.3 kg.s⁻¹ (3% production rate) were used for the drag head source term in the case of the small TSHD. For the large TSHD, values of 31.15 kg.s⁻¹ and 62.3 kg.s⁻¹ were applied.

The propeller wash component depends on many factors that are likely to vary in time and space (i.e. grain size, draft between prop and seabed, horsepower of dredger, angle of dredger relative to the ambient current etc) and is often included in the term related to overflow (Becker J. et al., 2015). For the purposes of this study, the propeller wash source term is considered separate to the overflow, and defined with rates of 25 and 80 kg.s⁻¹ for the small and the large TSHD, respectively, which is considered conservative but not unrealistic for these environs. This initial “dredging phase” will continue until the hopper is full and is expected to last up to 25 minutes in the present application.

After the initial hopper infilling, the actual content of the hopper is a sediment/water mixture which is expected to contain ~20% solids by volume (Spearman, J. et al., 2007). To maximize the amount of sediment in the hopper, the vessel can continue to pump sediment and water into the hopper, which will result in “overflowing” and thereby releasing some sediment into the water column. This phase is referred to as the “overflow phase”, and is shown as the source “2” in Figure 7.1. Depending on how the dredge is operated, the overflow rates can create highly-evident sediment plumes.

The overflow load consists of a highly concentrated mixture of sediment and water and the bulk behavior of that sediment mixture becomes dominant over the individual particle settling processes (Winterwerp, 2002). As a result, it is expected that the overflow release will be followed by a dynamic plume phase where the sediment mixture descends to the bottom as a jet-like feature, and impacts the seabed, suspending sediment and forming an initial density driven near-field plume. A fraction of the sediment load will also be de-entrained from the dynamic plume during descent and become suspended in the water column. This is comparable to processes involved during the offshore disposal presented in Section 8 (see Figure 8.1).

The general length scales expected for the overflow process are an order of magnitude smaller than the discharge of sediment at the offshore disposal ground.

Additionally, the overflow sediment mixture is less concentrated than in an offshore sediment disposal context. In the present study, this overflow phase was modelled considering two sources of sediment to the passive plume:

- Suspension of sediment de-entrained from the dynamic plume descent uniform released within the entire water column, and
- Passive plume generated following the dynamic plume impact: release within a cylinder of 2 m height and 60 m radius on the seabed (representing the boundary between the dynamic plume collapse and the passive plume). Sediment releases within cylinders of 2 m height and 100 m radius, and 4 m height and 60 m radius related to the large TSHD were also tested to assess the effect of larger release areas on the plume extension.

The release rate of the initial total raw overflow was taken as 63 kg.s^{-1} and 20 kg.s^{-1} for the large and the small TSHD, respectively.

In the present application, a fraction of 25% was considered appropriate for the sediment source term released within the entire column (i.e. sediment suspension due to dynamic plume descent). A similar proportion of 25% was used for the amount of the overflow load found in the bottom source release, i.e. resulting from the density current following the dynamic plume impact (see Figure 7.2). The impact of that overflow phase was tested considering overflow period times of 10, 20, and 50 minutes for both the small and the large TSHD. Maximum overflow period of 79 and 95 minutes were additionally tested for the large and the small TSHD respectively.

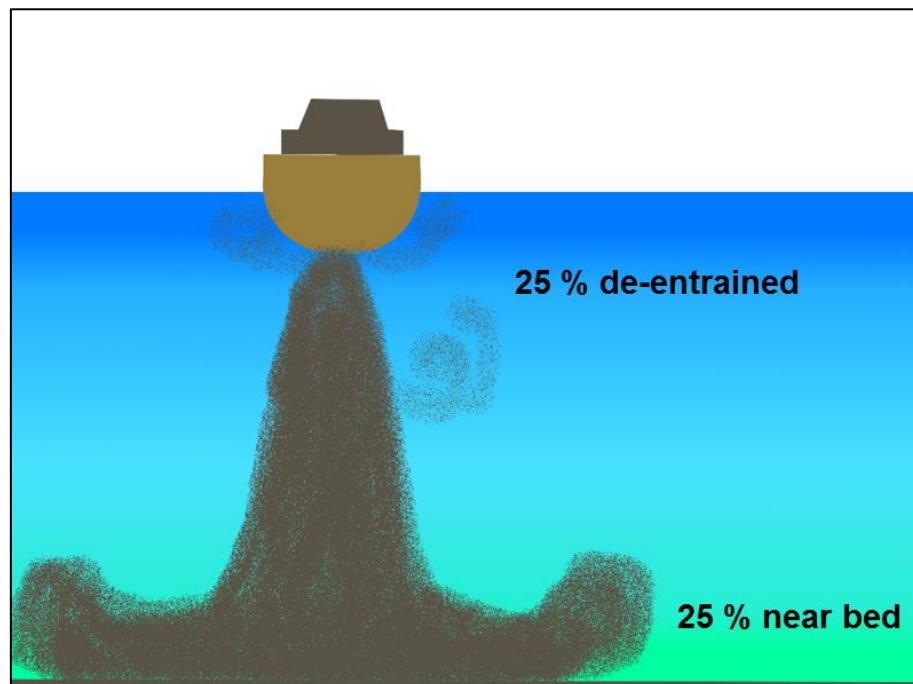


Figure 7.2 Percentages of sediment transferred from the near-field density driven plume to the far-field plume during overflowing

7.3.2. BHD

A BHD (Figure 7.3) is a stationary mechanical equipment, anchored by spuds and usually used for the dredging of small volumes in confined areas. The release mechanisms from a BHD include three main components:

- impact and excavation
- hoisting
- slewing to the barge

The release of sediments associated with a BHD varies with operator expertise and the use of open or closed buckets. A realistic discharge rate corresponding to the bucket source term was defined in Becker et al. (2015) as between 0 – 4 % of the production rate. For dredging at the jetty pocket area three BHD are considered, with production rates ranging between 270 – 475 m³.h⁻¹. At a realistic, but conservative production rate (i.e. 500 m³.h⁻¹), this corresponds to a discharge rate 8 kg.s⁻¹ released through the entire water column

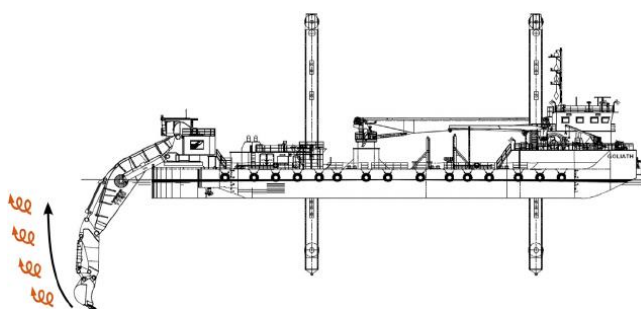


Figure 7.3 Source of a dredge plume for a Backhoe Dredger (after Becker et al., 2015).

7.3.3. CSD

The dredging operations associated with a CSD (Figure 7.4) include two simultaneous phases:

- The (hard) sediments are cut and fragmented by a rotating cutter head using different rotation and swing speeds.
- Sediment is sucked up by dredge pumps, and typically discharged through floating pipeline and pipes to a deposit area.

The sediment release mechanisms are thus largely associated with the rotating cutter head action and are located near the seabed. A fraction of the fragments are expelled during the fragmentation while the turbulence induced by the centrifugal force result in the suspension of sediments around the cutter head.

Although the corresponding sediment source term depends on specific parameters including the cut height and step length, the cutter head rotation and swing speeds, and the suction velocity, discharge rates are typically in the order 1 – 5% of the production rate (Becker et al., 2015). For this project, the CSD was characterised as having an average dredge work rate of 1600 m³.h⁻¹. The resultant sediment discharge associated with the cutter head source term in the plume model was thus taken as 31 kg.s⁻¹ near the seabed, based on a 5% conservative discharge rate. Note that CSDs are usually fitted with spuds which increase their precision and avoid any suspension of sediments associated with the propeller wash (e.g. Figure 7.4).

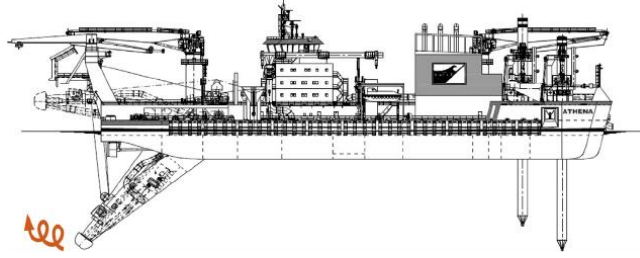


Figure 7.4 Source of a dredge plume for a Cutter Suction Dredger (after Becker et al., 2015).

The use of a CSD for the dredging operations at the jetty pocket and within the inner section of the channel is not the preferred option of RNZ, this dredger has been tested in the present study for completeness in case it's required as an option.

7.4. Post-processing

The results of the 28-day particle tracking simulations were post-processed to produce maps of the instantaneous and probabilistic suspended sediment concentration fields. The probabilistic approach aimed to provide sufficient statistical power (capturing the effect of the monthly tide variability) to investigate the 3D plume dispersion associated with the sediments released by the dredging operations. This process, which is statistically more robust than a case by case approach, nevertheless requires a significant computational runtime. In the model, sediments are released continuously for 28 days, allowing consideration of two complete spring / neap tidal cycles.

The general methods employed to reconstruct concentration fields from the particle tracking model outputs are outlined below.

7.4.1. Concentration and depositional thickness computation

To reconstruct concentrations from the particle tracking simulations at chosen receptors, a kernel method with variable bandwidth was used. The use of a variable bandwidth (kernel size) attempts to represent true variability of spatial concentration, while minimizing statistical variability that inevitably occurs away from the source due to a necessarily finite number of particles. A small kernel is used in regions gathering a high number of particles, where it is statistically appropriate to infer relatively small scale changes in concentration. Conversely, a larger kernel is used in regions presenting a low number of particles, so as to prevent unrealistically high concentrations around the precise (but partially random) locations of a few isolated particles.

In practice, the concentration C at a given receptor location (x,y) is computed as:

$$C(x, y) = \sum_{i=1}^n \frac{m_i}{\lambda_x(x, y) \lambda_y(x, y)} K\left(\left|\frac{x_i - x}{\lambda_x}\right|\right) K\left(\left|\frac{y_i - y}{\lambda_y}\right|\right) \quad (7.8)$$

where (x_i, y_i) is the location of each particle i , n is the total number of particles, m_i is the loading for each particle, λ_x and λ_y are the kernel bandwidth in the x and y directions for location (x,y) and K is the kernel function.

Following Vitali et al. (2006), an Epanechnikov kernel function was used:

$$K(q) = \begin{cases} 0.75(1 - q^2), & |q| \leq 1 \\ 0, & |q| > 1 \end{cases} \quad (7.9)$$

where q is the ratio of the particle distance from receptor to bandwidth ($q_x = d_x / \lambda_x$, or $q_y = d_y / \lambda_y$).

A receptor-based method derived from the RL3 method in Vitali et al. (2006) was used to define the bandwidths λ_x and λ_y .

For each receptor location, a neighborhood was defined as the region enclosing the 1/20th closest particles. Then, for each direction x and y , the bandwidths λ_x and λ_y were defined as the minimum value between the maximum projected distance of the particles within the neighborhood and twice the standard deviation of the projected distances within the neighborhood. Finally, in order to prevent unrealistically elongated kernels, the aspect ratio λ_x / λ_y was limited to be no greater than 5:1, with the smaller value increased.

The loading of each particle directly depends on the quantity being modelled. Here, each discrete particle was attributed a certain sediment mass which was determined as the ratio from the total true sediment volume of a given class released per step, to the total number of particles of that class introduced in the model at each release.

7.4.2. Application to the present study

Sediment concentration fields were determined following the methods outlined above for the suspended particle cloud associate with each sediment class. The individual sediment concentration fields were then combined to produce total SSC magnitudes considering all sediment classes. The particle load governs the concentration magnitudes and is a function of the amount of sediment released into the environment and the number of particles modelled. The predicted suspended sediment concentrations should be interpreted as dredging-related SSC only, and would add to any ambient SSC from other sources, such as river inputs or catchment run-offs.

7.5. Sites for dredge plume modelling

Nine sites along the navigation channel were used to simulate the dredge plume dispersion. The maps of peak ebb and flood tide flows over the channel (presented in MSL Report P0297-02) shows limited spatial variability in current velocities within each proposed dredged area. Using a limited number of points over the channel to perform the dredge plume modelling was thus justified in the present study. Locations and water depths associated with the different sites are presented in Table 7.2 and Figure 7.5.

The plume modelling at positions R0 to R8 was undertaken using the existing hydrodynamic fields from the SELFIE model. Note however that hydrodynamic conditions at positions R2, R3 and R8 were derived from both the existing and the post-dredging configurations to assess the impact of changes in the hydrodynamic field on the plume dispersion.

Table 7.2 Depths and depth changes of release sites along the dredged channel.

Positions	Existing depth [m]	Depth_{post-dredging} – depth_{existing} [m]
R0	12.4	5.3
R1	16.3	2.1
R2	15.0	3.7
R3	15.2	4.4
R4	16.5	3.5
R5	16.7	3.8
R6	16.2	2.7
R7	17.2	1.1
R8	17.8	0.5

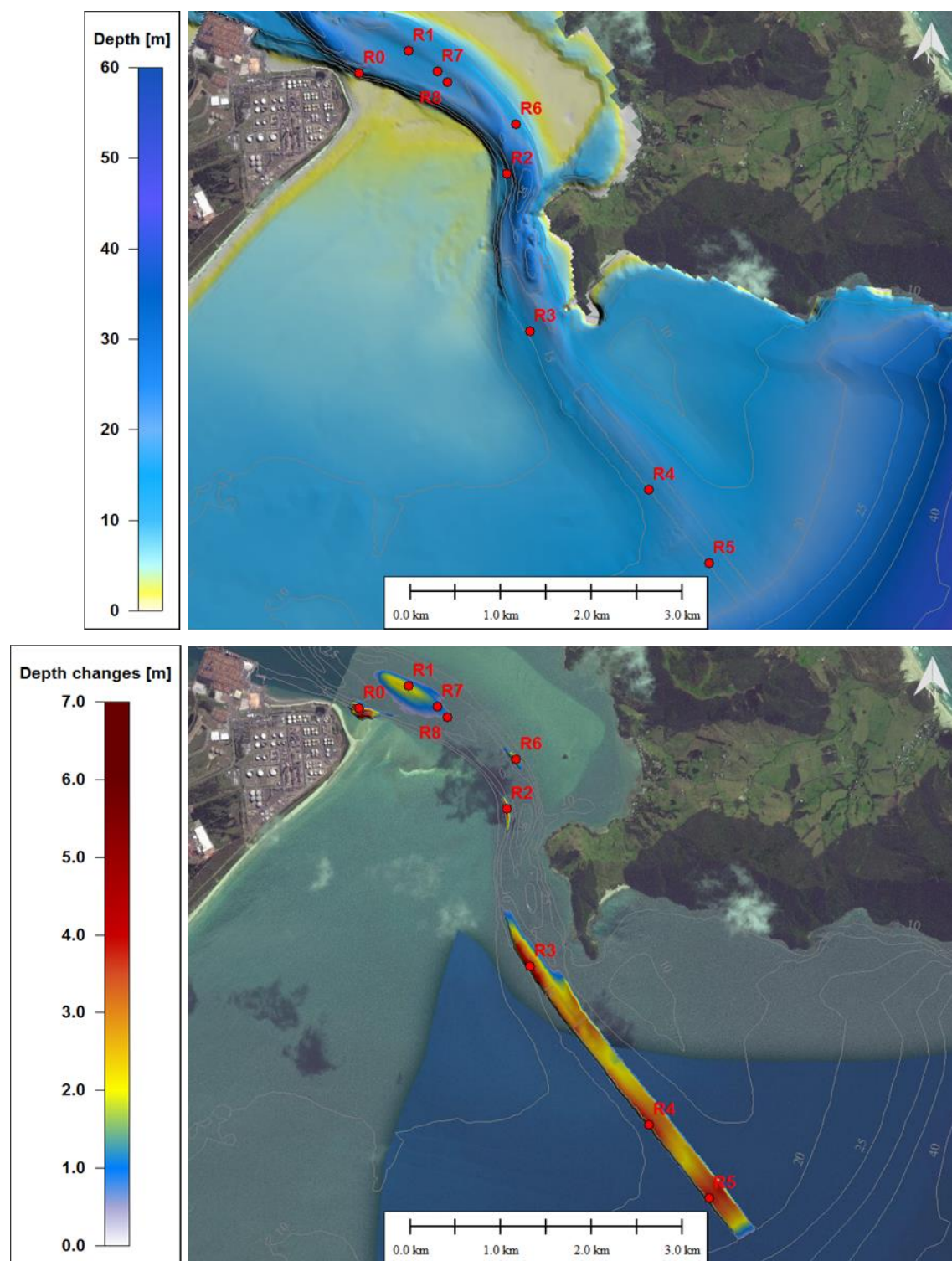


Figure 7.5 Simulated release sites along the dredged channel. Existing depth and depth changes are provided in Table 7.2. Geographic coordinates are presented in Appendix B.

8. DISPOSAL PLUME MODELLING

The placement of the dredged material over the proposed disposal areas is expected to produce a temporary plume of sediments in the water. The behaviour of this plume is driven by both the sediment grain-size distribution and the local hydrodynamics which control both the vertical and horizontal transport. In this context, a probabilistic approach was used to anticipate the plume dispersion under several hydrodynamic conditions.

This section presents the methodology applied, and the different scenarios considered, to assess the disposal plume dispersion.

8.1. Trajectory modelling

ERcore, the Lagrangian model used for the dredge plume modelling (Section 7) was applied to simulate the disposal plume in Bream Bay. The existing 2D Eulerian current field for the trajectory modelling was derived from the 10-year ROMS hindcast (Section 4) to ensure both residual and tidal current velocities were considered. This was chosen based on the importance of the non-tidal component of the current in the eastern region of Bream Bay characterised by increasing depths. In contrast, the hydrodynamic conditions used for the dredge plume modelling (Section 7) included only the tidal component which dominates the entrance region. A different vertical diffusivity was used for the disposal plume modelling, with a value of $0.0001 \text{ m}^2\text{s}^{-1}$ chosen due to increasing water depths and decreasing current velocities compared to the navigation channel. The parameters for the trajectory modelling described in Section 7.1 were conserved, except those previously cited above.

8.2. Simulated scenarios

8.2.1. Sources terms

The processes by which sediment is released and suspended in the water column during disposal operations are briefly outlined here in the context of the choice of the source term magnitudes and release depths for the particle tracking simulations.

In the case of silt to fine sand, the content of a loaded dredge consists of a highly concentrated mixture of sediment and water and the bulk behaviour of that sediment mixture becomes dominant over the individual particle settling processes. When the dredge opens its bottom door for release, the contents will typically be released as a jet-like sediment flux quickly descending to the seabed. The behaviour of the released sediment can be separated in the three main phases illustrated on Figure 8.1.

During the convective descent, the dense sediment material quickly descends to the bottom. Ambient water can become entrained around the perimeter of the jet which can strip, or de-entrain some sediment, which becomes suspended in the water column. The proportion lost is expected to be small, commonly cited as 1-5% of the disposed load (Bokuniewicz et al., 1978; Bokuniewicz and Gordon, 1980; Gordon, 1974; Truitt, 1988).

Following its descent, the dredge material collapses on impact with the seabed; this phase is known as the dynamic collapse phase. The collapse results in a large fraction of the disposed sediment depositing on the seabed and is often coupled to

the generation of the density current generated by the excess energy available following collapsing, whereby a fraction of the disposed sediment is suspended and propagates radially from the point of impact. The density current is expected to be contained within the bottom 15-20% of the water column, with excursion length scales of order 100-500 m (e.g. Aarninkhof and Luijendijk, 2010).

These two initial phases relating to the dissipation of the initial plume momentum are also referred to as dynamic plume stage (e.g. Spearman et al., 2007). The passive dispersion phase relates to the subsequent dispersion of the sediment that became suspended in the water column during the dynamic phase, i.e. de-entrained during descent, sediment entrained during the collapse of the dynamic plume, and sediment suspension by the density current developing near the seabed.

In the present study, the focus is on characterising the extents and concentrations of the plume resulting from this passive dispersion phase, as these plumes have the potential to effect order of magnitude greater spatial extents than the dynamic plume (which settles quickly). In that respect, the particle tracking simulations considered two main source terms:

- A. De-entrained sediment during descent – release at the bottom of the vessel used for disposal as a point source.
- B. Entrained sediment resulting from the collapse of the dynamic plume - release within a cylinder near the seabed of given height and radius.
- C. Surface sediment losses - release within the top layer of the water column (from the sea surface to bottom of vessel hull)

Note a degree of conservatism is introduced by releasing the sediment de-entrained from the descending plume at the vessel bottom rather than distributed within the water column, as these sediments have further to fall. The present application also considered an additional sediment source released at near-surface, representative of sediment which, in the unlikely event, is entrained vertically around the hull of the dredger due to turbulence associated with the discharge of sediment.

Entrained sediment resulting from the collapse of the dynamic plume (B above) was simulated assuming 20% of the discharged sediment enters the passive plume phase. This entrained sediment was distributed within a circular volume of 100 m radius and a 2 m height centred on the discharge location. This was combined with the mid-water and near surface release source terms (i.e. de-entrained and surface loss) which were assumed to consist of 5% and 0.5% of the disposed load respectively (see Figure 8.2).

The use of ratios for the proportion of sediment involved transferred in the passive plumes due to de-entrainment during descent and other losses near the surface (i.e. 5 and 0.5% respectively), is a relatively simplistic approach. Sensitivity testing of the ratio suggests it does not significantly alter the predicted SSC magnitudes, particularly in the surface.

The release depths for the source terms and total discharged volumes were varied according to the dredge being simulated (i.e. for the large and small dredge). Details of the dredging vessels are summarized in Table 8.1 and associated source terms are given in Table 8.2.

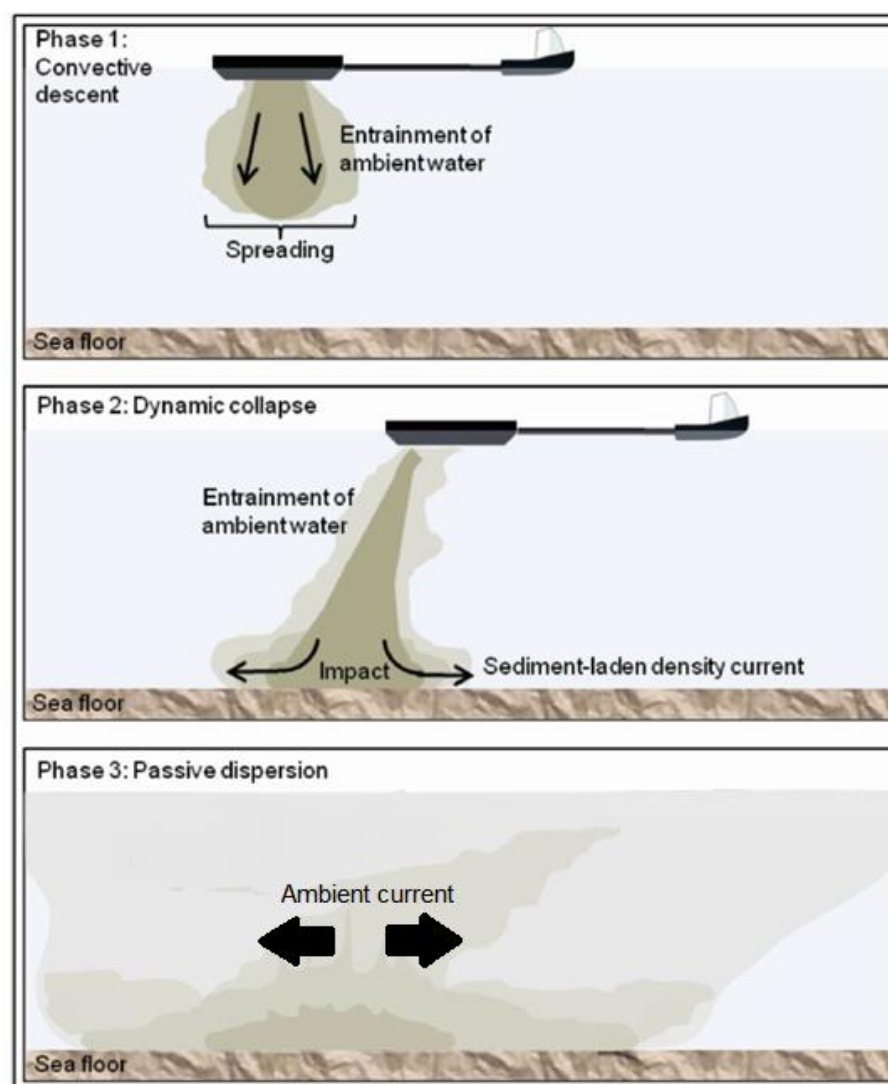


Figure 8.1 Three main phases occurring during the disposal of dredged material: 1) convective descent, 2) dynamic collapse, and 3) passive plume dispersion.

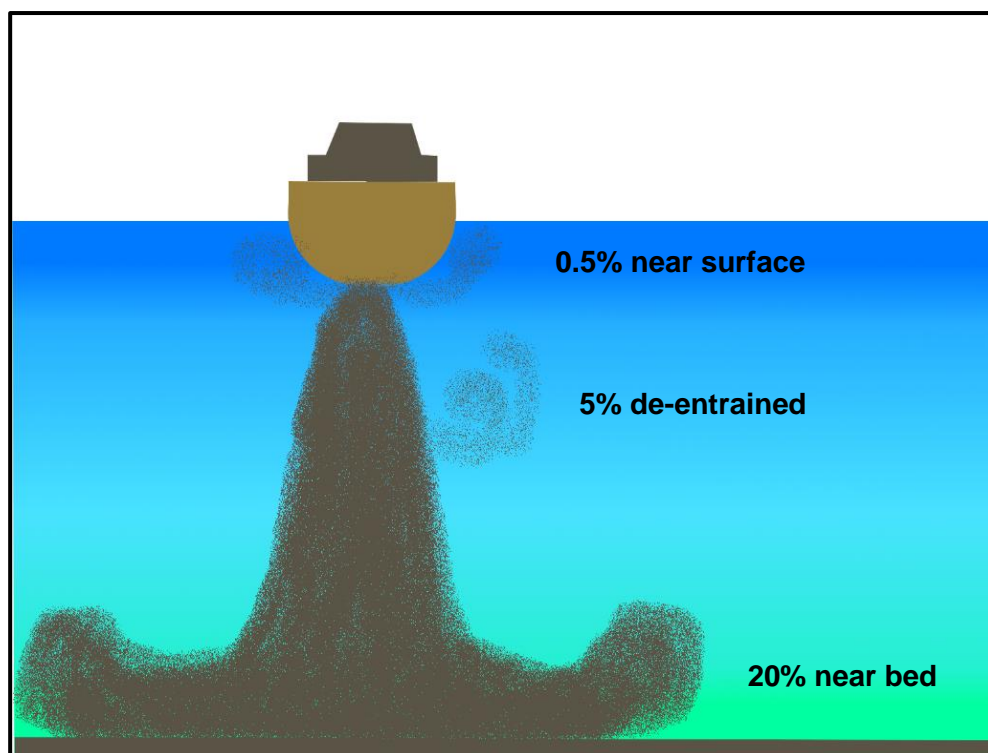


Figure 8.2 Percentages of sediment transferred from the near-field density driven plume to the far-field plume.

Table 8.1 Details of the dredging vessels likely to be used for dredging and disposal works.

Vessel	Hopper load [m3]	Draft [m]	Disposal load [min]
Large	10,830	-9.5	10
Small	2,130	-5.6	10

Table 8.2 Source terms and release depths.

Sources Terms	Percent of hopper volume	Release depth	Release type
Surface losses	1%	sea-surface to vessel draft	point source
De-entrained during descent	5%	vessel draft	point source
Density current	21%	2 m layer above seabed	100 m radius circle

8.2.2. Sediment distribution and settling velocity

The particle size distribution of the sediment to be disposed was conserved from the sediment distribution used for the dredge plume modelling. It includes three sediment fractions of silt (60 μm), fine sand (130 μm) and medium sand (400 μm). The coarse sand and gravel sediment fractions identified in the sampling results were not included within the disposal plume modelling as they directly settle to the bottom.

The particle size distribution and associated fall velocity of the sediment discharged at the proposed disposal site was identical to that of the distribution simulated during the dredging operations (see Table 7.1). The coarse sand and gravel sediment fractions identified in the sampling results were not included within the disposal plume modelling as they are expected to directly settle to the bottom.

8.2.3. Release sites and events

Five sites were considered for the discharge of dredge material (see Figure 8.3, Appendix C and Appendix B); one at each corner of the disposal and one in the centre where measured current data was collected using an ADCP current profiler.

The dispersion model was run for two discrete periods during which the hydrodynamic conditions were representative of the expected range at the disposal site, including strong west-directed currents at surface and bottom levels, respectively. This last scenario is considered as “worst case scenario” due to the location of 3 Mile Reef from the disposal area 3.2.

These discrete short-term simulations were also supplemented by two 1-month periods during summer and winter months (i.e. January and August, 1995 see Table 8.3). For the historical simulations, discharges were simulated at 140 minutes and 185 minutes interval for the large and small TSHD, respectively. These intervals were estimated based on the periods of dredging, overflow, travel and disposal.

The long-term simulation of the plume dispersion over a 6-month period assumed continuous release of sediment throughout the period, allowing statistical analysis of the predicted plume concentrations and extents. The choice of the modelling period was motivated by the necessity to consider a large range of weather conditions without increasing dramatically the computational runtime. Simulating plumes from the near-bed, near-surface and de-entrained from the dynamic phase of the plume descent for each of the representative grain sizes, while computationally expensive, provides the necessary information to allow realistic climatic and representative statistical measures of the predicted plume extents.

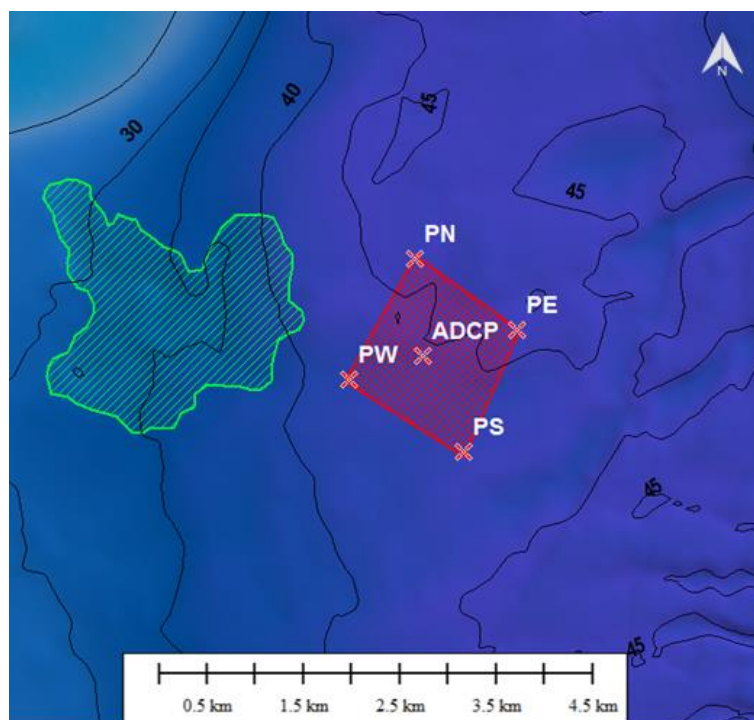


Figure 8.3 Location of the sites over the disposal ground used for the release of particles as part of the disposal plume modelling. The green polygon indicates the contour of a reef classified as sensitive.

Table 8.3 Summary of simulation periods.

Disposal simulations	Period
Strong west-directed current on surface	10/12/1995-12:00
Strong west-directed current near bottom	06/02/1995-12:00
Summer hydrodynamic conditions	January (1995)
Winter hydrodynamic conditions	August (1995)

9. DISPOSAL GROUND MODELLING

This section describes the numerical modelling that was adopted to estimate the long-term dynamics of the proposed disposal grounds 1.2 and 3.2 (see Figure 1.4) for the placement of maintenance and capital volumes, respectively. The present work aims to provide solid information regarding the predicted effect of the disposal mound on the physical and ecological components of the coastal system in Bream Bay. Main expected outcomes are listed below:

- Estimation of the degree of stability of the disposal mound under a range of wave and tidal forcing.
- Prediction of the magnitudes of the sediment transport over adjacent areas.
- Identification of potential ecological harm related to the transport of large amount of disposed sediments.
- Impact of the depth changes on the wave climate in Bream Bay and adjacent beaches associated to the disposal of material.

9.1. Modelling approach

The Delft3D model was implemented to predict the disposal ground dynamic using an input reduction approach. A limited number of representative forcing conditions (including tides, waves, residual currents and residual water elevations) was used to reproduce the long-term residual sediment transport patterns and associated morphological evolutions. This methodology was combined with the application of morphological acceleration factors (MORFAC) based on the occurrence of each scenario to improve computational efficiency by acceleration computed morphological evolution. Details about the input reduction approach and corresponding references are provided in Section 6.3.1.

Outcomes of the consultation process involving RNZ and the relevant experts resulted in the identification of two offshore disposal sites referenced as Disposal Sites 1.2 and 3.2. At Disposal Site 3.2 it is intended to place up to 97.5% of the capital dredge volume and up to 100% of the maintenance dredge volume. Although the capital dredge volume for this area is estimated at 3.7 million m³, a 4 m high disposal mound was set-up over a proposed 2 km² area - equivalent to a total volume of 8 million m³. This conservative approach aimed to consider both the total capital dredge volume and the maintenance dredge volumes accumulated over 35 years based on a stable disposal mound. The effect of the disposal mound on the wave climate within Bream Bay was assessed based on the wave modelling of the 16 representative scenarios presented in Section 6 (see Table 6.1) including both the pre-disposal and the post-disposal bathymetries in the model.

Disposal Site 1.2 is intended to receive 2.5 – 5% of the capital dredge and up to 100% of the maintenance dredge volume. The assessment of the nearshore disposal dynamics was undertaken based on the numerical modelling of a representative value for a low mound, which was taken to be a 0.6 m high disposal mound (1.5 million m³) defined on the ebb tide delta.

This corresponds to a conservative approach considering 5% of the capital dredge volume and 100% of the maintenance dredge volume accumulated over 10 years. The relative low water depth (less than 10m) of the Disposal ground 1.2 is expected to make the mound morphologically unstable with a relative high rate of erosion per annum. In this context, considering 35 years of accumulation of sediments (as for the Disposal ground 3.2) for a total volume of 4.3 million m³ would have been largely unrealistic. The 1-year disposal ground dynamics for disposal sites 1.2 and 3.2 were simulated using a sequence of 16 representative scenarios (Table 6.1). The modelled sediment thickness and depth changes obtained at the end of each scenario were used for the initialisation of the next one.

The distribution of sediments used to characterise the disposal mound composition included five classes according to the results of the vibrocoreing (Tonkin and Taylor, 2016c):

- 5% of silt (D50 = 60 µm)
- 26% of fine sand (D50 = 130 µm)
- 59% of medium sand (D50 = 400 µm)
- 4% of coarse sand (D50 = 1300 µm)
- 6% of gravel (D50 = 2000 µm)

9.2. Model domains

The Delft3D – FLOW domain includes the whole of Bream Bay from Bream Head to Langa Beach. To the North, the grid extends to Busby Head excluding Mair Bank and the Whangarei Harbour entrance (Figure 9.1). The resolution of the hydrodynamic/morphologic model grid ranges between 35 and 180 m, with higher resolution focused over the proposed disposal grounds. Delft3D – WAVE model was implemented on the same high-resolution curvilinear grid than Delft3D – FLOW. However, a nesting approach was implemented, including a coarser grid (Figure 9.2) to correctly reproduce the spectral wave transformation during the propagation of wave energy from deep to shallow water.

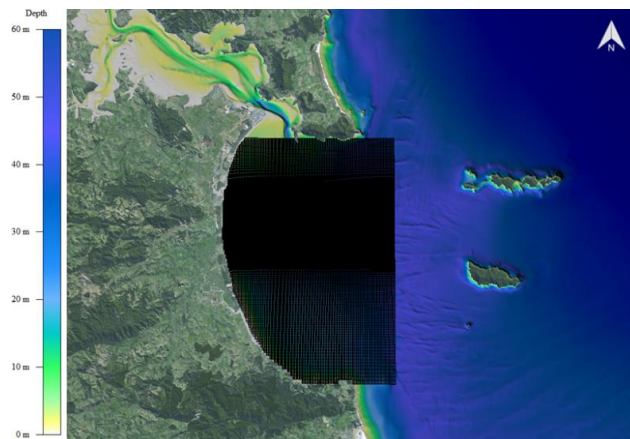


Figure 9.1 Bathymetry and Delft3D – FLOW model grid for the proposed disposal ground modelling.

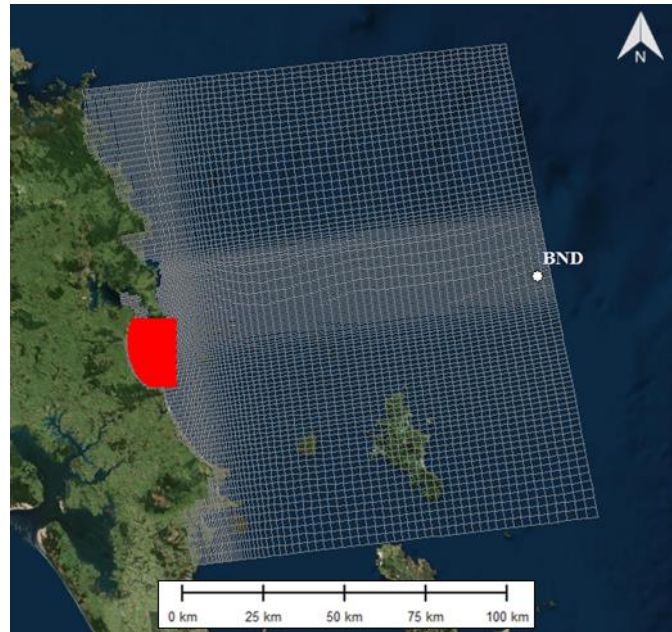


Figure 9.2 Delft3D –WAVE model grid for the proposed disposal ground modelling. Location (BND) for representative wave climate is shown at the centre of the eastern boundary.

REFERENCES

- Aarninkhof, S., Luijendijk, A., 2010. Safe disposal of dredged material in an environmentally sensitive environment. *Port Technol. Int.* 47, 39–45.
- Ardhuin, F., Rascle, N., Belibassakis, K.A., 2008. Explicit wave-averaged primitive equations using a generalized Lagrangian mean. *Ocean Model.* 20, 35–60. doi:10.1016/j.ocemod.2007.07.001
- Ardhuin, F., Roland, A., 2013. The development of spectral wave models: coastal and coupled aspects, in: *Proceedings of Coastal Dynamics*. p. 7th.
- Bagnold, R.A., 1966. An approach to the sediment transport problem. *Gen. Phys. Geol. Surv. Prof. Pap.*
- Becker J., van Eekelen E., van Wiechen J., de Lange W., Damsma T., Smolders T., van Koningsveld M., 2015. Estimating source terms for far field dredge plume modelling. *J. Environ. Manage.* 149, 282–293.
- Bennis, A.-C., Ardhuin, F., Dumas, F., 2011. On the coupling of wave and three-dimensional circulation models: Choice of theoretical framework, practical implementation and adiabatic tests. *Ocean Model.* 40, 260–272. doi:10.1016/j.ocemod.2011.09.003
- Black, K.P., 1983. *Sediment Transport and Tidal Inlet Hydraulics*. Hamilton, New Zealand: University of Waikato. Ph. D. thesis, 331p.
- Bokuniewicz, H.J., Gebert, J., Gordon, R.B., Higgins, J.L., Kaminsky, P., 1978. *Field Study of the Mechanics of the Placement of Dredged Material at Open-Water Disposal Sites. Volume I. Main Text and Appendices A-1*. DTIC Document.
- Bokuniewicz, H.J., Gordon, R.B., 1980. Sediment transport and deposition in Long Island Sound. *Adv Geophys. States* 21.
- Booij, N., Ris, R.C., Holthuijsen, L.H., 1999. A third-generation wave model for coastal regions: 1. Model description and validation. *J. Geophys. Res. Oceans* 104, 7649–7666. doi:10.1029/98JC02622
- Brown, J.M., Davies, A.G., 2009. Methods for medium-term prediction of the net sediment transport by waves and currents in complex coastal regions. *Cont. Shelf Res.* 29, 1502–1514.
- Camenen, B., Larroudé, P., 2003. Comparison of sediment transport formulae for the coastal environment. *Coast. Eng.* 48, 111–132.
- Collins, J., 1972. Prediction of Shallow Water Spectra. *J. Geophys. Res.* 77, 2693–2707.
- Dastgheib, A., 2012. *Long-term process-based morphological modeling of large tidal basins*. UNESCO-IHE, Institute for Water Education.
- De Vriend, H.J., Capobianco, M., Chesher, T., De Swart, H. de, Latteux, B., Stive, M.J.F., 1993. Approaches to long-term modelling of coastal morphology: a review. *Coast. Eng.* 21, 225–269.
- Deltares, 2013. *User Manual Delft3D-FLOW*. version: 3.15.2789. Deltares.
- Dissanayake, D., Ranasinghe, R., Roelvink, J.A., 2012. The morphological response of large tidal inlet/basin systems to relative sea level rise. *Clim. Change* 113, 253–276.
- Dodet, G., 2013. *Morphodynamic modelling of a wave-dominated tidal inlet: the Albufeira lagoon*. La Rochelle.
- Egbert, G.D., Erofeeva, S.Y., 2002. Efficient inverse modeling of barotropic ocean tides. *J. Atmospheric Ocean. Technol.* 19, 183–204.
- Elder, J.W., 1956. The dispersion of marked fluid in turbulent shear flow. *J. Fluid Mech.* 5, 544–560.
- Engelund, F., Hansen, E., 1967. *A monograph on sediment transport in alluvial streams*. TEKNISKFORLAG Skelbregade 4 Copenhagen V, Denmark.
- Fairall, C.W., Bradley, E. F., Hare, J. E., Grachev, A. A., Edson, J. B., 2003. Bulk parameterization of air-sea fluxes: Updates and verification for the COARE algorithm. *J. Clim.* 16, 571–591.
- Fischer, H.B., Koh, R.C.Y., Imberger, J., Brooks, N.H., 1979. *Mixing in Inland and Coastal Waters*. Academic Press, San Diego, California USA.

- Fredsøe, J., 1984. Turbulent boundary layer in wave-current motion. *J. Hydraul. Eng.* 110, 1103–1120.
- Gordon, R.B., 1974. Dispersion of dredge spoil dumped in near-shore waters. *Estuar. Coast. Mar. Sci.* 2, 349–358.
- Grunnet, N.M., Walstra, D.-J.R., Ruessink, B.G., 2004. Process-based modelling of a shoreface nourishment. *Coast. Eng.* 51, 581–607.
- Haidvogel, D.B., Arango, H., Budgell, W.P., Cornuelle, B.D., Curchitser, E., Di Lorenzo, E., Fennel, K., Geyer, W.R., Hermann, A.J., Lanerolle, L., others, 2008. Ocean forecasting in terrain-following coordinates: Formulation and skill assessment of the Regional Ocean Modeling System. *J. Comput. Phys.* 227, 3595–3624.
- Holthuijsen, L.H., Booij, N., Ris, R.C., Haagsma, I.J., Kieftenburg, A.T.M.M., Kriezi, E.E., Zijlema, M., van der Westhuysen, A.J., 2007. SWAN cycle III version 40.51, Technical Documentation. Delft, 2600 GA Delft The Netherlands.
- Latteux, B., 1995. Techniques for long-term morphological simulation under tidal action. *Mar. Geol.* 126, 129–141.
- Lesser, G.R., 2009. An approach to medium-term coastal morphological modelling. UNESCO-IHE, Institute for Water Education.
- Lesser, G.R., Roelvink, J.A., van Kester, J.A.T.M., Stelling, G.S., 2004. Development and validation of a three-dimensional morphological model. *Coast. Eng., Coastal Morphodynamic Modeling* 51, 883–915. doi:10.1016/j.coastaleng.2004.07.014
- Morgan, K.M., Kench, P.S., Ford, R.B., 2011. Geomorphic change of an ebb-tidal delta: Mair Bank, Whangarei Harbour, New Zealand. *N. Z. J. Mar. Freshw. Res.* 45, 15–28.
- MSL, 2016. Crude Shipping Project, Whangarei Harbour - Predicted physical environmental effects from channel deepening and offshore disposal.
- Okubo, A., 1971. Oceanic diffusion diagrams. *Deep-Sea Res.* 18, 789–802.
- OMC International, 2016. Mardsen Point Channel Optimisation.
- Pinto, L., Fortunato, A.B., Freire, P., 2006. Sensitivity analysis of non-cohesive sediment transport formulae. *Cont. Shelf Res.* 26, 1826–1839.
- Prediction of shallow-water spectra - Collins - 1972 - *Journal of Geophysical Research* - Wiley Online Library [WWW Document], n.d. URL <http://onlinelibrary.wiley.com/doi/10.1029/JC077i015p02693/full> (accessed 4.25.16).
- Ramli, A., de Lange, W.P., Bryan, K.R., Mullarney, J., 2015. Coupled flow-wave numerical model in assessing the impact of dredging on the morphology of Matakana Banks, in: *Proceedings of the Australasian Coasts & Ports Conference*.
- Ranasinghe, R., Pattiaratchi, C., Masselink, G., 1999. A morphodynamic model to simulate the seasonal closure of tidal inlets. *Coast. Eng.* 37, 1–36. doi:10.1016/S0378-3839(99)00008-3
- Ris, R.C., Holthuijsen, L.H., Booij, N., 1999. A third-generation wave model for coastal regions: 2. Verification. *J. Geophys. Res. Oceans* 104, 7667–7681. doi:10.1029/1998JC900123
- Royal HaskoningDHV, 2016a. Shipping Channel - Concept Design Report, prepared for Refining NZ., Refining NZ Crude Freight Project.
- Royal HaskoningDHV, 2016b. Dredging Methodology Assessment. Technical Memo, prepared for Refining NZ., Refining NZ Crude Freight Project.
- Royal HaskoningDHV, 2015. Desktop Simulation Study, prepared for Refining NZ., Refining NZ Crude Freight Project.
- Smart, G.M., Duncan, M.J., Walsh, J.M., 2002. Relatively rough flow resistance equations. *J. Hydraul. Eng.* 128, 568–578.
- Smith, S.J., Friedrichs, C.T., 2011. Size and settling velocities of cohesive flocs and suspended sediment aggregates in a trailing suction hopper dredge plume. *Cont. Shelf Res.* 10.
- Spearman, J., Bray, R.N., Land, J., Burt, T.N., Mead, C.T., Scott, D., 2007. *Estuarine and Coastal Fin Sediments Dynamics*.
- Tolman, H.L., Chalikov, D., 1996. Source terms in a third-generation wind wave model. *J. Phys. Oceanogr.* 26, 2497–2518.

- Tolman, H.L., 1991. A Third-Generation Model for Wind Waves on Slowly Varying, Unsteady and Inhomogeneous Depths and Currents. *J. Phys. Oceanogr.* 21, 782–797.
- Tonkin and Taylor, 2016a. Crude Freight Project, Whangarei Harbour - Dredging and disposal options - synthesis report. Tonkin and Taylor.
- Tonkin and Taylor, 2016b. Crude Shipping project, Mid-point multi-criteria alternatives assessment. Prepared for ChanceryGreen for Refining NZ.
- Tonkin and Taylor, 2016c. Marsden point Refinery - Crude Freight Project, Vibrocore report (No. 30488.1000). Tonkin and Taylor.
- Truitt, C.L., 1988. Dredged material behavior during open-water disposal. *J. Coast. Res.* 489–497.
- van der Wegen, M., Dastgheib, A., Jaffe, B.E., Roelvink, D., 2011. Bed composition generation for morphodynamic modeling: case study of San Pablo Bay in California, USA. *Ocean Dyn.* 61, 173–186.
- Van der Wegen, M., Roelvink, J.A., 2008. Long-term morphodynamic evolution of a tidal embayment using a two-dimensional, process-based model. *J. Geophys. Res. Oceans* 113.
- van der Westhuysen, A.J., Zijlema, M., Battjes, J.A., 2007. Nonlinear saturation-based whitecapping dissipation in SWAN for deep and shallow water. *Coast. Eng.* 54, 151–170. doi:10.1016/j.coastaleng.2006.08.006
- Van Rijn, L.C., van Rijn, L.C., van Rijn, L.C., 1993. Principles of sediment transport in rivers, estuaries and coastal seas. Aqua publications Amsterdam.
- Van Rijn, L.C., Walstra, D.J.R., Ormond, M. van, 2004. Description of TRANSPOR2004 and implementation in DELFT3D-ONLINE: final report. Deltares (WL).
- Van Rijn, L.C., 2007. A unified view of sediment transport by current and waves, Part II: Suspended transport. *J. Hydraul. Eng. ASCE* 22.
- Van Rijn, L.C., 1984. Sediment Transport Part II: Suspended Load Transport. *J. Hydraul. Eng.* 110, 1613–1641.
- Vitali, L., Monforti, F., Bellasio, R., Bianconi, R., Sachero, V., Mosca, S., Zanini, G., 2006. Validation of a Lagrangian dispersion model implementing different kernel methods for density reconstruction. *Atmos. Environ.* 40, 8020–8033.
- Walstra, D.J.R., Hoekstra, R., Tonnon, P.K., Ruessink, B.G., 2013. Input reduction for long-term morphodynamic simulations in wave-dominated coastal settings. *Coast. Eng.* 77, 57–70.
- Walstra, D.J.R., Roelvink, J.A., Groeneweg, J., 2001. Calculation of wave-driven currents in a 3D mean flow model, in: Coastal Engineering Conference. ASCE AMERICAN SOCIETY OF CIVIL ENGINEERS, pp. 1050–1063.
- WEPPE, S., MCCOMB, P., COE, L., 2015. NUMERICAL MODEL STUDIES TO SUPPORT THE SUSTAINABLE MANAGEMENT OF DREDGE SPOIL DEPOSITION IN A COMPLEX NEARSHORE ENVIRONMENT, in: The Proceedings of the Coastal Sediments 2015. World Scientific.
- Whitehouse R., et al, 2000. Dynamics of estuarine muds, Thomas Telford, London. ed.
- Williams, J.R., Hume, T.M., 2014. Investigation into the decline of pipi at Mair Bank, Whangarei Harbour. Prepared for Northland Regional Council (No. AKL2014-022). NIWA.
- Winterwerp, J.C., 2002. Near-field behavior of dredging spill in shallow water. *J. Waterw. Port Coast. Ocean Eng.* 128, 96–98.
- Zhang, Y.L., Baptista, A.M., 2008. A semi-implicit Eulerian-Lagrangian finite element model for cross-scale ocean circulation. *Ocean Model.* 21, 71–96.

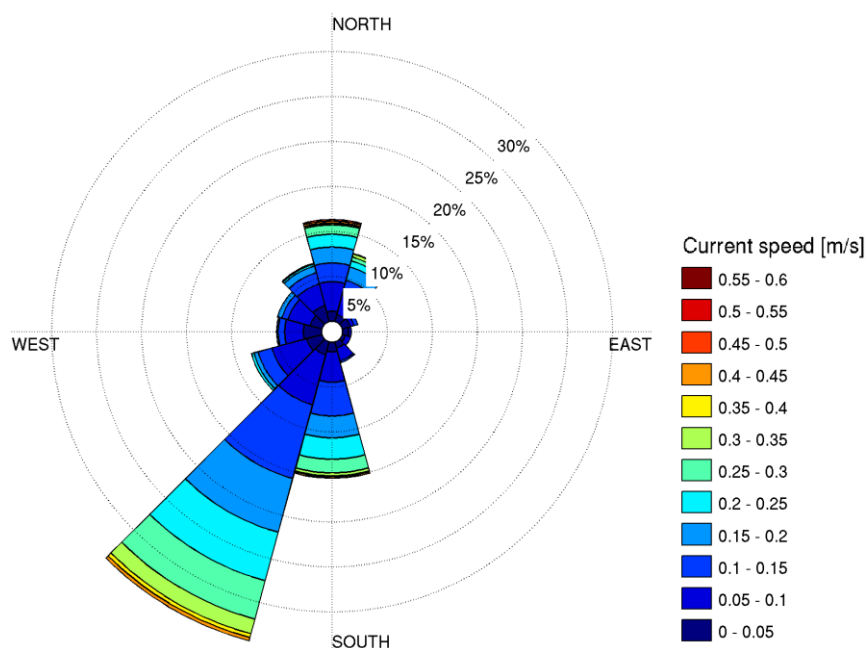
APPENDIX A – LOCATION OF INSTRUMENTS

Geographic coordinates of instruments used to collect data and validate the different models implemented in the present study.

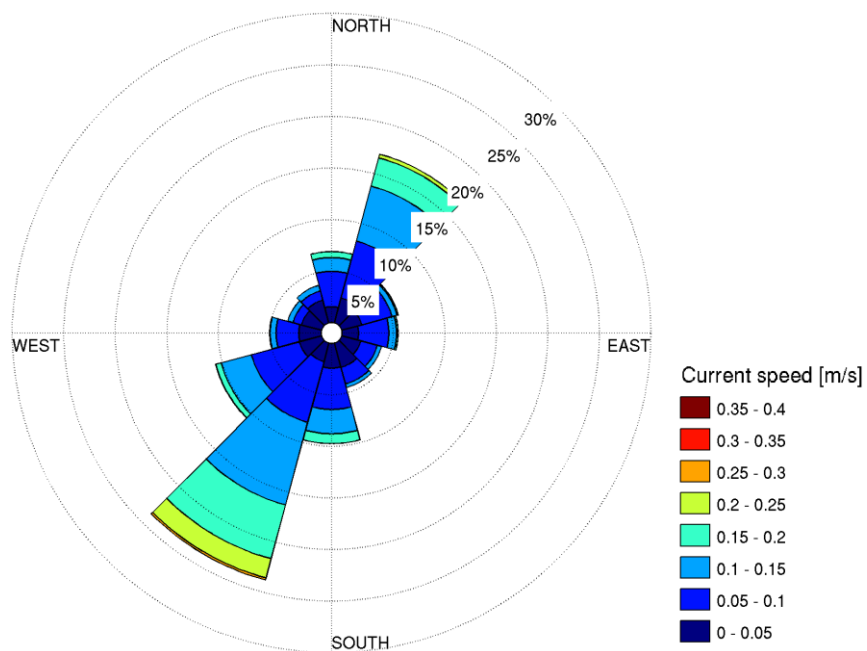
Positions	Description	Geographic coordinates (WGS 84 datum)	
		Longitude (East)	Latitude (North)
WS	Wind station location at Mardsen Point	174.48700	-35.84000
WRB	Wave measurement at tidal delta entrance	174.54830	-35.88310
w1	Wave measurement along Ruakaka Beach	174.46720	-35.90740
w2	Wave measurement along Ruakaka Beach	174.47050	-35.88930
w3	Wave measurement along Ruakaka Beach	174.48140	-35.86800
w4	Wave measurement along Ruakaka Beach	174.50110	-35.84930
ADCP1	Current profiler position in the Parry Channel	174.66077	-35.89648
ADCP2	Current profiler position at Disposal site 3.2	174.59075	-35.912833
ADCP3	Current profiler position at Disposal site 1.2	174.50742	-35.886233
ADCP4	Current profiler position at Disposal site 2.2	174.53307	-35.937559
K17	Water elevation measurement at Port Whangarei (near Hatea river)	174.35120	-35.75750
P10	Water elevation measurement near Portland	174.34890	-35.80330
Parua	Water elevation measurement at the Parua Bay entrance	174.37950	-35.77600
W2	Water elevation measurement between Tamaterau and Rat Island	174.45160	-35.79970

APPENDIX B – MEASURED CURRENTS

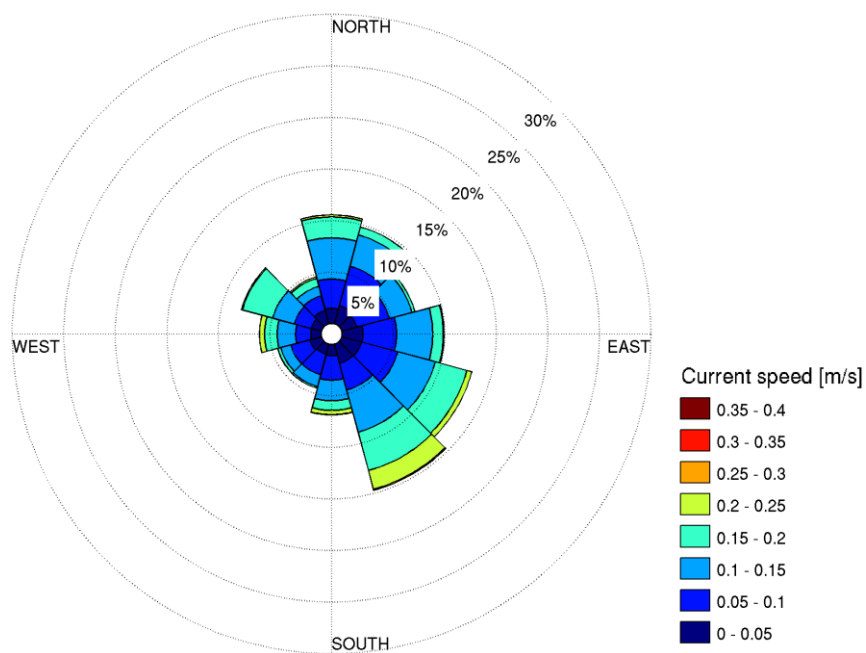
Time series and rose plots of the depth-averaged measured currents at sites ADCP1-4.



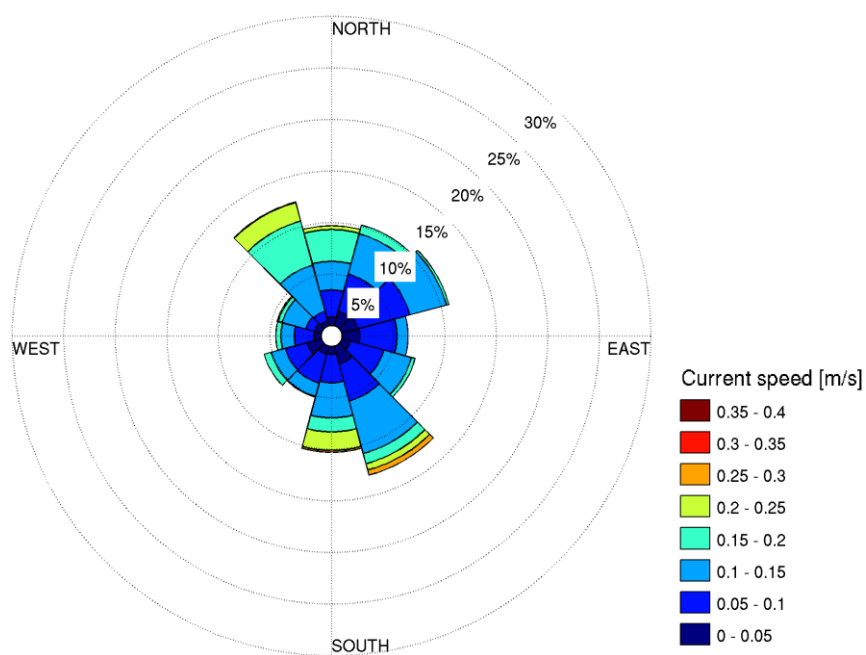
ADCP1



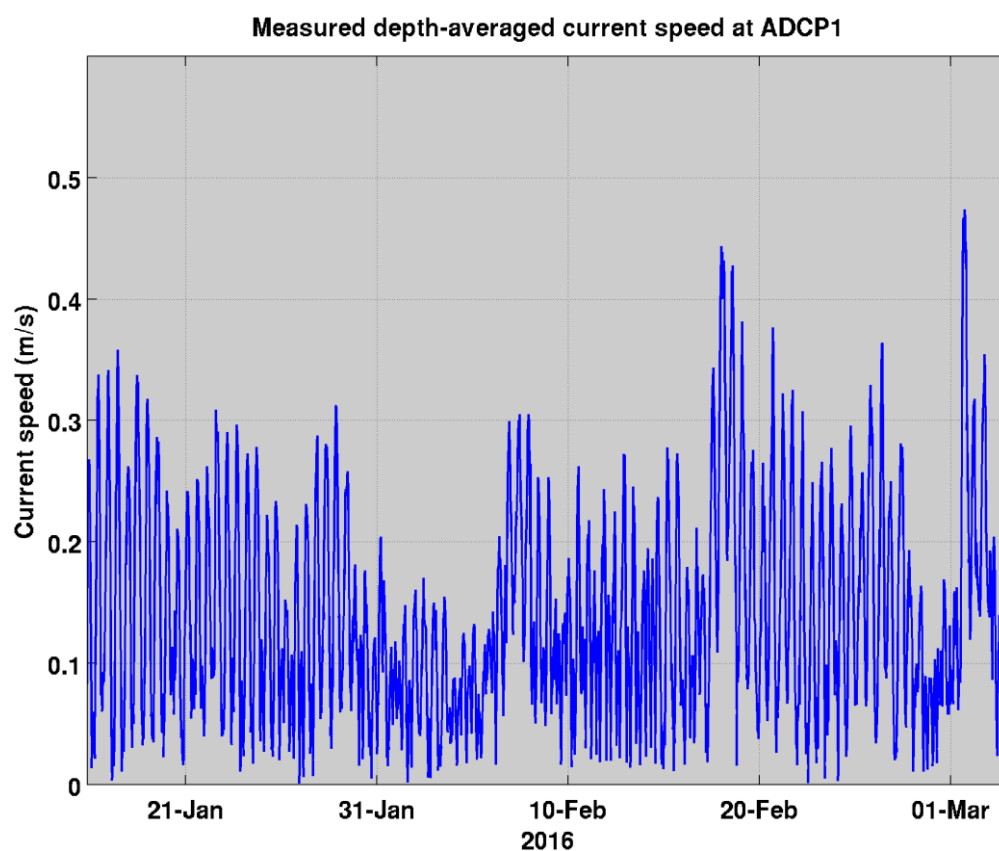
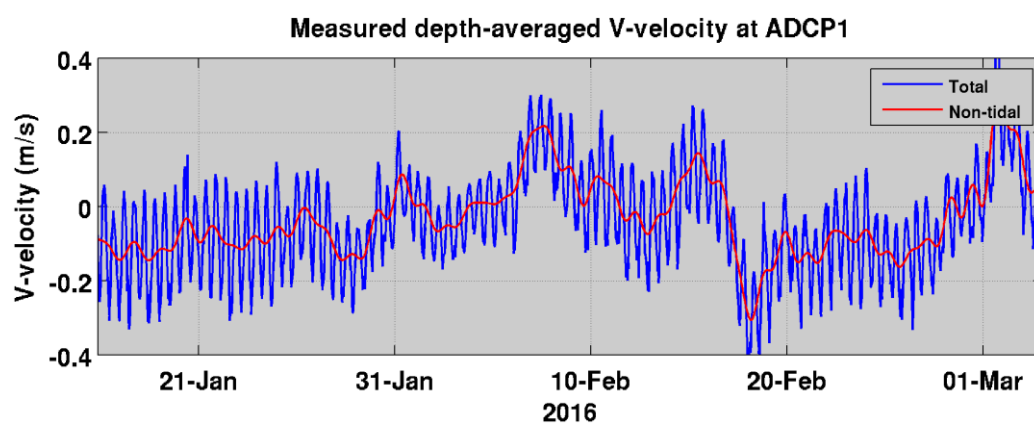
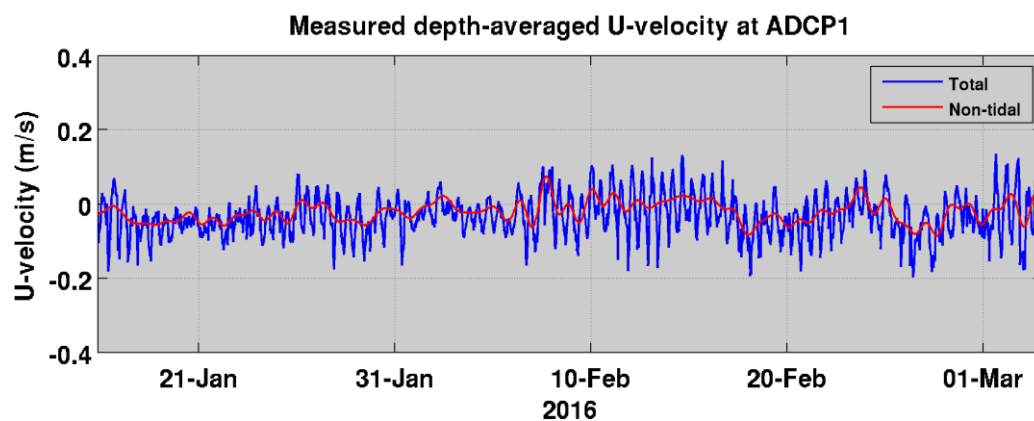
ADCP2

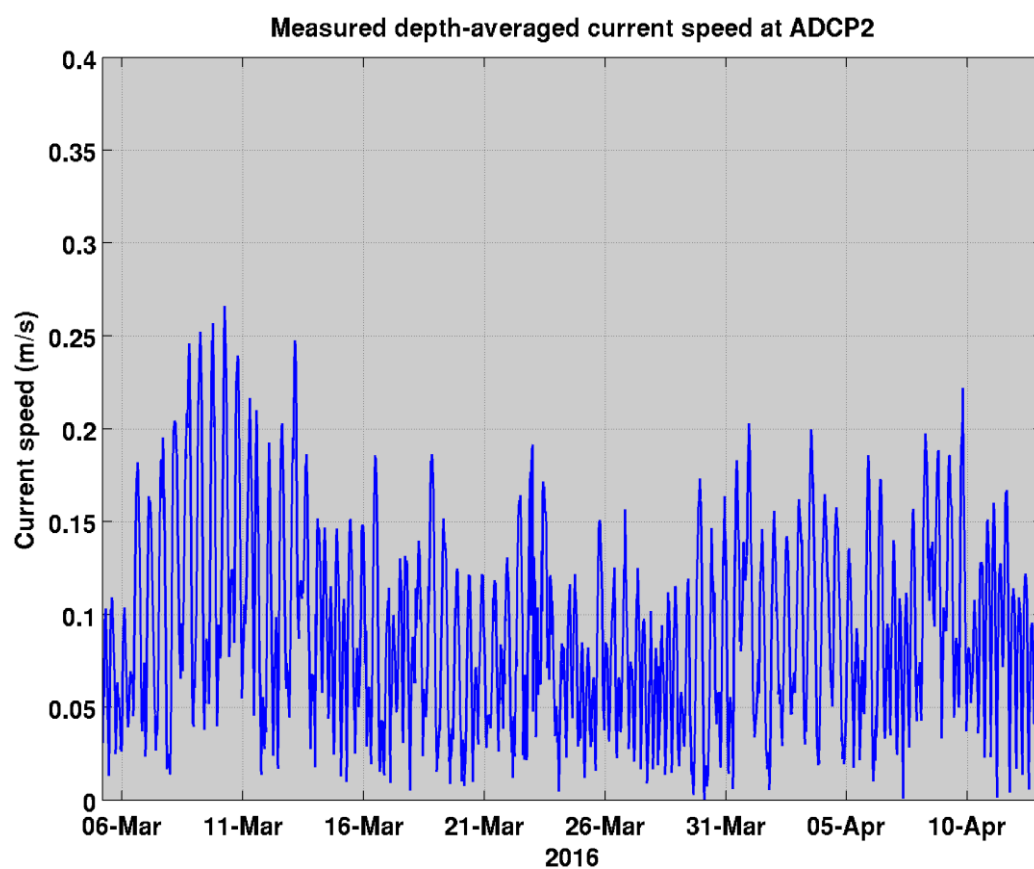
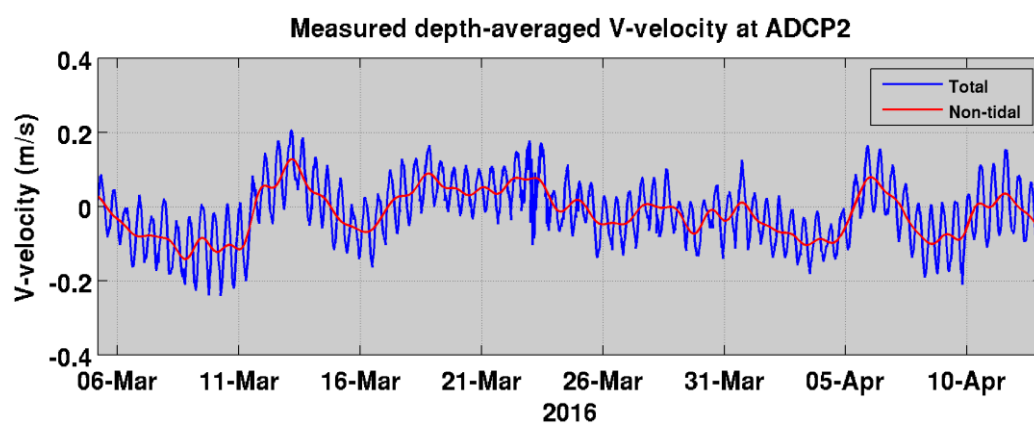
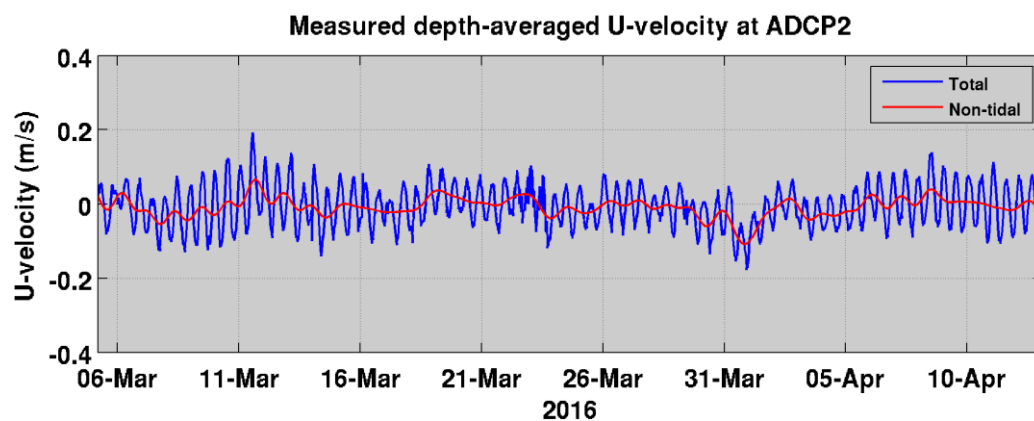


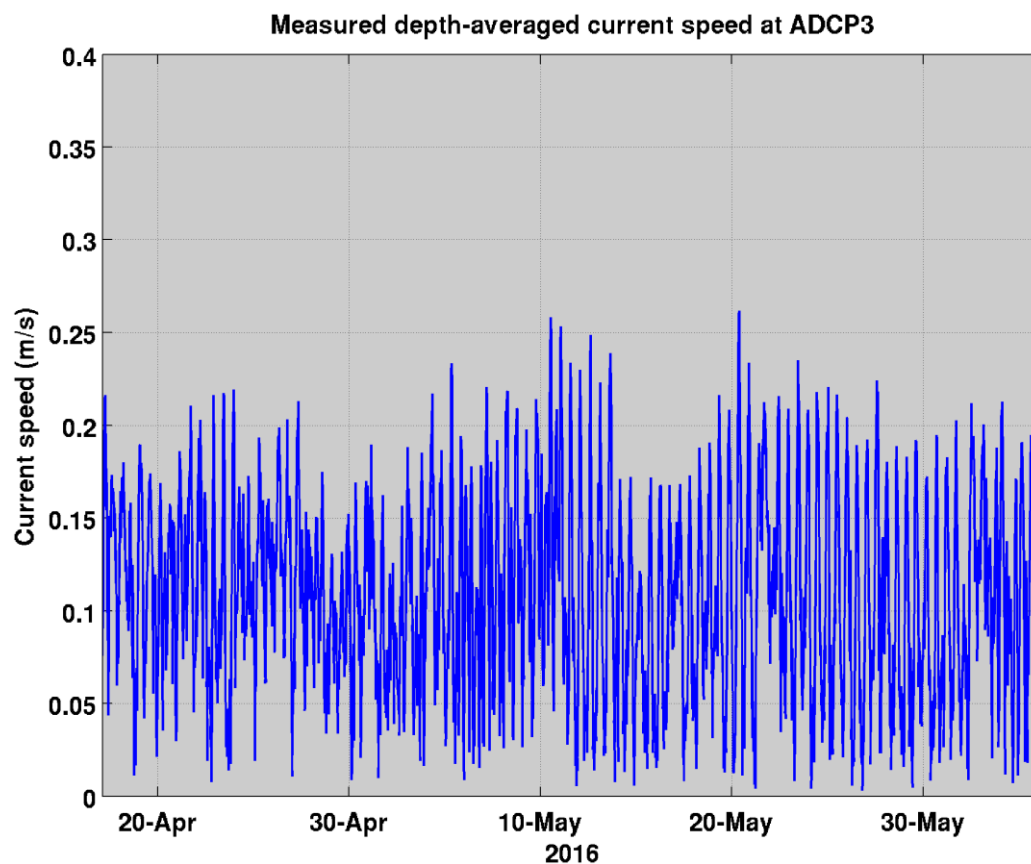
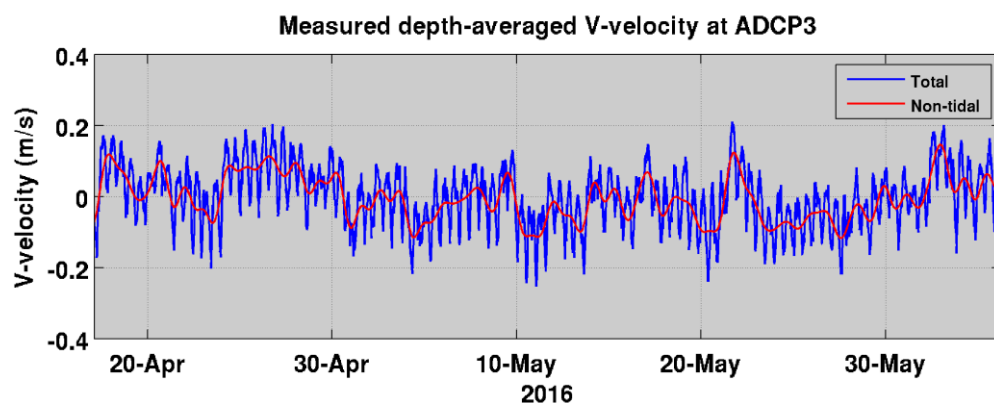
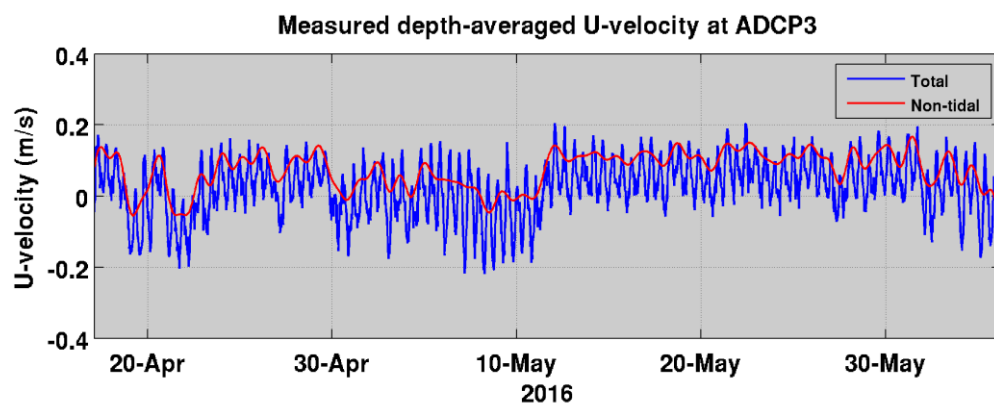
ADCP3

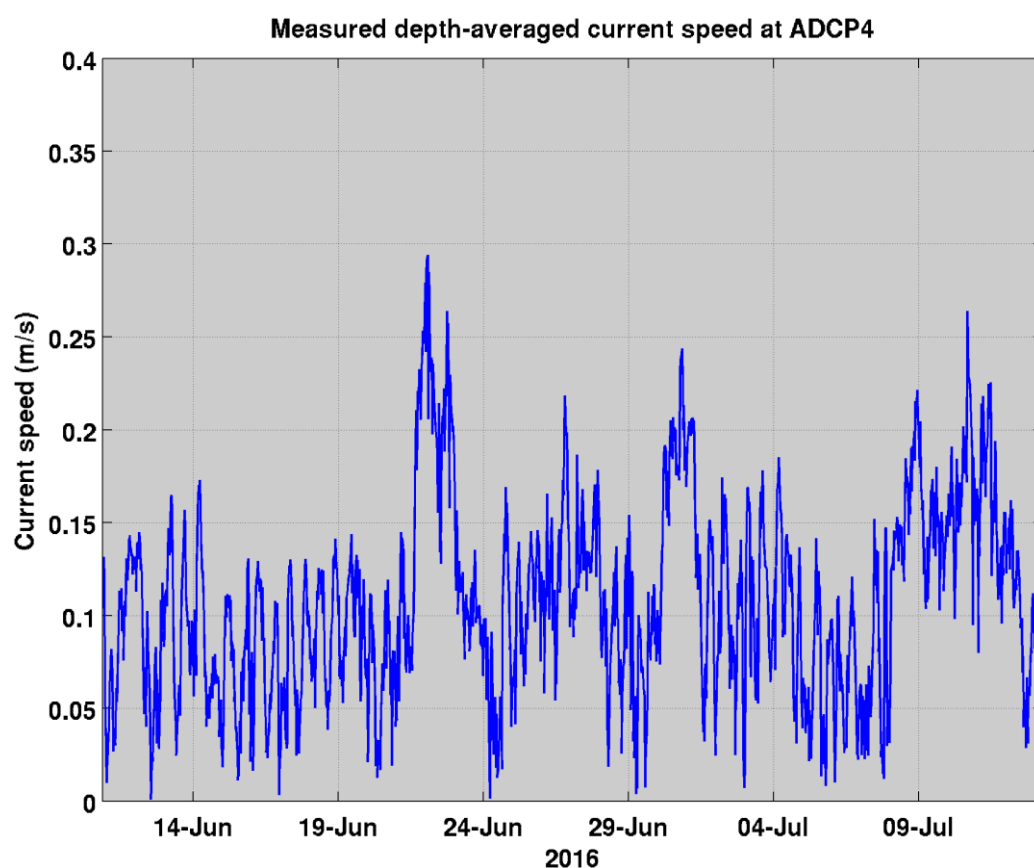
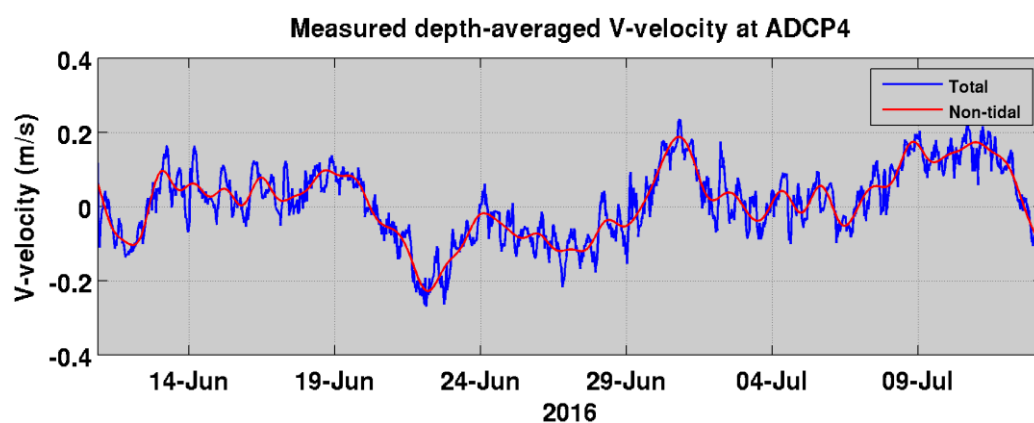
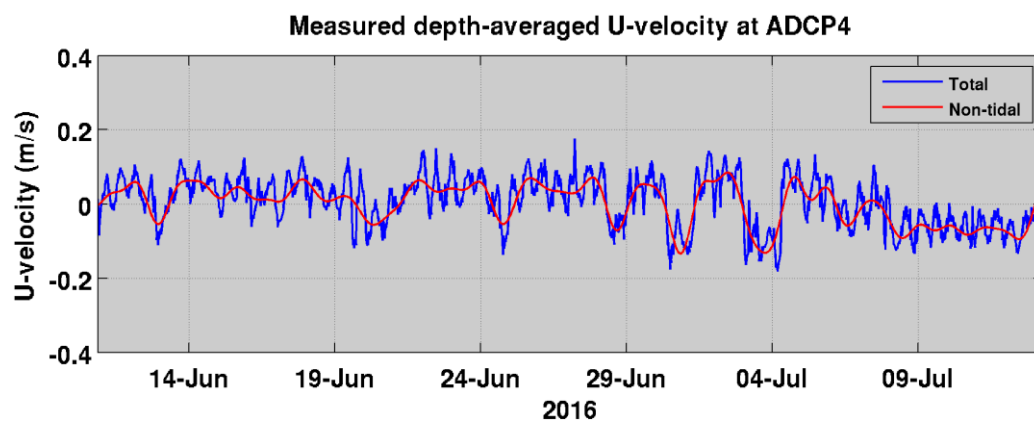


ADCP4









APPENDIX C – LOCATION OF RELEASE SITES

Geographic coordinates of release sites used for the dredging and the disposal plume modelling.

Positions	Geographic coordinates (WGS 84 datum)	
	Longitude (East)	Latitude (North)
R0	174.501963	-35.837500
R1	174.507890	-35.835210
R2	174.520148	-35.847333
R3	174.523247	-35.862960
R4	174.538100	-35.878500
R5	174.545600	-35.885700
R6	174.521125	-35.842327
PW	174.581275	-35.915609
PN	174.588669	-35.904212
PE	174.600443	-35.910711
PS	174.594556	-35.922250
ADCP	174.590750	-35.912833